Norwegian University
of Life Sciences

Master's Thesis 2020 30 ECTS
Faculty of Science and Technology

A Study of the Light and Elevated Temperature Induced Degradtion in p-type Multicrystalline PERC Wafers with Hyperspectral Imaging

Rasmus Svebestad
Master of Science in Technology
Environmental Physics and Renewable energy

This page is intentionally left blank.

Preface

The completion of this master's thesis leads to the end of my studies in Environmental Physics and Renewable Energy at the Norwegian University of Life Sciences (NMBU). My five years at NMBU has been a great experience, for this I am grateful and I would like to thank some people.

For the help with this master's thesis I would like to thank my supervisor Ingunn Burud, for helping me sketching the outlines of it and for her feedback throughout the process of creating it. I would also like to give a big thank you to my co-supervisor Torbjørn Mehl, who has helped me a lot with both the imaging process and the data analysis. A thank will also be given to Espen Olsen who has contributed with a highly appriciated domain knowledge and feedback on the results. In addition to the internal academic staff at NMBU, I would like to thank Rune Søndenå at IFE who has pre-processed and prepared the samples used in this study, and who has given important advices and feedback along the way.

For the completion of my studies I would like to thank all the students studying Environmental Physics and Renewable Energy, who has contributed to the friendly and helpful environment that surrounds the study. It is important to maintain this environment, I have benefited a lot from it during my studies and I hope that future students will experience it the same way. The academic staff and alumni students who has facilitated this environment, should also be thanked. In the end I would like to thank my family and friends for all the support throughout the years. A special thank should be given to my flatmates for their work as proofreaders and psychologists over the last few weeks.

Rasmus Svebestad

Ås, June 2nd 2020

Summary

Since 2012 a lot of research has been done to understand the phenomenon of light and elevated temperature induced degradation (LeTID), which can limit the efficiency of a solar cell by as much as 20 %. In this study LeTID was investigated by studying samples of multicrystalline p-type passivated emitter and rear cell (PERC) wafers with hyperspectral imaging. Eight samples were invesigated in the study. Among these, five were cut from wafers pre-processed with phosphorus diffusion gettering and hydrogenation (PDGH) while three were cut from wafers pre-processed with phosphorus diffusion gettering (PDG). Samples of different pre-processings were chosen to study the involvement of hydrogen in LeTID. To study the effect of the placement of a wafer in the ingot, the samples were from wafers cut from different heights in the ingot. To study LeTID, the samples were first pre-processed with an illumination of 0.08 suns with a 1.5 AM spectrum at room temperature. This was done to mitigate the influence of boron-oxygen light induced degradation (BO-LID) on the results. Then the samples were treated with 1 sun of illumination with a 1.5 AM spectrum at a temperature of 110 °C to trigger the LeTID. This treatment lasted more than 300 hours, and throughout the treatment, hyperspectral images was taken continuously.

It seems clear from the results of this study that hydrogen is participating in the LeTID, as only hydrogenated samples showed LeTID. From the results it could be seen that at least one defect were passivated in dislocation clusters of the hydrogenated samples when the temperature was elevated. This indicates that hydrogen is activated in the samples when the temperature is raised. The results of the study indicates that LeTID is disappearing towards the top of the ingot, as the sample of the wafer from highest in the ingot showed no signs of LeTID. The most plausible reason for the disappearence of LeTID towards the top of the ingot is that LeTID is caused by the activated hydrogen passivating the dopant atoms of the samples. This theory is strengthened by the dislocation cluster of the second highest hydrogenated sample, which shows increased resiliance towards LeTID. It seems plausible that this resiliance originates from the hydrogen atoms being more likely to passivate impurities in the dislocation cluster, rather than passivating the dopant atoms. LeTID disappearing towards the top of the ingot contradicts the theory of LeTID being caused by either cobalt or nickel, as the concentration of these elements increases towards the top of the ingot.

Sammendrag

Siden 2012 har det blitt forsket mye for å oppnå en økt forståelse av LeTID, som kan forårsake en degradering på opp mot 20 %. I denne studien har prøver av multikrystalinske p-type PERC wafere blitt undersøkt ved hjelp av hyperspektrale bilder for å studere LeTID. Åtte prøver ble brukt i forsøket, og av disse var fem preparert med PDGH behandling og tre preparert med PDG behandling. Grunnen til at både PDG behandlede prøver og PDGH behandlede prøver ble studert var for å finne ut mer om hydrogens rolle i LeTID. Prøvene ble kuttet ut fra wafere tatt fra forskjellige høyder i ingoten, for å studere hvilken effekt dette ville ha på utviklingen av LeTID. Før forsøket begynte ble prøvene bestrålt med et 1.5 AM spektrum med styrke på 0.08 sol i romtemperatur. Dette ble gjort for å unngå at resultatene ble påvirket av bor-oksygen degradering som følge av bestrålingen. Da dette var gjort ble prøvene eksponert for stråling med et 1.5 AM spektrum med styrke på 1 sol, mens de ble varmet opp til omkring 110 °C. Denne behandlingen varte i over 300 timer og det ble tatt hyperspektrale bilder jevnlig underveis.

Det virker klart fra studiens resultater at hydrogen deltar i LeTID. Dette fordi bare prøver som var hydrogenerte viste LeTID. Resultatene viste også at minst en defekt ble passivert i dislokasjonklustrene til de hydrogenerte prøvene når temperaturen økte. Dette indikerer at hydrogen aktiveres i prøvene når temperaturen øker. Studiens funn tyder også på at wafere hentet fra toppen av ingoten er motstandsdyktige mot LeTID. Den mest sannsynlige forklaringen til dette er at LeTID blir forårsaket av aktiverte hydrogen atomer i waferne som passiverer dopeatomene. Denne teorien styrkes også av at dislokasjonsklusteret fra den nest øverste hydrogenerte prøven viser en økt motstandsdyktighet mot LeTID, sammenlignet med resten av den prøven. Det virker sannsynlig at denne motstandsdyktigheten skyldes at hydrogenatomer i et dislokasjonkluster vil passivere urenheter fremfor dopeatomer. At LeTID forsvinner mot toppen av ingoten motsier teorien om at LeTID forårsakes av kobolt og/eller nikkel, fordi konsentrasjonen av disse atomtypene minsker mot toppen.

Contents

1 Introduction **1**

2 Theory **5**
2.1 PV Technology fundamentals 5
2.1.1 Semiconductors 5
2.1.2 pn-junction 8
2.1.3 Bandgap 9
2.1.4 Illumination of the solar cell 11
2.2 Recombination and photoluminescence 12
2.2.1 Minority carrier lifetime and recombination mechanisms . . 12
2.3 Photoluminescence 16
2.3.1 Band-to-band photoluminescence 16
2.3.2 Defect related luminescence 17
2.4 Light and Elevated Temperature Induced Degradation 17
2.5 Hyperspectral imaging 19
2.6 Foreign elements and defects in silicon wafers 20

3 Methodology **23**
3.1 Samples and sample processing 23
3.1.1 Pre-processing 25
3.1.2 Processing 26
3.2 The hyperspectral imaging process 28
3.2.1 The imaging setup 28
3.2.2 Cooling of the samples 31
3.2.3 Image aquisition 32
3.3 Data processing 33

4 Results **39**
4.1 Spatial BB-signal development 39
4.2 Spectrum development 43
4.3 A deeper look on the dislocation clusters 51
4.4 A closer look on the DRL development 67

5 Discussion **73**
5.1 Discussion of methodology: Weaknesses and considerations 73
5.2 Hydrogens role in LeTID 74
5.3 Variation due to the samples' height in the ingot 75
5.4 Discussion of the results for the dislocation clusters 76
5.5 Further discussion of the signal development 77

6 Conclusion and further work **79**
6.1 Conclusion 79
6.2 Further work 80

A Extra figures **89**
A.1 Extra spectrum development figures 89
A.2 Extra figures relative DRL development 93

B Example Matlab Codes **95**

List of Figures

2.1 Illustration of a silicon crystal lattice. The figure shows the silicon atoms and the covalent bonds between the valence electrons. The figure is inspired by Boylestad et al. [16]. 6

2.2 Simple illustration of the distribution of charge carriers and electric potential through the depth of a solar cell. p is concentration of free holes, n is concentration of free electrons and V is the electric potential. The figure is inspired by Smets et al. [15]. 9

2.3 Illustration of the bandgap and how a photon with higher energy than the bandgap is exciting an electron. The figure is inspired by Boylestad et al. [16] and Smets et al. [15]. 10

2.4 The figure shows the difference between a) the valence and conduction band of a direct semiconductor and b) the valence and conduction band of a indirect semiconductor. The figure show the differnce in energy, E, and the difference in momentum, p, between the top of the valence band and the bottom of the conduction band. The figure is inspired by Smets et al. [15]. 11

2.5 Illustration of the four recombination mechanisms a) direct recombination, b) SRH-recombination, c) Auger rebombination and d) surface recombination. E_C is the energy level at the bottom of the conduction band, E_V is the energy level at the top of the valence band and E_T is the energy level of the traps created by defects. The red dots illustrates electrons, while the white dots illustrates holes. The figure is inspired by Smets et al. [15]. 16

2.6 Illustration of the three dimensions of the hyperspectral image and the hypercube. Where the x and y axis are the spatial dimensions and the λ axis is the spectral dimension. 19

3.1 Picture of the samples a) sample 1, b) sample 2, c) sample 3, d) sample 4, e) sample 5, f) sample 6, g) sample 7 and h) sample 8. The full sample names were burned in on the samples' left corners. A black line coveres the names to protect the indentity of the manufacturer. 24
3.2 Illustration of the two different pre-processing treatments, PDG and PDGH. The figure is inspired by Adamczyk et al. [39] and Søndenå et al. [26]. 26
3.3 Illustration of the setup used to take hyperspectral images of the samples. A) camera, B) laser, C) long pass filter, D) sample, E) sample holder, F) cardboard to reduce fog over the sample, G) cardboard to reduce fog in front of the laser and H) translation stage. 29
3.4 Picture of the samples on a tissue paper. During the experiment sample 4 and 5 was interchanged and so was sample 6 and 8. The picture is taken after the experiment was done and it shows how sample 3, 6 and 8 was shattered. 33
3.5 The plot of the BB-signal for all the samples' upsides. The curves are normalized with regard to the signal after light soaking. In this plot the signal for sample 4 is called data5 and sample 5 is called data4. Also sample 6 and 8 are interchanged. Otherwise the BB-signal of the samples are called: data[insert number of sample]. 34
3.6 The plot of the BB-signal for all the samples, divided by sample 7's signal. The curves are also normalized with regard to the signal after light soaking. In this plot the signal for sample 4 is called data 5 and sample 5 is called data 4. Also sample 6 and 8 are interchanged. Otherwise the BB-signal of the samples are called: data[insert number of sample]. 35
3.7 A photoluminescence image taken at IFE of sample 5's wafer. The black square marks approximately where the sample was cut from. The scale on the right side is in µs, and the pixel colour is given from the minority carrier lifetime in that pixel. 36

4.1 Spatial development of the BB-signal over time for: a) sample 1, b) sample 6 and c) sample 2. The images are from left the initial image, image after light soaking, fully degraded and fully regenerated. The colour of each pixel shows the strength of BB-signal in that pixel. . 40
4.2 Spatial development of the BB-signal over time for: a) sample 3, b) sample 7, c) sample 4 and d) sample 4D. The images are from left the initial image, image after light soaking, fully degraded and fully regenerated. The colour of each pixel shows the strength of BB-signal in that pixel. 41

4.3 Spatial development of the BB-signal over time for: a) sample 5, b) sample 8, c) sample 5D and d) sample 8D. The images are from left the initial image, image after light soaking, fully degraded and fully regenerated. The colour of each pixel shows the strength of BB-signal in that pixel. 42
4.4 Photoluminescence spectrum of sample nr. 1. The red line is the initial spectrum, the green line is the spectrum after light soaking, the blue line is the spectrum when the sample is fully degraded and the yellow line is the spectrum after the sample has regenerated. . . 44
4.5 Photoluminescence spectrum of sample nr. 6. The red line is the initial spectrum, the green line is the spectrum after light soaking, the blue line is the spectrum when the sample is fully degraded and the yellow line is the spectrum after the sample has regenerated. . . 45
4.6 Photoluminescence spectrum of sample nr. 2. The red line is the initial spectrum, the green line is the spectrum after light soaking, the blue line is the spectrum when the sample is fully degraded and the yellow line is the spectrum after the sample has regenerated. . . 46
4.7 Photoluminescence spectrum of sample nr. 3. The red line is the initial spectrum, the green line is the spectrum after light soaking, the blue line is the spectrum when the sample is fully degraded and the yellow line is the spectrum after the sample has regenerated. . . 47
4.8 Photoluminescence spectrum of sample nr. 7. The red line is the initial spectrum, the green line is the spectrum after light soaking, the blue line is the spectrum when the sample is fully degraded and the yellow line is the spectrum after the sample has regenerated. . . 48
4.9 Photoluminescence spectrum of sample nr. 4. The red line is the initial spectrum, the green line is the spectrum after light soaking, the blue line is the spectrum when the sample is fully degraded and the yellow line is the spectrum after the sample has regenerated. . . 49
4.10 Photoluminescence spectrum of sample nr. 5. The red line is the initial spectrum, the green line is the spectrum after light soaking, the blue line is the spectrum when the sample is fully degraded and the yellow line is the spectrum after the sample has regenerated. . . 50
4.11 Photoluminescence spectrum of sample nr. 8. The red line is the initial spectrum, the green line is the spectrum after light soaking, the blue line is the spectrum when the sample is fully degraded and the yellow line is the spectrum after the sample has regenerated. . . 51
4.12 The image displays where the dislocation cluster investigated on sample 2 is situated. The image also shows the spatial distribution of the D3-signal of sample 2. 52

4.13 The figure shows the photoluminescence spectrum of the dislocation cluster of sample 2. 53

4.14 The image displays where the dislocation cluster investigated on sample 3 is situated. The image also shows the spatial distribution of the D3-signal of sample 3. 54

4.15 The figure shows the photoluminescence spectrum of the dislocation cluster of sample 3. 55

4.16 The image displays where the dislocation cluster investigated on sample 4 is situated. The image also shows the spatial distribution of the D3-signal of sample 4. 56

4.17 The figure shows the photoluminescence spectrum of the dislocation cluster on the upside of sample 4. 57

4.18 The figure shows the spatial development of a) the BB-signal, b) the D3 signal and c) the D4 signal of the dislocation cluster on the upside of sample 4. The colour of the pixels indicates the strength of the signal. 58

4.19 The image displays where the dislocation cluster investigated on the downside of sample 4 is situated. The image also shows the spatial distribution of D3-signal on the downside of sample 4. 59

4.20 The figure shows the photoluminescence spectrum of the dislocation cluster on the downside of sample 4. 60

4.21 The image displays where the dislocation cluster investigated on the downside of sample 5 is situated. The image also shows the spatial distribution of the D3-signal on the downside of sample 5. 61

4.22 The figure shows the photoluminescence spectrum of the dislocation cluster on the downside of sample 5. 62

4.23 The image displays where the dislocation cluster investigated on sample 7 is situated. The image also shows the spatial distribution of the D3-signal of sample 7. 63

4.24 The figure shows the photoluminescence spectrum of the dislocation cluster of sample 7. 64

4.25 The image displays where the dislocation cluster investigated on the downside of sample 8 is situated. The image also shows the spatial distribution of the D3-signal on the downside of sample 8. 65

4.26 The figure shows the photoluminescence spectrum of the dislocation cluster on the downside of sample 8. 66

4.27 Spatial development of the D3-signal over time for: a) sample 3, b) sample 7, c) sample 5D and d) sample 8D. The images are from left the initial image, image after light soaking, fully degraded and fully regenerated. The colour of the pixel indicates the strength of the signal. 68
4.28 The figure compares the relative changes in the PL-signal of: a) sample 1 and b) sample 6. The PL spectrums are divided by their respective initial PL spectrum, to show how the signals develop through prossesing. 69
4.29 The figure compares the relative changes in the PL-signal of: a) sample 3 and b) sample 7. The PL spectrums are divided by their respective initial PL spectrum, to show how the signals develop through prossesing. 70
4.30 The figure compares the relative changes in the PL-signal of: a) sample 5 and b) sample 8. The PL spectrums are divided by their respective initial PL spectrum, to show how the signals develop through prossesing. 71

A.1 Photoluminescence spectrum of the downside of sample nr. 4. The red line is the initial spectrum, the green line is the spectrum after light soaking, the blue line is the spectrum when the sample is fully degraded and the yellow line is the spectrum after the sample has regenerated. 90
A.2 Photoluminescence spectrum of the downside of sample nr. 5. The red line is the initial spectrum, the green line is the spectrum after light soaking, the blue line is the spectrum when the sample is fully degraded and the yellow line is the spectrum after the sample has regenerated. 91
A.3 Photoluminescence spectrum of the downside of sample nr. 8. The red line is the initial spectrum, the green line is the spectrum after light soaking, the blue line is the spectrum when the sample is fully degraded and the yellow line is the spectrum after the sample has regenerated. 92
A.4 Spatial development of the D3-signal over time for: a) sample 1 and b) sample 6. The images are from left the initial image, image after light soaking, fully degraded and fully regenerated. The colour of the pixel indicates the strength of the signal. 93
A.5 The figure compares the relative changes in the PL-signal of: a) sample 2 and b) sample 4. The PL spectrums are divided by their respective initial PL spectrum, to show how the signals develop through prossesing. 94

List of Tables

3.1 List of the samples used in this study. 25
3.2 List that shows how much time of treatment with illumination and elevated temperature the samples took to be fully degraded and fully regenerated. 35

Abbreviations

Abbreviation	Meaning
AM	Air Mass
BB	Band-to-Band
CCD	Charge-Coupled Device
DRL	Defect Related Luminescence
D1, D2, D3, D4	The four known DRL signals
hpmc-Si	High Performance Multicrystalline Silicon
LeTID	Light and Elevated Temperature Induced Degradation
LID	Light Induced Degradation
LS	Light Soaking
mc-Si	Multicrystalline Silicon
NIR	Near Infrared
NMBU	The Norwegian University of Life Sciences
PDG	Phosphorus Diffusion Gettering
PDGH	Phosphorus Diffusion Gettering and Hydrogenation
PERC	Passivated Emitter and Rear Cell
PV	Photovoltaic
SRH	Shockley-Read-Hall
SWIR	Short Wavelength Infrared

Chapter 1

Introduction

The total global energy consumption is raising. The consumption growth between 1990 and 2017 corresponds to an average growth in energy consumption per year of approximately 1.7 %, calculated with numbers from IEA [1]. Meanwhile, the Earths climate is changing due to a rise in the global temperature. This temperature rise is mainly caused by human emissions of green house gases, in particular CO_2 [2]. The human emissions of CO_2 mainly comes from burning of fossil fuels [3], to meet the growing energy demand. A solution to mitigating the global temperature rise would be shifting towards cleaner energy sources [2].

Photovoltaic (PV) solar energy is a much cleaner energy source than fossil fuels and the production of PV energy is already saving millions of tons of CO_2 equivalents each year. It has been calculated that the production of PV energy in 2019 reduced the energy related CO_2 emissions of the world with around 2 %. 2019 was the third year in a row where over 100 GW of PV energy was installed globally. The installed capacity of PV in 2019 was at least 114.9 GW, which is around 18 % of the total installed capacity of around 627 GW at the end of 2019 [4]. This shows a market in rapid growth, and the International Energy Agency (IEA) predicts that PV will be leading the electric power production by 2040 [5].

The mainstream PV cells today have an efficiency around 20 % and the efficiency is projected to raise to 22 % within the next 10 years [6]. To increase this efficiency, further research is needed. In addition to increasing the efficiency of the cells, it is important that the efficiency do not fall dramatically during the lifetime of the solar cells. In 2012, an effect that substantially lowers the the solar cells efficiency was detected by Ramspeck et al. [7]. In 2015 it was detected that this effect also were present in outdoor PV modules by Kersten et al., who named the effect *light*

and elevated temperature induced degradation (LeTID) [8].

At NMBU this defect has been studied in cooperation with a government funded research group called LeTUP. NMBU's contribution to the research group has been investigating LeTID with hyperspectral imaging [9]. The main goal of this thesis is contributing to the research on LeTID utilizing hyperspectral imaging. The thesis is supposed to contribute either by verifying already excavated results or find new results that can shed new light on LeTID.

The main goal was broken down to 4 sub goals. The first one is to find out more about hydrogens participation in LeTID. Results from many reports has pointed at hydrogen as a probable participant in LeTID [10] [11] [12]. Thus, a further exploration of hydrogens involvement in LeTID will be a contribution to the research of the domain. The second sub goal is to find out if, and how, the LeTID of a wafer is affected by the height in the ingot the wafer is cut from. It has been seen in research from Søndenå et al. [13] and Petter et al. [14] that a wafer's height in the ingot is of importance to how much the wafer is affected by LeTID. Therefore this thesis aims to explore this phenomenon.

Sub goal number three is to find a defect related luminescence (DRL) signal that can be tied to the LeTID. If a DRL signal is significantly increasing when the samples is degraded, and significantly decreasing when the samples regenerate, it will be plausible that this signal can be tied to the mechanism causing LeTID. If such a signal should be found it would be of great significance to the further research of LeTID. The last sub goal is to set the results of this thesis into context with the already existing research on the subject, and perhaps refute or strengthen already existing theories. The goals of this thesis is listed below.

The main goal of this thesis is as following:

- Contributing to the research on light and elevated temperature induced degradation (LeTID) utilizing hyperspectral imaging.

The sub goals leading up to the main goal of this thesis is:

1 Gain a deeper understanding of hydrogens participation in LeTID.

2 Investigating if, and how, a wafer's development of LeTID is affected by the height in the ingot it is cut from.

3 Find a defect related luminescence (DRL) signal that can be tied to the

LeTID effect.

4 Tie the results of this study to already existing theories.

Chapter 2

Theory

The theory chapter will explain the necessary theory to understand what is done in this master's thesis. The chapter will start by explaining how solar cell technology works. It will then continue with an explanation of recombination and the different recombination mechanisms in silicon solar cells. After that an explanation of photoluminescence will be given both band-to-band photoluminescence and defect related luminescence. Then a basic explanation of the hyperspectral image will be given, before the chapter is rounded off with theory about foreign elements and defects in silicon wafers.

2.1 PV Technology fundamentals

PV technology is based on fundamentals from semiconductor physics. This section will discuss some of them. The section will explain semiconductors, intrinsic and doped semiconductors, the band gap and the pn-junction. The theory of this section and the section about recombination is taken from [15], if no other reference is cited.

2.1.1 Semiconductors

Semiconductors are materials that have conductivity between conductors and insulators. There are in general two types of semiconductors, single-crystal and compound. Both types of semiconductors may be used in solar cells, two expamples

of single-crystal materials are silicon and germanium, and two examples of compound materials are gallium arsenide and cadmium telluride [16]. The samples investigated in this thesis are made of crystalline silicon and the rest of this section will focus on crystalline silicon.

Silicon Semiconductors

Silicon is element number 14, which means it has 14 electrons and 14 protons. Two of the electrons are in the 1. shell, eight are in the 2. shell and four are in the 3. shell. The electrons in the 1. and 2. shells are tightly bound to the silicon atom, but the four electrons in the 3. shell are more loosely bound. These four electrons are called valence electrons and are more interactive. In a silicon crystal each silicon atom is bonded with four other silicon atoms. They are bonded through covalent bonds between the valence electrons as shown in fig 2.1.

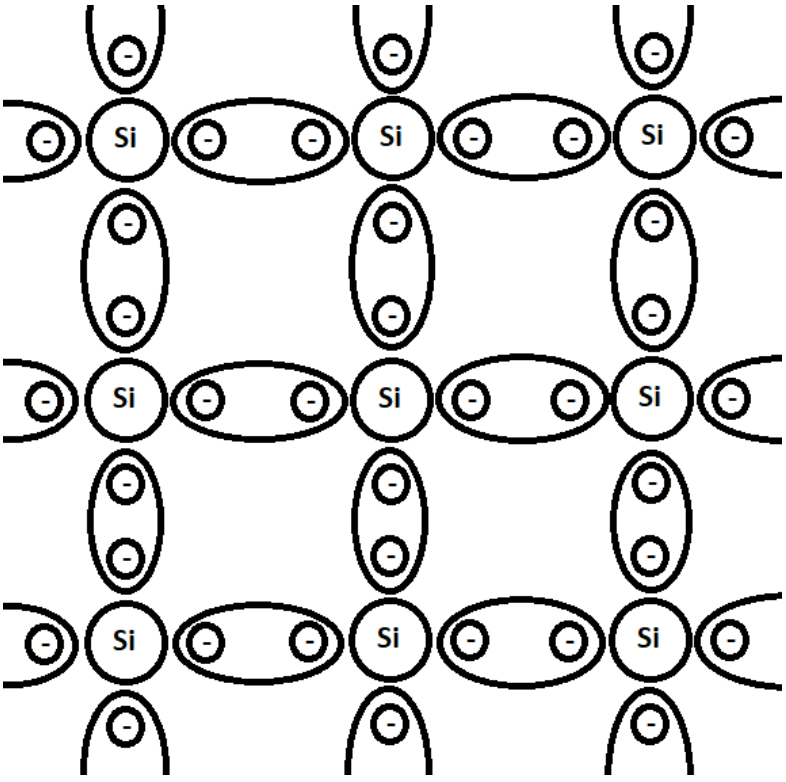

Figure 2.1: Illustration of a silicon crystal lattice. The figure shows the silicon atoms and the covalent bonds between the valence electrons. The figure is inspired by Boylestad et al. [16].

The bonds to the neighbouring atoms are equally long and the angle between them is 109.5°, together they form a lattice. The atoms in the lattice share valence electrons within the covalent bonds and by these bonds the electrons are bound thighter to their parent atoms. Despite this, if the valence electrons are added sufficient energy they break free from their bond and become free electrons. Free electrons are electrons in the silicon lattice that can drift with applied electric fields and diffuse with regard to consentration.

When the temperature is equal to 0 K there are no free electrons within the silicon lattice, but as the temperature increase more valence electrons are excited. At room temperature there are 1.5 x 10^{10} free electrons per cubic centimeters in silicon crystals. These free electrons are called intrinsic carriers as they are the materials natural charge carriers without external modification or influence. The concentration of silicon atoms in a silicon crystal is approximately 5 x 10^{22} cm^{-3}. Thus the value of intrinsic carriers is negligible. This makes intrinsic silicon a poor conductor, as there are few electrons that can move within the lattice. To create more free charge carriers the material can be doped.

Doped Silicon Semiconductors

Doping of crystaline silicon is replacing some silicon atoms in the lattice with other elements. There are two types of doping, n-type and p-type. For n-type doping, some silicon atoms are replaced by atoms of an element with one more valence electron than silicon, normally phosphorus. These new atoms are called donors as they create four covalent bonds with the silicon atoms around them, but still have one excess electron that cannot form bonds with any other atom. These excess electrons are loosely bound to the donor atoms and are thus likely to be excited to free electrons. p-type doping is the opposite of n-type doping. In p-type doping atoms with one less valence electron are added to the silicon lattice, normally boron. These atoms are called acceptors as they form covalent bonds with three neighbouring silicon atoms, but to make the fourth bond they have to accept electrons from an atom nearby. In room temperature the thermal energy in the lattice may enable an electron to shift from one bond to another, this creates a hole. A hole is a positive charge that comes from a lack of electrons. When a semiconductor is doped, the charge carrier concentration can be increased from negligible to values that greatly increases the conduction ability of the semiconductor. Typical levels of doping span from low doping around 10^{12} cm^{-3} to heavy doping around 10^{20} cm^{-3}.

When an electron connects to the acceptor atom the acceptor atom with its electrons

becomes negatively charged, but the silicon atom the electron left becomes positively charged. Thus the net charge remains neutral, but an acceptor atom creates a lower concentration of electrons that attracts electrons that wants to even out the concentration difference. In n-type doping the net charge also remains neutral. Because, when the excess electron is excited from the donor atom the donor atom becomes positively charged, and a negative charge follows the electron as it bounces around. Thus doping does not cause net charge of either negative or positive values. Doping creates a concentration difference that causes charge carriers to diffuse in the lattice to even it out, and this diffusion creates local net charges. This is made use of in the pn-junction which is the key to generating electric power from a solar cell.

2.1.2 pn-junction

The pn-junction creates the electrical potential in a photovoltaic cell. A pn-junction is formed when a p-type semiconductor and a n-type semiconductor are next to each other. The difference in electron concentration causes electrons to diffuse from the n-type semiconductor to the p-type semiconductor, and holes to diffuse in the opposite direction. This diffusion generates differences in electric charge as the n-type semiconductor now has more protons than electrons and the p-type semiconductor has more electrons than protons. This creates an electric field, which drags the electrons and holes in the oppsite direction of the concentration gradient. The system reaches an equilibrium when the force on the electrons from the electric field is equally big and in opposite direction of the force from the concentration gradient.

When the equilibrium is reached, there has been generated a depletion region in the interface between the two semiconductors. In this region the charge carrier concentration varies. The charge carrier concentration difference within this depletion region raises an electric potential across it, which makes it possible to generate electric power under illumination. A simple illustration of the charge carrier distribution and electric potential across a photovoltaic cell can be seen in figure 2.2.

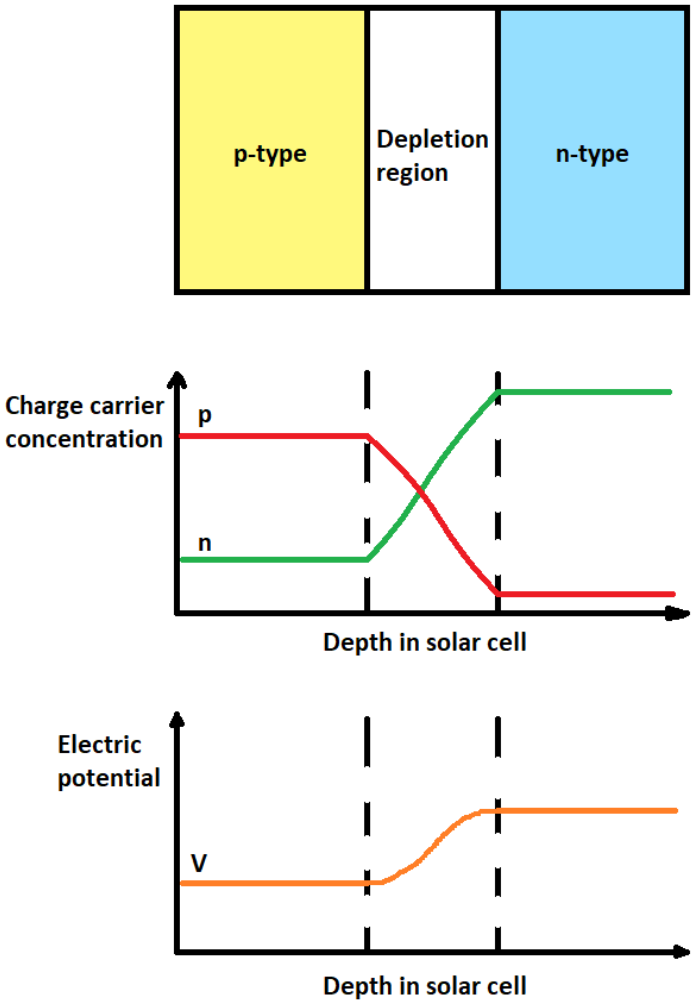

Figure 2.2: Simple illustration of the distribution of charge carriers and electric potential through the depth of a solar cell. p is concentration of free holes, n is concentration of free electrons and V is the electric potential. The figure is inspired by Smets et al. [15].

2.1.3 Bandgap

The electrons of an atom has certain energy levels they can occupy. When electrons orbits an atom, they will be in certain shells. Each shell has a discrete energy value associated with it, and the values for all the shells makes up the allowed energy values for the atoms electrons. When atoms are organized in a crystal lattice, the interaction between the atoms will cause a slight shift for each atoms energy levels.

As a result of this the electrons in a crystal lattice can occupy a lot of different energy levels that are very close to each other. This creates a band of continuous energy values the electrons can occupy instead of some discrete values. Thus, the valence electrons of crystaline silicon will have occupy an energy level within an energy band, called the valence band. For the valence electrons to become free electrons, they need sufficient energy to lift them from the valence band to a valid energy level for a free electron. This set of valid energy levels for free electrons is called the conduction band. The electrons cannot occupy energy levels that lay between the valence and the conduction band. This gap of invalid energy levels are called the bandgap, and equals the energy a valence electron needs to receive to be excited [16]. For crystalline silicon at room temperature this bandgap, E_g, is 1.12 eV. In a solar cell extra electrons are excited from the valence band to the conduction band by photons, illustrated in figure 2.3.

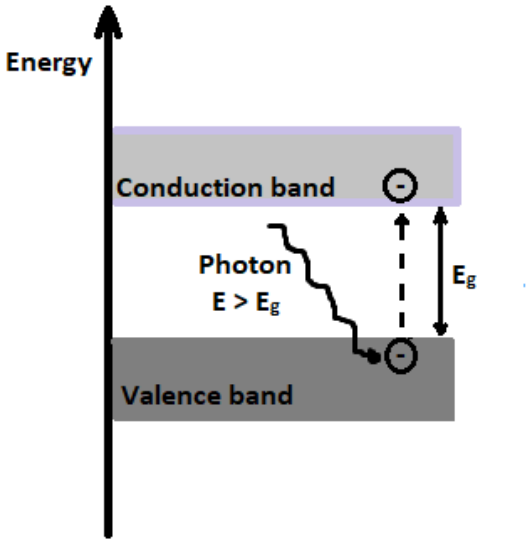

Figure 2.3: Illustration of the bandgap and how a photon with higher energy than the bandgap is exciting an electron. The figure is inspired by Boylestad et al. [16] and Smets et al. [15].

The illustration in figure 2.3 displays the simple idea of the bandgap, but the real bandgap is not that simple. The figure only takes energy into account, but allowed energy levels also depends on momentum. The allowed energy levels of the electrons vary dependant on their momentum. Thus, the top line of the valence band and the bottom line of the conduction band is a function dependent on momentum. The valence band might have a top that aligns with the bottom of the conduction

band, but that may also not be the case. When the top and the bottom aligns the semiconductor is a direct semiconductor, and when they do not it is an indirect semiconductor. Crystalline silicon is an indirect semiconductor. Which means, for the electrons to be excited they do not only need to be provided energy, they will also need a shift of momentum. While the electrons can be given energy when they interact with a photon, a shift of momentum is provided by interaction with phonons. Phonons comes from vibrations in the crystal lattice and are a quantized form of the lattice vibrations. Since electrons in an indirect semiconductor needs to interact with both a photon and a phonon to be excited to the conduction band, they are less likely to become excited than the electrons in a direct semiconductor. This leads to a lower electron current and is also important when we later discuss recombination mechanisms. The bandgap of direct and indirect semiconductors are illustrated in figure 2.4.

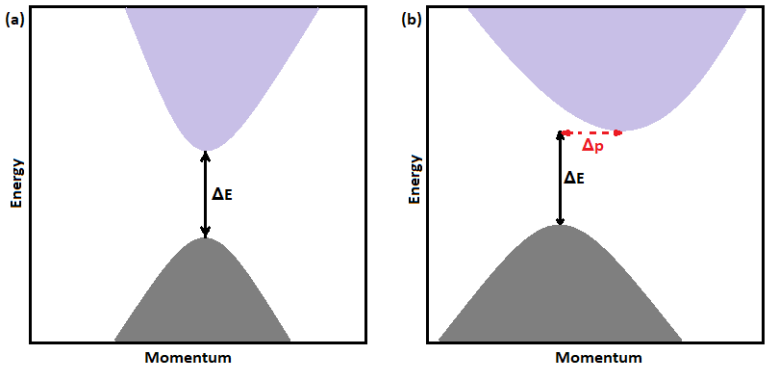

Figure 2.4: The figure shows the difference between a) the valence and conduction band of a direct semiconductor and b) the valence and conduction band of a indirect semiconductor. The figure show the differnce in energy, E, and the difference in momentum, p, between the top of the valence band and the bottom of the conduction band. The figure is inspired by Smets et al. [15].

2.1.4 Illumination of the solar cell

When a solar cell is illuminated, additional electrons are excited from the valence band to the conduction band by photons with higher energy than the bandgap. The excitation of electrons creates electron-hole pairs, which is one free electron and one hole, as a hole is generated whenever a free electron is generated. This extra generation of electron-hole pairs increases the concentration of minority carriers, which is the least present charge carrier in each region, electrons for the p-type

region and holes for the n-type region. As the minority carrier concentration increases in the n-type and p-type region, a new quasi-equilibrium enforces itself as minority carriers constantly diffuse across the depletion region. When an outer circuit is connected to the solar cell, a portion of the photogenerated electrons may flow through this instead of the depletion region to recombine with a hole. These electrons generates electric power.

2.2 Recombination and photoluminescence

A solar cell is not able to convert all the energy of the solar irradiance into electric energy. Some of the losses comes from the leak current across the depletion region, and some occures as a result of the solar cell not being able to make use of the excess energy of photons with more energy than the bandgap. Other losses comes from the solar cell not being able to convert the energy of photons with lower energy than the bandgap. Of these loss mechanisms, the two latter is impossible to do anything about in simple silicon solar cells, while the first one will not be discussed in this thesis. One portion of the energy losses that are important when improving solar cell technology is the losses caused by unwanted recombination.

When electrons goes through the outer circuit from the p-type region to the n-type region it recombines with a hole, and evens out the local net charge. This is the kind of recombination that is wanted in a solar cell as the electron has passed through the outer circuit, but the electron may also recombine before its energy can be utilised in the outer circuit. This is unwanted recombination, and the different types of recombination mechanisms will be explained in this section. When an electron of higher energy recombines with a hole of lower energy, one photon with the energy of the discrepancy between them is released. Thus, a solar cell will radiate photoluminescence. Photoluminescence will also be explained later in this chapter.

2.2.1 Minority carrier lifetime and recombination mechanisms

An important measure in solar cell physics is the *minority carrier lifetime*, τ_{eff}. The minority carrier lifetime is a measure of how long a minority carrier, either an electron or a hole, exists before it recombines. It can be compared with the lifetime of a radioactive particle and describes how long an electron or hole on average will

take to recombine after excitation. It has been shown that the efficiency of a solar cell depends on the minority carrier lifetime. This follows from the open circuit voltage being dependent on the minority carrier lifetime as shown in equation 2.1, and the efficiency of the solar cell depends linearly on the open circuit voltage, shown in equation 2.2. In equation 2.1 V_{oc} is the open circuit voltage, k_B is the boltzmann constant, T is the temperature, G_L is the rate of which free electrons are generated and n_i is the intrinsic density of charge carriers. For equation 2.2 η is the efficiency of the solar cell, which means how much of the incident energy the solar cell converts to electric energy. J_{sc} is the short circuit current of the solar cell, V_{oc} is again the open circuit voltage of the solar cell and FF is the fill factor which gives the portion of losses a solar cell has because of its operating point of voltage and current. P_{in} is the power irradiated onto the solar cell. The equations 2.1 and 2.2 shows that higher minority carrier lifetime will lead to a higher efficiency and a low lifetime will lead to a lower efficiency.

$$V_{oc} \approx \frac{2k_BT}{q} \ln\left(\frac{G_L\tau_{eff}}{n_i}\right). \tag{2.1}$$

$$\eta = \frac{J_{sc}V_{oc}FF}{P_{in}}. \tag{2.2}$$

The minority carrier lifetime is inversly proportional to the total recombination rate. The total recombination rate is the sum of the recombination rate of each recombination mechanism. And each recombination mechanisms recombination rate is inversly proportional to the lifetime of the minority carrier with regard to that recombination mechanism. This leads to the invers of the minority carrier lifetime to be the sum of the invers of the lifetime related to each recombination mechanism. This is given in formula 2.3:

$$\frac{1}{\tau_{eff}} = \sum_i \frac{1}{\tau_i}. \tag{2.3}$$

Where τ_i the minority carrier lifetime related to an arbitrary recombination mechanism.τ_{eff} is the total minority carrier lifetime of the solar cell. τ_{eff} depends mainly on the 4 main recombination mechanisms in solar cells: direct recombination, Shockley-Read-Hall (SRH) recombination, Auger recombination and surface recombination. An equation like this also indicates that the τ_{eff} never is higher than any of the individual recombination mechanisms lifetime. Thus,

the recombination mechanisms that has the lowest individual lifetime is of most importance. Which one that is will vary with the characteristics of the solar cell.

Direct recombination

As electrons are excited from the valence band to the conduction band they can also be deexcited, relaxed, from the conduction band to the valence band. This is called direct recombination and occurs when an electron in the conduction band recombines directly with a hole in the valence band. This process is illustrated in figure 2.5a). This recombination is most common in semiconductors with a direct bandgap, as the electrons then can recombine by releasing only a photon and do not need to have a shift of momentum. As the samples of this thesis are made of silicon this recombination mechanism is not that important for the minority carrier lifetime, because silicon has an indirect bandgap.

Shockley-Read-Hall recombination

Shockley-Read-Hall (SRH) recombination is recombination through energy levels in the bandgap created by metal impurities or lattice defects. This can be seen in figure 2.5b). A metal atom in the silicon lattice is called an impurity, as it creates allowed energy states for the electrons and holes within the bandgap. The allowed energy states are called traps, and the traps facilitates recombination of electrons and holes. Recombining via a trap is easier than directly over the bandgap as lower change of energy is needed to access them, rather than going directly from the conduction band to the valence band. SRH recombination is typically non-radiative, which means that typically no photons will be released when an electron hole pair regenerates by this mechanism. Although it is typically non-radiative the energy loss from this mechanism may be released as photons which will generate photoluminescence signals that will be discussed later in the theory.

Auger recombination

Auger recombination is in contrast to direct recombination and SRH recombination a three particle process. In Auger recombination an electron in the conduction band is relaxed by giving energy and/or momentum to another electron in the conduction band, before it recombines with a hole in the valence band. It can also

happen through a hole being excited after receiving energy and momentum from another hole in the valence band. Both these processes is illustrated in figure 2.5c). In neither of the cases a photon is released as the change of energy is deposited in the third particle, which either in the electrons case is excited to a higher level in the conduction band or in the holes case is relaxed deeper into the valence band. The energy of the electrons is then normally dissipated in the lattice, while the holes normally regains the energy from the lattice. Despite this, it has been shown by Hangleiter et al. that these particles may recombine directly with either an electron or a hole with participation of a phonon. If such recombination occurs, a photon with energy slightly lower than twice the bandgap is released [17].

Surface recombination

While the three recombination mechanisms mentioned earlier has been mechanisms that are active inside the bulk, the last one is surface recombination. The surface recombination are similar to the SRH recombination as the imperfect lattice on the surface creates traps inside the bandgap. The atoms on the surface are unable to connect to another atom to create a covalent bond with the last electron, which creates what is called *dangling bonds*. These dangling bonds on the surface creates multiple trap states which makes it easy for electrons to recombine with holes. Surface recombination can to a high degree be avoided by surface passivation. Surface passivation is done by adding a layer on to the surface with atoms that connects to the dangling bonds. The samples in this thesis are surface passivated, and therefore surface recombination is not of great importance to these samples. An illustration of surface recombination can be seen in figure 2.5d).

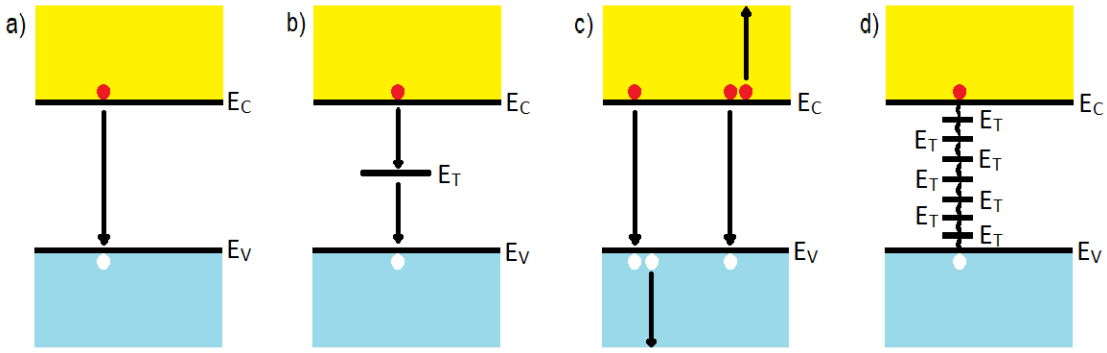

Figure 2.5: Illustration of the four recombination mechanisms a) direct recombination, b) SRH-recombination, c) Auger rebombination and d) surface recombination. E_C is the energy level at the bottom of the conduction band, E_V is the energy level at the top of the valence band and E_T is the energy level of the traps created by defects. The red dots illustrates electrons, while the white dots illustrates holes. The figure is inspired by Smets et al. [15].

2.3 Photoluminescence

As mentioned earlier in this chapter, often when an electron recombines with a hole a photon is released. This is called radiative recombination, as photons are radiated from the semiconductor because of it. The energy of the photons corresponds to energy discrepancy between the electrons energy before the recombination and the electrons energy after the recombination. When a solar cell is illuminated by a laser with photons of higher energy than the bandgap, as in this experiment, such recombinations are extensively happening in the cell. The radiation of photons from the solar cell when excited by photons from a laser is called photoluminescence (PL) [18].

2.3.1 Band-to-band photoluminescence

When an electron recombines over the bandgap the released photon will have energy equal to the bandgap. The resulting band-to-band (BB) photoluminescence, is in this thesis referred to as the BB-signal. For crystalline silicon the BB-signal has an energy level of 1.10 eV at 90 K. The BB-signal will also have phonon replicas

in the area around 1.05 eV [18]. A solar cell that mainly radiates a BB-signal when illuminated by a laser will be of high quality and have few impurities. As more impurities would lead to more electrons being relaxed by releasing smaller amounts of energy as photons and phonons. Thus a high BB-signal indicates less recombination through the other recombination mechanisms. Which again indicates a high lifetime, which indicates an efficient cell.

2.3.2 Defect related luminescence

Photoluminescene related to defects in silicon crystals was first detected in 1976, by Drozdov et al. [19]. In this study it was discovered 4 defect related luminescence (DRL) signals, by introducing dislocations into silicon. The four DRL signals were called D1, D2, D3 and D4. The signals' peaks at 4.2 K were found to be: D1: 0.812 eV, D2: 0.875 eV, D3: 0.934 eV and D4: 1.000 eV. Subsequent of this report a lot of research has been done and other signals have been found. These signals include D07: 0.68-0.78 eV and D5: 0.826 eV at 16 K [20]. The D3 and D4 signal has been linked together and are suspected to have the same origin, and the same is the case for the D1 and D2 signal. It has also been shown that a signal can be extracted from the D3/D4 region called VID3, very intense D3 [21]. Despite all the research in the area of DRL it has proven hard to tie any specific defects to the different DRL signals. This has led to a lot of different explanations for the different signals [22], and this makes it hard to identify a specific defect from a PL signal. The DRL signal will increase with lower temperatures, as the phonon activity will decrease, and thus more SRH recombination will be radiative [23]. This also leads to better images in general as low phonon activity sharpenes the signals of the PL-spectrums.

2.4 Light and Elevated Temperature Induced Degradation

In 2012, Ramspeck et al. presented a discovery of an unexpectedly strong light induced degradation (LID) in mc-silicon PERC solar cells [7]. This strong degradation was present when the samples where illuminated at temperatures higher than 50 °C. The degradation effect was later named light and elevated temperature induced degradation (LeTID) by Kersten et al. in 2015 [8]. In this article it was proven that the degradation was present in solar cell modules outdoor aswell as in

the laboratory. Kersten et al. detected degradation of efficiency above 10 % and later studies have shown relative efficiency loss of 20 % due to LeTID [24]. It has in later years also been shown that LeTID is not exclusive for mc-silicon, but it is believed to be an effect affecting all silicon solar cells [12]. Although it was shown already in the article by Kersten et al. that the LeTID effect could be avoided by special engineering the solar cell, there was a need for a greater understanding of the underlaying causes to LeTID.

The development of LeTID is a rapid degradation followed by a slow regeneration [25]. The degradation will in a laboratory with temperatures around 100 °C and illumintation of 1 sun typically take somewhere around 24 h and the regeneration some days [24]. This varies a lot with temperature and illumitnation, and in a lab with high temperature and illumination the entire process can be done in under 24 h [26]. Outdoors the process is way slower and it may take a few weeks for the solar cells to degrade and years to regenerate [8].

It has been shown that the LeTID effect cannot be explained by the BO-LID process [8], which is a light induced degradation due to formation of boron-oxygen complexes. This is a known and understood degradation mechanism that happens only by illumination and not elevated temperatures, and has been shown to decrease the efficiency up to 2 % [27]. Neither can it be explained by FeB separation, which also is a known process behind LID [8].

Søndenå et al. presented an article in 2019 that showed a variation of LeTID with regard to the wafers height in the ingot [13]. Petter et al. saw a reduction of LeTID towards the top of the ingot, but they did not see an increase in LeTID when they trippeled the boron concentrion in 2016 [14]. In 2017 Luka et al. saw that the LeTID occured rather homogeneously in a solar cell, but structural defects such as grain boundaries was less affected by LeTID. The study also indicated that at least one of the fast diffusers, Cu, H, Ni and Co, was involved in the LeTID [24].

In the most recent years there have been more and more articles relating the LeTID effect to hydrogen [12]. One theory proposed by Bredemeier et al. suggests that the degradation is caused either by Ni or Co, and the regeneration is caused by hydrogen diffusing from the surface to the bulk to passivate these [28]. Another theory by Chen et al. suggests that the LeTID effect is caused by migrating hydrogen atoms that interact with the dopant atoms. Chen et al. also observed a surface degradation after the regeneration process and proposed that this could be caused by the hydrogen migrating towards the surface, as they postulated that the pn-junction repels hydrogen [12].

2.5 Hyperspectral imaging

To study the LeTID-effect it was in this thesis made use of hyperspectral imaging. In RGB-images, normally referred to as colour pictures, there are two spatial dimensions and in addition to them there is one colour dimension. This is because RGB-images consists of three images one red, one green and one blue. A hyperspectral image also has a "colour dimension", called the spectral dimension. Instead of different colours the spectral dimension consists of different wavelengths. A hyperspectral camera detects up to hundreds of different wavelengths, and creates a continuous spectrum for each pixel [29]. A hyperspectral image will have three dimensions two spatial and one spectral, as is depicted in figure 2.6:

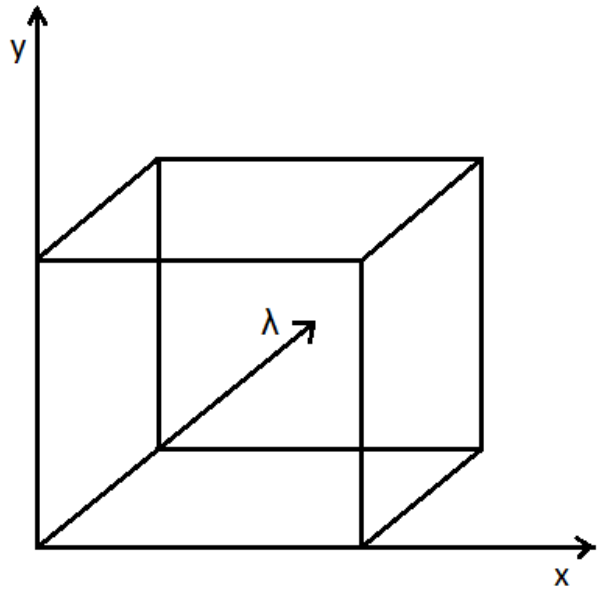

Figure 2.6: Illustration of the three dimensions of the hyperspectral image and the hypercube. Where the x and y axis are the spatial dimensions and the λ axis is the spectral dimension.

The three dimensional image of a hyperspectral carmera is called a hypercube. The hypercube can be assembled in different ways depending on which type of hyperspectral camera is used. In this thesis a line-scan camera was used. A line-scan camera assembles the hypercube by scanning lines of the sample. When one line

is scanned the camera makes a spectra for every pixel of the scanned line. All the spectras makes up a 2D-matrix with the spatial value along the line on one axis and the wavelengths on the other axis. The camera scans lines until it have covered the entire sample and puts the 2D-matrices together to a cube. The cube consist of values that are linear with the number of photons it has detected for every pixel and every wavelength. If we name the cube X, $X(x, y, \lambda)$ will have a value that describes how many photons of a wavelength λ the camera detects in pixel (x, y). Thus a hyperspectral image explains what kind of and how many photons a sample radiates, and also the spatial distribution of them [29]. This has a broad application, e.g. in agriculture and food industry [30] and in recent years also in studies of solar cells and wafers [22] [18].

2.6 Foreign elements and defects in silicon wafers

Defects in silicon materials, such as impurities, affect the properties of the material [31]. Some typical impurities in solar cells are iron, aluminium, copper, tin, cobalt, nickel, cadmium, titanium, gold, zinc, lithium, silver, germanium, antimony, chromium and oxygen [32], but impurities are not limited to these. Impurities limits the minority carrier lifetime, as they create recombination centers [31]. In solar cells this is not wanted as it is important to maintain a high minority carrier lifetime. Impurities and dopant atoms varies with the height of the ingot. The concentration of different elements follow equation 2.4, called the Scheil equation [33]:

$$C_s(x) = k_{eff} C_0 (1 - x)^{(k_{eff} - 1)}. \tag{2.4}$$

In this equation $C_s(x)$ is the concentration of the element at height x, C_0 is the initial concentraion of the element in the melt and k_{eff} is the effective segregation coefficient. The effective segregation coefficient varies with a lot of variables and varies from element to element. If the effective segregation coefficient is below 1 the element concentration will be higher at the top of the wafer and if the effectiv segregation coefficient is higher than 1 the concentration of the element will be higher towards the bottom. For the dopant atoms phosphorus, boron and gallium the value is below 1, which means that the level of doping will raise towards the top of the ingot. The concentration raise is slow in the bottom of the ingot, but rapid in the highest 20 % [33]. Except for oxygen all the impurities mentioned above has an effectiv segregation coefficient under 1, which means that they also accumulate

towards the top of the ingot [32].

For multicrystalline silicon, which is the material used for the samples in this thesis, the main crystal defect is dislocation clusters. A dislocation cluster is a network of sub-grain boundaries, which is a smaller version of a grain boundary situated within a grain. The dislocation clusters significantly lowers a solar cells efficiency [34]. The effect of a dislocation cluster on a solar cells efficiency varies a lot. It has been seen in experiments that the negative effect of dislocation clusters that are highly decorated with metal impurities are much bigger than for dislocation clusters that are not. In fact, clean dislocation clusters has shown little or no effect on the cells efficiency. Thus, it is believed that the negative effect of a dislocation cluster mainly originates from the metal impurities that decorates it [35]. Some elements of the dislocation clusters, such as kinks, are known to be electrically active and will interact with metal impurities in the bulk [36]. The dislocation clusters size and occurrence varies with the height in the ingot [37].

Hydrogen are now commonly used to passivate defects in solar cells and hence increase performance. It is used for surface passivation as the hydrogen atoms can connect to the dangeling bonds to passivate their energy levels within the bandgap. This is done by coating the wafers with hydrogenated dielectrics. It is also common to infuse hydrogen into the bulk. This is done by coating the wafer with hydrogenated dielectric layers, followed by a firing process. The firing causes the hydrogen atoms to diffuse into the bulk. Inside the bulk the hydrogen passivate defects. Hydrogen has been a major factor in the improvements of the solar cell efficiency, but its properties in the silicon is still not fully understood [38].

Chapter 3

Methodology

This chapter aims at descriping the samples used in this experiment, how they were processed and how they were taken images of. It will give an in-depth explanation of the equipment and methods used in the hyperspectral imaging. The chapter will also explain the methods used in the data analysis.

3.1 Samples and sample processing

The wafers studied in this thesis are boron-doped multicrystalline Passivated Emitter and Rear Cell (PERC) wafers. This type of technology is amongst the high performance multicrystalline silicon (hpmc-Si) types. The samples were cut from 10 different wafers, among which five were treated with phosphorus diffusion gettering (PDG) and five were treated with phousphorus diffusion gettering and hydrogenation (PDGH). The different treatments will be explained in the pre-processing section. The five PDGH-treated wafers were from different heights within the same ingot, the same was the case for the PDG-treated wafers. From each of the wafers used in this study, there were made two samples of size 50mm x 50mm. The samples were cut with a laser cutter, by Rune Søndenå at IFE, the Norwegian Institute for Energy and Technology. From each wafer maximum one sample was used in the experiment and the other one was kept as safety, in case there would be problems during the experiment that would necessitate a repetition of the experiment. A picture of the eight samples, which were used in this thesis, can be seen in figure 3.1. The picture is taken after the experiment was done, and one can see the bruises and contamination on the surface of the samples.

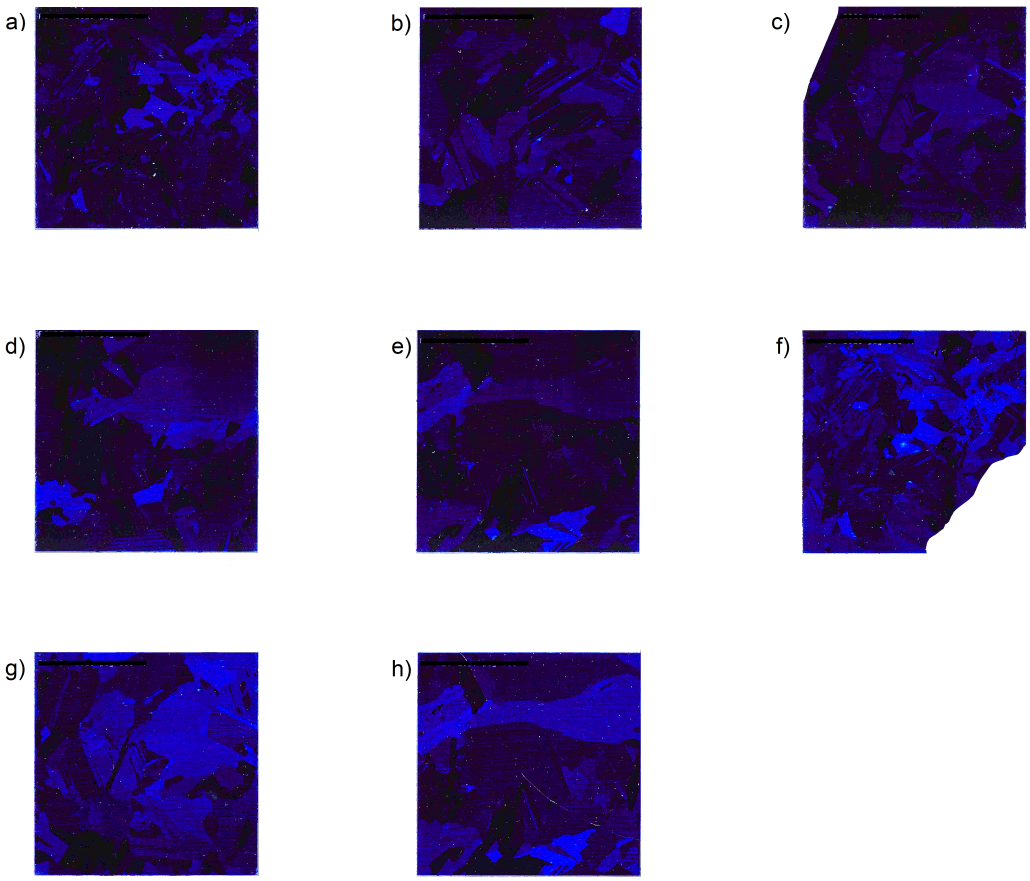

Figure 3.1: Picture of the samples a) sample 1, b) sample 2, c) sample 3, d) sample 4, e) sample 5, f) sample 6, g) sample 7 and h) sample 8. The full sample names were burned in on the samples' left corners. A black line coveres the names to protect the indentity of the manufacturer.

In table 3.1 it is given an overview of the different samples used in the experiment. They are numbered from 1 to 8 according to their preproccesing, the first five samples were PDGH treated and the last three were PDG treated. Within the different treatments they were numbered after their respective height in the ingot. The sample names consists of a number which indicates where in the ingot the sample's wafer are cut from. For example, if a sample name contain the number 001 that sample's wafer was cut from the bottom of the ingot, and 002 was the

Table 3.1: List of the samples used in this study.

Sample nr.	Sample name	Treatment	Height in ingot [%]*
1	007 A	PDGH	1
2	264 A	PDGH	29
3	391 A	PDGH	43
4	597 A	PDGH	65
5	894 A	PDGH	97
6	009 A	PDG	1
7	390 A	PDG	42
8	893 A	PDG	97

* The height in ingot is just a simple approximation that does not take into account the cut-off from the top and bottom it is simply appriximated by dividing the wafer number by the total number of wafers, which is 920. The approximation does not either take the kerf loss into account.

next one. As commented in the table the wafers height in the ingot is a plump approximation that does not take into account the top and bottom cut-off nor the kerf-loss. The kerf-loss is the loss of ingot due to the sawing-process [15]. This was done because both the kerf-loss and how much the manufacturer cuts off from the ingots top and bottom is unknown. The real percentage value of the wafer's height in the ingot would therefore be more squeezed as the top and bottom cut-off is not taken into account. Which means the wafers are closer to the middle than indicated in the simple approximation.

3.1.1 Pre-processing

The samples in this experiment underwent two different pre-processing treatments. The first set of samples in table 3.1, 1-5, went through phosphorus diffusion gettering and hydrogenation, PDGH. While the second set of samples, 6-8, only went through phosphorus diffusion gettering, PDG. The two pre-processing treatments are illustrated in figure 3.2. The pre-processing was done by Rune Søndenå at IFE.

In both cases of pre-processing the wafers were etched to remove the damages from the sawing, this was done with a HF:nitric acid:Acetic acid solution, called CP5. Then both groups were in-diffused with phosphorus from $POCl_3$ gas on both sides at approximately 830 °C, to create the emitter. This was done in a tube furnace.

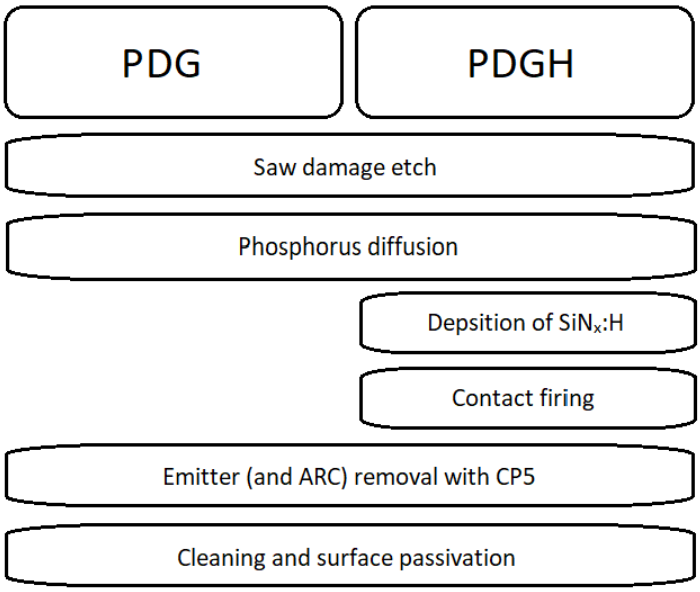

Figure 3.2: Illustration of the two different pre-processing treatments, PDG and PDGH. The figure is inspired by Adamczyk et al. [39] and Søndenå et al. [26].

After this the PDGH wafers were hydrogenated by deposition of a hydrogen rich SiN_x:H anti-reflective coating, ARC. This was followed by a simulated contact firing process to infuse the hydrogen, the temperature during the contact firing was up to 720 °C. After the hydrogenisation the PDGH wafers had a removal of the ARC and the emitter layers and the PDG wafers had a removal of the emitter layer. This removal was done in a CP5 solution. In the end all the wafers were cleaned and surface passivated. The surface passivation was done by depositing a stack of hydrogen rich amorphus silicon and SiN_x:H, followed by heating the wafers to 230 °C for 20 minutes. The pre-processing is close to that of a normal solar cell, but is done especially to study the bulk silicon PL signal development. It is the same treatment that has been used by Adamczyk [39] and Søndenå [26].

3.1.2 Processing

The processing of the samples in this experiment consisted of light soaking the samples to trigger the BO LID-degradation, and then expose the wafers to light

and elevated temperature. This was done with a solar simulator and heating plate. It was done to see if the PL-signal changed during the processing. Hyperspectral images was taken of the wafers continously throughout the experiment. These images was later analysed to see the treatment's effect on the wafers.

The solar simulator had a light spectrum of 1.5 AM (air mass). The light intensity was adjustable. First the wafers were lightsoaked for 66.5 hours at approximately 0.08 suns, which corresponds to a light intensity of $8\,\mathrm{mW/cm^2}$. After this the wafers were taken images of to see the degradation during the lightsoaking. Then the samples were put on a metal plate with a temperature of 100 °C and the light intensity was turned up to approximately 1 sun, $100\,\mathrm{mW/cm^2}$. There was a small difference of the illumination on the different samples as the illumination was not uniform. This difference was not more than .

The temperature and illumination of the treatment was chosen after investegation of the conditions used by Mehl et al. [9], Luka et al. [40] [24] and Søndenå et al. [26]. In the first article 1 sun of illumination was used by Mehl and since that experiment was done with the same equipment and by advice from Mehl it was decided to use an illumination of 1 sun. The temperature was harder to choose, because there was used several different temperatures in the articles. In one of the articles by Luka et al. [24] it was done a comparison between using 100 °C, 115 °C and 130 °C. At higher temperature the experiment consumes less time, but distinguishes less between the samples efficiency at full degradation and the efficiency after regeneration. It was therefore decided to use the lowest of the three temperatures, 100 °C. The temperature and illumination was verified, during the experiment by a termometer and a pyranometer.

After 2 hours of degradation with 100 °C and $100\,\mathrm{mW/cm^2}$ the degradation was interrupted to take new images of the samples. After the images was taken it was decided to raise the temperature to 115 °C. This was decided on the basis of a more thorough investigation of the article by Luka et al. [24]. It was seen that the difference between the top and bottom of the samples efficiency at 100 °C and 115 °C was small and amplifying the temperature would save a lot of time. After 4 hours of the new treatment new images was taken. During this imaging process the temperature of the metal plate was measured to 110 °C. It was than decided to use this temperature throughout the rest of the experiment.

The light and elevated temperature treatment was interrupted for imaging after (given in time treated after lightsoaking): 2h, 6h, 10h, 14h, 18h, 21.5h, 24.75h, 29.75h, 44h, 55h, 66h, 75h, 87h, 96h, 108h, 114.67h, 127.33h, 136.67h, 145.33h, 157.33h, 169.33h, 177.33h, 191.33h, 214.33h, 223.33h, 240.83h, 262.33h, 286.33h,

305.33h, 327.33h, 369.33h and 394.33h. The experiment was ended when the BB-signal of the samples started to fall for consecutive measurements after the samples had regenerated.

There were four accidents during the experiment. Before the experiment started a corner were knocked off sample nr. 6. Thus all the images of sample nr. 6 is without this corner. In the course of the imaging after 66 hours a corner broke off from sample nr. 3. The later images of sample nr. 3 is therefore without that corner, which necessitated to not use the entire area of the sample in later analysis. Sample nr. 8 broke in two before the imaging after 177 hours, and the later images of that sample is taken of the two bits put together. Figure 3.1 is a picture of the samples after the experiment was done, which displays the bruises of the different samples. There was also a power outage of approximately two hours during the degradation after the imaging at 286 hours. Thus, it is uncertan whether or not there was 19 whole hours of degradation between that imaging process and the next one. This is due to uncertainties regarding when the power was put on and how long the system used to stabilize again to 1 sun and 110 °C.

3.2 The hyperspectral imaging process

As described in the processing section hyperspectral images was taken througout the experiment, this section will explain the setup used for the imaging. The section will describe the methods of imaging and maintainance. The setup is heavily based on the setup used by Mehl in his doctoral thesis [18], and that thesis is also the main reference for this section.

3.2.1 The imaging setup

The setup used in this experiment is illustrated in figure 3.3. The setup consists of a hyperspectral camera and a line laser that are attached to a translation stage that moved to image the samples. The samples were contained on a cryogenic cooler and were covered with a cardboard that had an opening to let the laser beam through to excite them. The laser was also covered by a cardboard, which had a narrow slit to let the laser beam through. The camera lense was covered with a high pass filter that filtered out long wavelenghts.

The camera used in this experiment is a hyperspectral line scan camera from

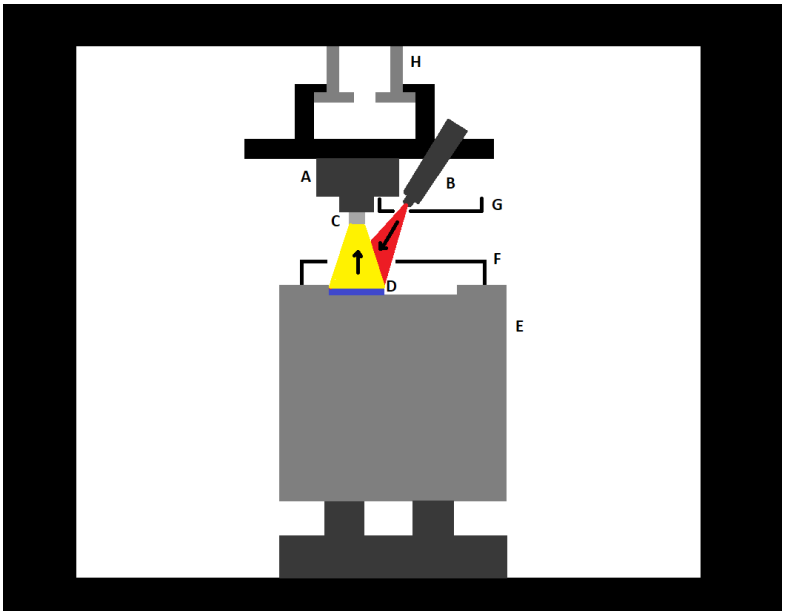

Figure 3.3: Illustration of the setup used to take hyperspectral images of the samples. A) camera, B) laser, C) long pass filter, D) sample, E) sample holder, F) cardboard to reduce fog over the sample, G) cardboard to reduce fog in front of the laser and H) translation stage.

Specim. The camera detects light from 929.11 nm to 2531.70 nm, these wavelengths lies within the near infrared (NIR) and short wavelength infrared (SWIR) part of the light spectrum. This means that the camera detects light within the energy intervall 0.4899-1.334 eV. An intervall that suits the purpose of this experiment well, as it contains the BB-signal and the known DRL-signals. The camera has 256 bands in the spectral dimension, the bands are not linearly distributed as the width of the bands vary from 6.32 nm for the shortest wavelength to 6.23 nm for the longest wavelength.

The camera has 320 pixels in the line it scans, the x-direction. And the number of pixels in the y-direction varies with: the spatial resolution in the scan direction, the framerate, the scanning speed and the length of the area that are scanned. For this experiment the spatial resolution was set to 100 µm in both spatial directions. For the x-direction this was done by adjusting the distance between the sample and the camera. For the y-direction the resolution was set by adjusting the scanning speed. This was done with respect to the relation between the resolution R, the scanning speed v_s, and the framerate F, given in equation 3.1:

$$v_s = R * F. \tag{3.1}$$

Since the framerate of the camera was at 25 Hz and the desired resolution was 100 µm, the scanning speed was set to 2.5 mm/s.

The laser used in this experiment is a line laser of the type Lasiris Magnum II, produced by Coherent. The wavelength of the laser is 808 nm which corresponds to each photon having an energy of 1.53 eV. An energy that is sufficient to overcome the bandgap of the samples. The laser beam is adjustable and has a maximum power of 5600 mW, in this experiment the power was fixed to 5.00 W.

The cameras detector is of the type mercury-cadmium-tellurid (MCT), and detects the amount of photons of different wavelengths. In front of the detector there is a dispersing element to separate the different wavelengths. This dispersing element will also cause the reflection of the 808 nm laser beam to create second and third order light maximas. The light of 808 nm will not be detected by the MCT-detectro, but the second order maxima of this light lies at 1616 nm and would normally disturb the signal from the samples. To avoid this signal disturbance, a long pass filter is placed in front of the camera. A long pass filter is a filter that lets light with high wavelengths pass, but blocks light of lower wavelengths. When this filter is placed in front of the camera the light of 808 nm is blocked. As a result of this no second order maxima is generated, and the disturbance of the signal is avoided. The long pass filter used for this experiment is a high performance long pass filter with optical density >= 4. The high pass filter blocks wavelengths beneath 1000 nm and was manufactured by Edmund Optics.

The sample holder used in this experiment is made at NMBU to hold solar cells and cool them to low temperatures. On the top of the holder there is plate of polished aluminium, the plate can hold samples up to a size of 156 mm x 156 mm. The rest of the holder is covered with extruded polystyrene foam for isolation to keep it cool. The spatial resolution of the images in this experiment was wanted to be 100 µm. To get the right resolution of 100 µm the height of the aluminium plate was adjusted with blocks underneath the holder and squares made of paper underneath the aluminium plate. There is a hole on the top of the holder where liquid nitrogen can be poured into a tank inside of it. The tank can hold 2 L of liquid nitrogen, and the tank needs to be full for the holder to reach the bottom temperature around 84 K.

3.2.2 Cooling of the samples

The container is cooled with liquid nitrogen to improve the images, which gets better when the samples have a lower temperature. This is explained in the theory chapter. The samples are cooled by the aluminium plate, which is cooled by heat sinks that goes into the tank containing liquid nitrogen. The samples are also cooled by small nozzels that are placed around the aluminium plate right above the top of it. From these nozzles cold nitrogen vapor flies out to cool the samples.

To fill the tank of the sample holder with liquid nitrogen two containers of 20 L was used. The holder needed to be filled regularly to ensure that it held a low temperature. When preparing the sample holder for imaging it was filled with liquid nitrogen some minutes ahead to let the temperature stabilize. When the imaging started the temperature ranged from 84 K to 85 K, and during the imaging which took about 1 hour the temperature would raise to about 89 K. This gives raise to some uncertainties when comparing the images, since the temperature is not constant during the process. This is though compensated for when comparing images of the same wafers, since the images of the same wafer is taken approximately the same time after the imaging started each time. When comparing between wafers this may impact the absolute values of the wafers, but when we compare the relative difference of the wafers this should be partly compensated.

There are also other uncertainties linked to the cooling and these uncertainties comes from frost and fog. When the holders temperature is in the range it is during this experiment, frost and fog are created on and around it. This causes the air over the samples to be hazy, and lowers the quality of the images. Although this is impossible to avoid there are taken measures to lower the negative effect of it. To keep the laser clear of the fog it is covered with a cardboard that only lets the laser beam through and not the fog. Over the aluminium plate there is also a cardboard to minimize the effect of the fog. The frost is also a problem as a layer of frozen dew continuously lays on the aluminium plate, and the samples when they are placed on it. If there are frozen dew between the sample and the aluminium plate the contact between them are weakened. This leads to a higher temperature on the samples when imaged, and therefore it is of high importance to remove the layer of frozen dew from the aluminium plate before putting on the samples. This was done with excess PV-wafers because they were thin enough to remove the layer entirely. If the frozen dew would not be removed the images would not be comparable. To minimize the amount of frozen dew accumulated on the aluminium plate between the imaging processes, a dummy wafer was put on top of the plate when it was not used. Although the dew was removed before the imaging, a new layer appeared

during it. This cannot be avoided, and since it is equal for every image there was not taken measures to deal with it.

3.2.3 Image aquisition

The imaging was done in two parts. First two and two samples was put down onto the aluminium plate and imaged. Then the samples was rotated 180°, layed onto the aluminium plate and imaged again. This was done because the camera only covered about 3 cm of the samples in x-direction with a spatial resolution of 100 µm. The camera has 320 pixels in the x-direction and around 20 pixels are lost because of the rim around the aluminium plate. Later the two different images of the samples will be refered to as the upside and downside of the same sample. Where the upside will be called eg. sample 1 and the downside sample 1D.

There was taken 4 images at a time of the samples. This was done so that later in the data processing phase the median of the three last images could be taken, and used. The samples was imaged two and two: 1 and 2, 3 and 5, 4 and 8 and 7 and 6. Before the imaging all 8 samples were moved from the solar simulator to a tissue paper. The samples laying on the tissue paper can be seen in figure 3.4. In figure 3.4 sample 5 lies on sample 4's place and vica versa, the same was the case for sample 6 and 8. This was due to an interchanging in the beginning of the experiment. The interchanging is the reason why sample 5 was imaged with sample 3, sample 4 with sample 8 and sample 7 with sample 6.

When the sample holder was filled with liquid nitrogen and the temperature had stabilized the dummy wafer was removed from the top of the aluminium plate. Then an excess wafer was used to remove all the frozen dew on the aluminium plate, before two wafers were putted on the plate. After this cardboard F from figure 3.3 was put on top of the holder to minimize the fog and all the light in the room was turned off. Then the camera scanned the two samples. When this was done the samples was moved back to the tissue paper and the process was repeated for the next wafers. This was repeated until all the samples had been scanned on both sides and then the samples was moved to the solar simulator. When the imaging process was finished frozen dew was removed from the aluminium plate, the dummy wafer was put on top of it and two plates of styrofoam was put on top of the holder. This was done to minimize the heat entering the holder and thus minimizing the consumption of nitrogen.

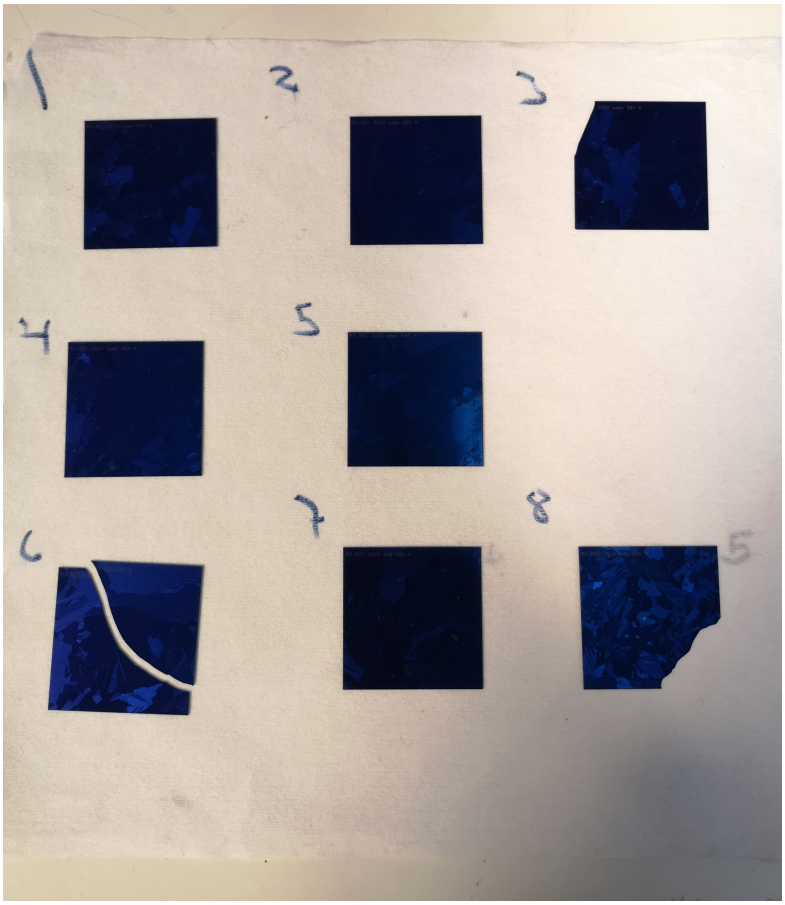

Figure 3.4: Picture of the samples on a tissue paper. During the experiment sample 4 and 5 was interchanged and so was sample 6 and 8. The picture is taken after the experiment was done and it shows how sample 3, 6 and 8 was shattered.

3.3 Data processing

Throughout the imaging phase the level of the BB-signal was tracked to know when the top of the regeneration was reached. This was done in Matlab and the script used for this is shown in appendix B. The track plot of the BB-signal for every samples' upsides can be seen in figure 3.5:

The signals in figure 3.5 were used to find the points of full degradation and full regeneration for every sample. The imaging was done without a reference sample. A reference sample is a sample with constant lifetime throughout the entire imaging process. It is imaged next to the samples and used to minimize

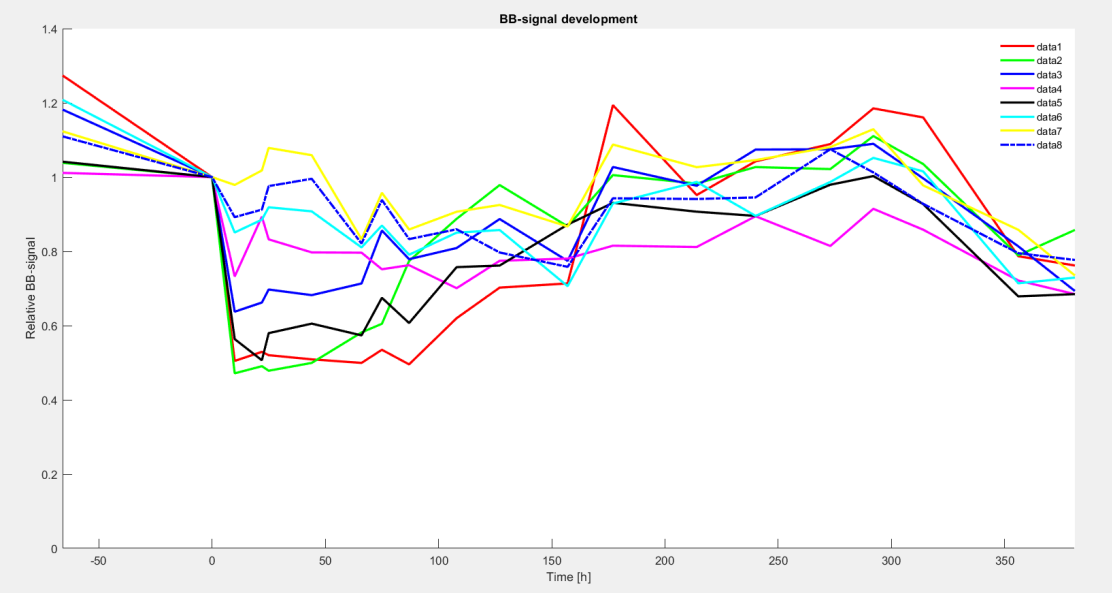

Figure 3.5: The plot of the BB-signal for all the samples' upsides. The curves are normalized with regard to the signal after light soaking. In this plot the signal for sample 4 is called data5 and sample 5 is called data4. Also sample 6 and 8 are interchanged. Otherwise the BB-signal of the samples are called: data[insert number of sample].

the uncertainties caused by the varitaion of external conditions for each image, like light contamination. This is done by normalizing each sample with respect to the reference sample. To compensate for this sample 7 was used to normalize the curves of figure 3.5. Sample 7 was used for this as it was the most stabile sample throughout the processing. Figure 3.6 shows the plot after the curves was normalized with regard to sample 7.

As it seemed unlikely that wafer 7 was sufficiently stabile throughout the experiment, the plots shown in figure 3.5 and 3.6 was used together to find points of full degradation and full regeneration for every sample. There was no clear top nor bottom for sample 4, 6, 7 and 8. For simplicity their times for full degradation and regeneration were set to the same as the most common value amongst the other samples. The time with treatment of illumination and elevated temperature that was selected as bottoms and tops for the samples are presented in table 3.2:

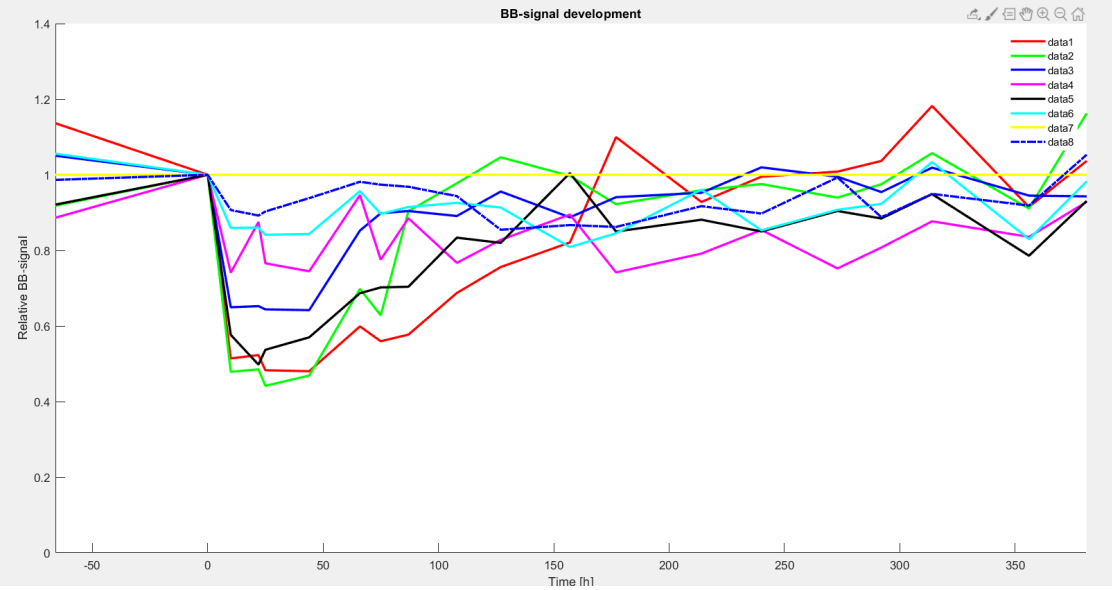

Figure 3.6: The plot of the BB-signal for all the samples, divided by sample 7's signal. The curves are also normalized with regard to the signal after light soaking. In this plot the signal for sample 4 is called data 5 and sample 5 is called data 4. Also sample 6 and 8 are interchanged. Otherwise the BB-signal of the samples are called: data[insert number of sample].

Table 3.2: List that shows how much time of treatment with illumination and elevated temperature the samples took to be fully degraded and fully regenerated.

Sample nr.	Fully degraded after [hours]	Fully regenerated after [hours]
1	25	292
2	25	292
3	22	240
4	22	292
5	22	292
6	22	292
7	22	292
8	22	292

A median image was made for each sample for the timesteps: initial, after light soaking, when fully degraded and when fully regenerated. The purpose of mak-

ing median images was to deal with uncertainties of each individual image, and specifically dead pixels. A dead pixel is created when the measurement of a pixel goes wrong and the value of that pixel is set to 0. The median image was made from the three last images out of the four that was taken by all the wafers at every timestep. The script used for this can be seen in appendix B.

The first step of the analysis was investigating the development of the spatial distribution of the BB-signal and the known DRL-signals. This was studied by generating images of each signal for all the samples and timesteps. The script used is shown in appendix B. Then the samples' spectral development was investigated by plotting the spectrums of every timestep for each sample. This script can be seen in appendix B.

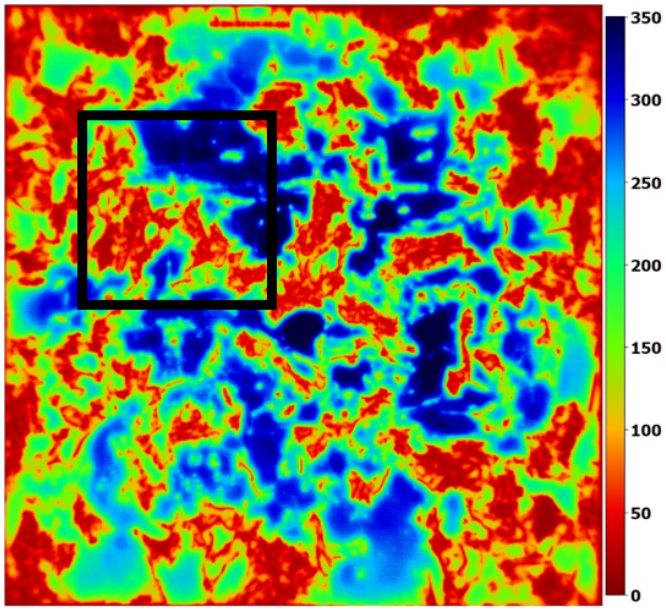

Figure 3.7: A photoluminescence image taken at IFE of sample 5's wafer. The black square marks approximately where the sample was cut from. The scale on the right side is in µs, and the pixel colour is given from the minority carrier lifetime in that pixel.

The generated images of the different signals was then used to find areas of interest from the samples. For example, this could be areas with a strong signal of any kind or areas with a distinct signal development. The images of the D3 signal was used together with BB photoluminescence images taken at IFE, by Rune Søndenå, to find dislocation clusters in the samples. At IFE it was used a uniform 808 nm laser to generate charge carriers, and a charge-coupled device (CCD) camera to detect the BB-signal. An example of these images can be seen in figure 3.7. In the

image the blue areas are areas with a high BB-signal and the red areas are areas of low BB-signal. The areas that are red in these images corresponds to a high degree with the areas of high D3 signal in the images taken in the study. The areas of low efficiency should be regarded as dislocation clusters. The dislocation clusters was then analysed in same way as the entire samples. The samples from furthest down in the ingot showed no dislocation clusters that were big and clear enough to be analysed. From all other heights there were found dislocation clusters that could be analysed in either the upside, the downside or both samples. Other than the dislocation clusters the areas of interest of other DRL signals, showed little significance when investigated closer.

As a last step of the analysis it was decided to look further into the relative development of the PL spectrums, because the spectrums were heavily dominated by the BB-signal. The spectrums were now normalized with regard to the initial PL spectrum, to show the development of the weaker signals. This was done by the same script as was used to investigate the spectrums, shown in appendix B.

Chapter 4

Results

This chapter will present the results of this study. Firstly, the spatial development of the BB-signal of the samples will be presented. Secondly, the spectral development of the wafers will be displayed. Then specific results of some dislocation clusters will be shown. In the end more results of the spectral development of the samples are presented, with a specially emphasis on the development of the DRL-signal.

4.1 Spatial BB-signal development

This section will present the spatial development of the samples BB-signal. First the results of the upside samples from lowest in the two ingots, of which one were hydrogenated and one were not, are shown along with the upside sample from second lowest in the ingot of the wafers that were hydrogenated. Then the results of the upside samples in the middle of the two different ingots are presented along with the upside and downside sample from second highest in the ingot of which wafers were hydronated. And lastly results of the upside and downside samples from highest in the two ingots are displayed.

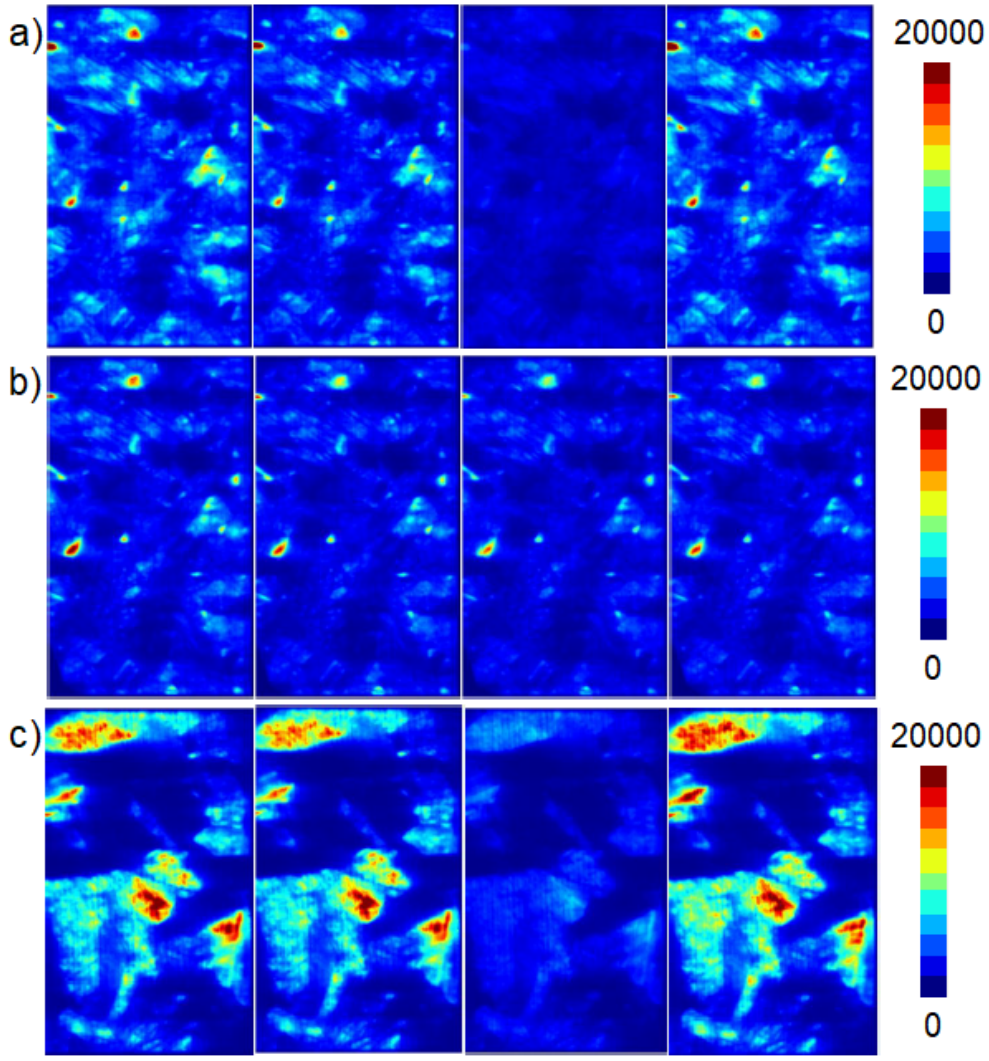

Figure 4.1: Spatial development of the BB-signal over time for: a) sample 1, b) sample 6 and c) sample 2. The images are from left the initial image, image after light soaking, fully degraded and fully regenerated. The colour of each pixel shows the strength of BB-signal in that pixel.

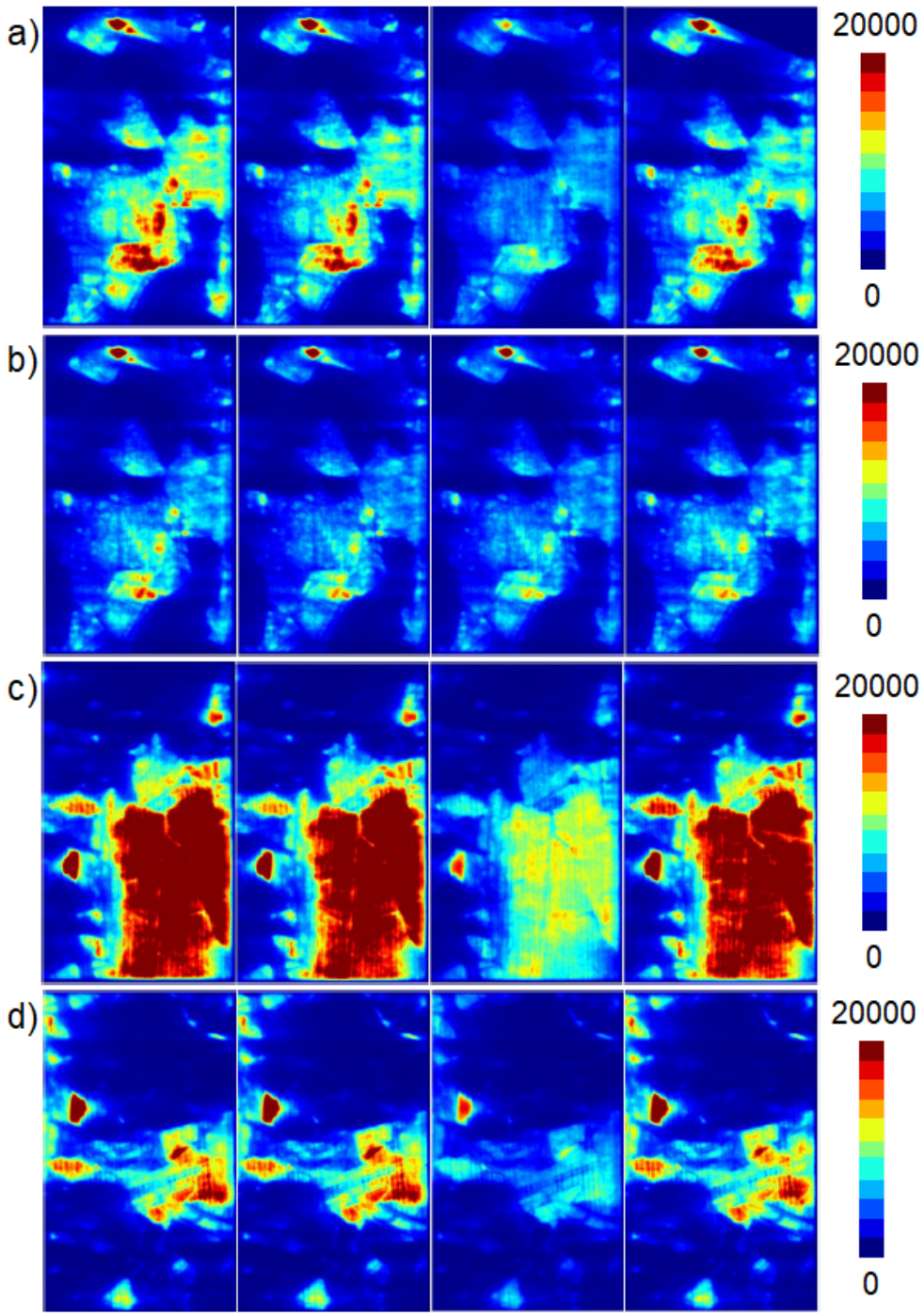

Figure 4.2: Spatial development of the BB-signal over time for: a) sample 3, b) sample 7, c) sample 4 and d) sample 4D. The images are from left the initial image, image after light soaking, fully degraded and fully regenerated. The colour of each pixel shows the strength of BB-signal in that pixel.

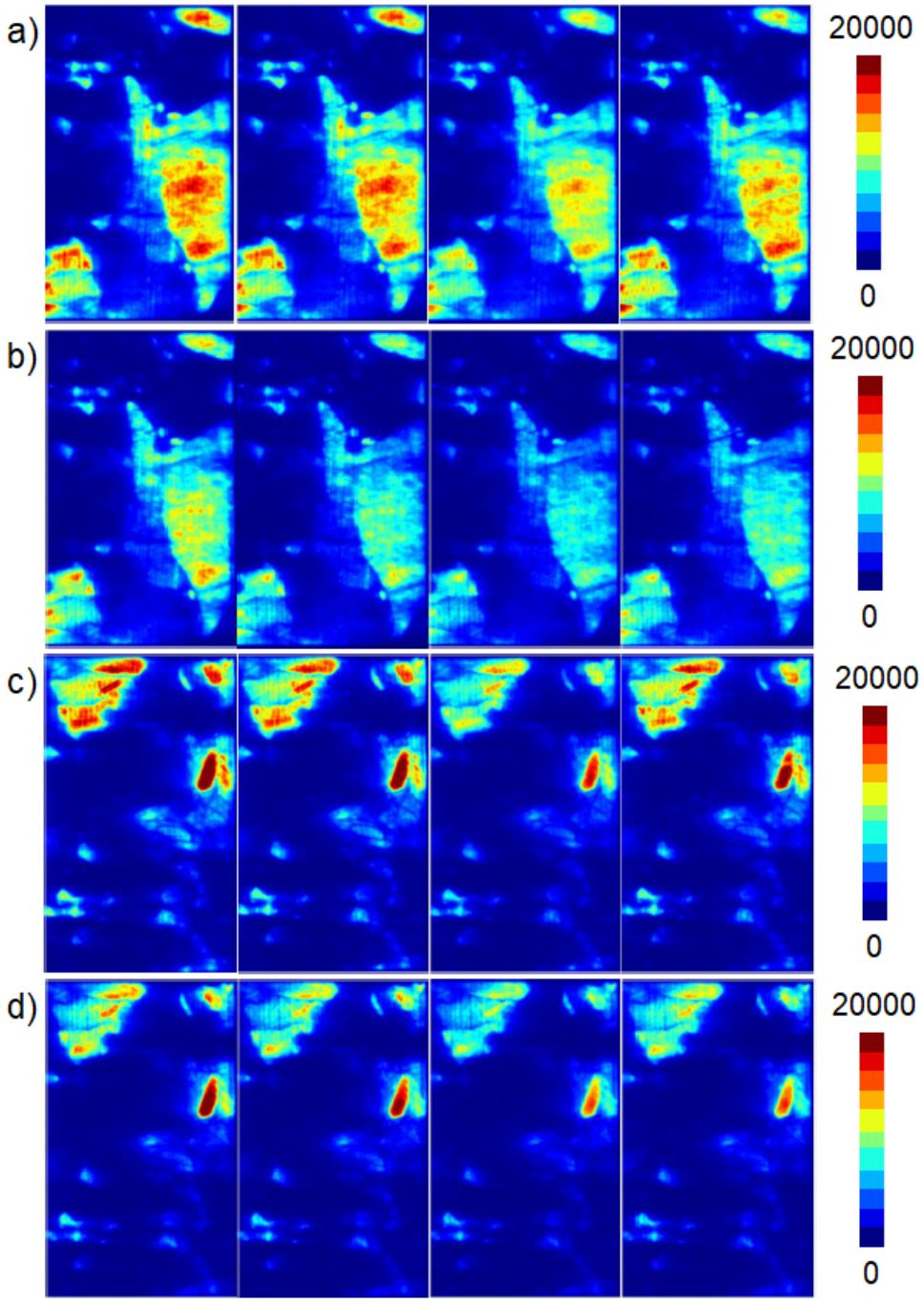

Figure 4.3: Spatial development of the BB-signal over time for: a) sample 5, b) sample 8, c) sample 5D and d) sample 8D. The images are from left the initial image, image after light soaking, fully degraded and fully regenerated. The colour of each pixel shows the strength of BB-signal in that pixel.

In figure 4.1 sample 1, 6 and 2 shows a slight degradation between the initial and light soaked image. Sample 1 and sample 2 shows strong degradation between the image taken after light soaking and the image at full degradation. Sample 6 shows a slight, and somewhat accelerated, degradation between the image taken after light soaking and the image taken after full degradation. Between the image of full degradation and full regeneration sample 1 and sample 2 shows strong regeneration to the same level of BB-signal that are shown in the initial image. Sample 6 shows some regeneration to the level where the BB-signal are at approximately the same level as after light soaking.

Figure 4.2 shows a slight degradation of the BB-signal for all the samples between the initial image and the image after light soaking. All the samples, except sample 7, shows strong degradation between the image after light soaking and the image after full degradation. Sample 7 shows a slight degradation between these images at the same level that was shown between the inital image and the image after light soaking. Sample 3 shows a strong regeneration of the BB-signal between the fully degraded and fully regenerated image, that brings the BB-signal up to approximately the same level as the two first images. Sample 7 shows a slight regeneration that brings the BB-signal up the same level as the image taken after light soaking. Sample 4 and 4D shows a strong regeneration that brings the BB-signal up to approximately the same level as the image taken after light soaking.

None of the samples in figure 4.3 shows strong degradation. All of the samples 5, 8, 5D and 8D shows a small degradation from the initial to the light soaked image. And all of the samples shows a new small degradation from light soaked to fully degraded. All the samples seems to have a somewhat accelerated degradation, except for sample 8. Sample 5 show a small regeneration to approximately the same level as after light soaking, except for the spot in the top right corner that does not reach the same level of BB-signal. Sample 8 and 5D shows a small regeneration of the BB-signal to approximately the same level as after light soaking. Sample 8D also shows a small regeneration, but the brightest spot on the right hand side of it does not show much regeneration, and clearly does not reach the same level as after light soaking.

4.2 Spectrum development

In this section the full spectrums for the four points in time that was shown spatially in the last section, initial, after light soaking, fully degraded and fully regenerated,

will be shown. The spectrums are made by summing the value for each photon energy level over all the pixels. The samples are presented from lowest in the ingot to highest.

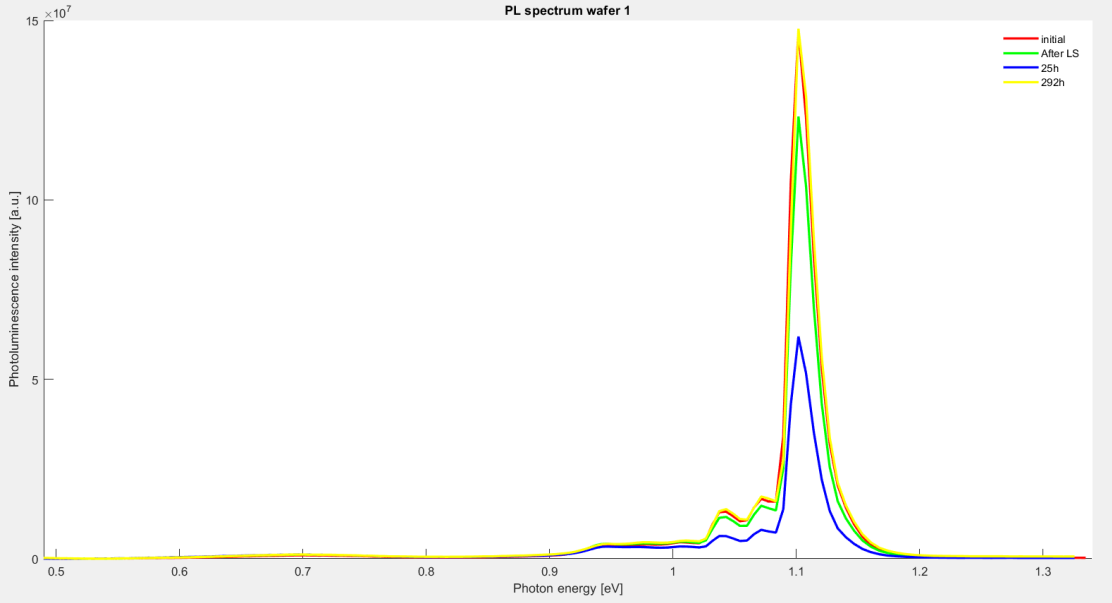

Figure 4.4: Photoluminescence spectrum of sample nr. 1. The red line is the initial spectrum, the green line is the spectrum after light soaking, the blue line is the spectrum when the sample is fully degraded and the yellow line is the spectrum after the sample has regenerated.

Figure 4.4 shows the spectrum of the initial image, the image after light soaking, the image after full degradation and the image after full regeneration of wafer 1. In figure 4.4 one can see the BB-signal just above 1.1 eV on all time steps. The BB-signal degrades to approximately 80 % of the initial signal after light soaking. It then degrades to 50 % of the initial signal when fully degraded and regenerates to a level a little bit higher than the initial signal after 292 hours. The figure also shows two phonon replicas of the BB-signal right to the left of real signal at approximately 1.07 eV and 1.04 eV. In addition the figure shows a signal in the region from 0.94 eV to a 1.02 eV, which is the region of the D3 and D4 signals. This signal is reduced from light soaked to fully degraded, but are regenerated to the same level as the initial signal after 292 hours. The less prominent signals of the samples will be further investigated in a later section.

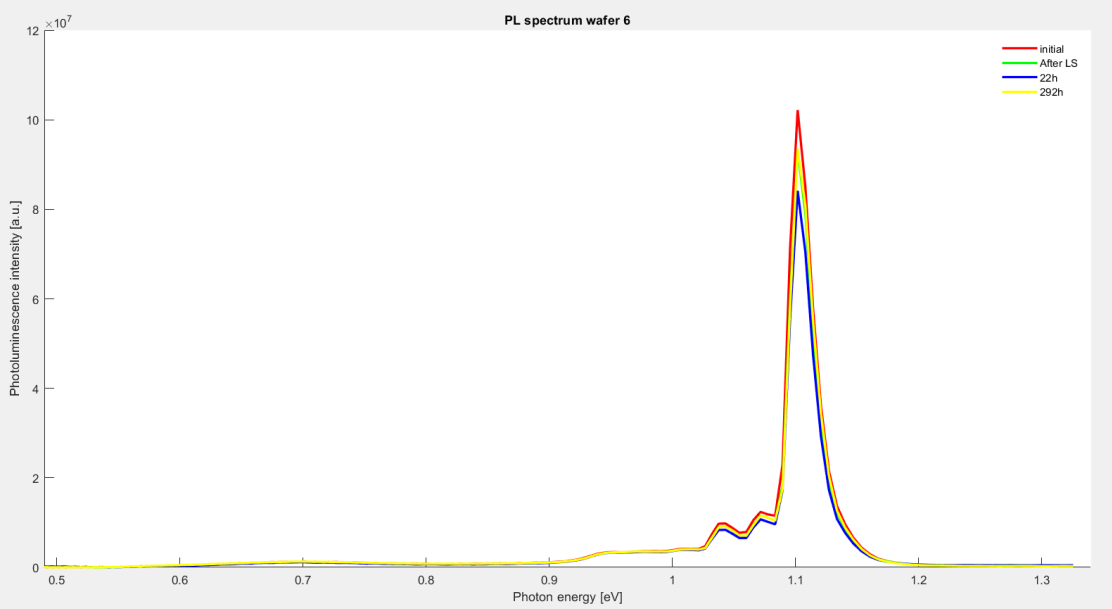

Figure 4.5: Photoluminescence spectrum of sample nr. 6. The red line is the initial spectrum, the green line is the spectrum after light soaking, the blue line is the spectrum when the sample is fully degraded and the yellow line is the spectrum after the sample has regenerated.

Figure 4.5 displays the spectrums from sample 6. The BB-signal can be seen right above 1.1 eV. The signal is reduced by almost 10 % from initial to light soaked and reduced again by almost the same amount from light soaked to fully degraded. Then the BB-signal is regenerated to the same level as after light soaking. Again the two phonon replica signals can be seen right to the left of the real BB-signal. Sample 6 also shows a signal in the range of D3 and D4, but this signal are not degraded and regenerated as in figure 4.4.

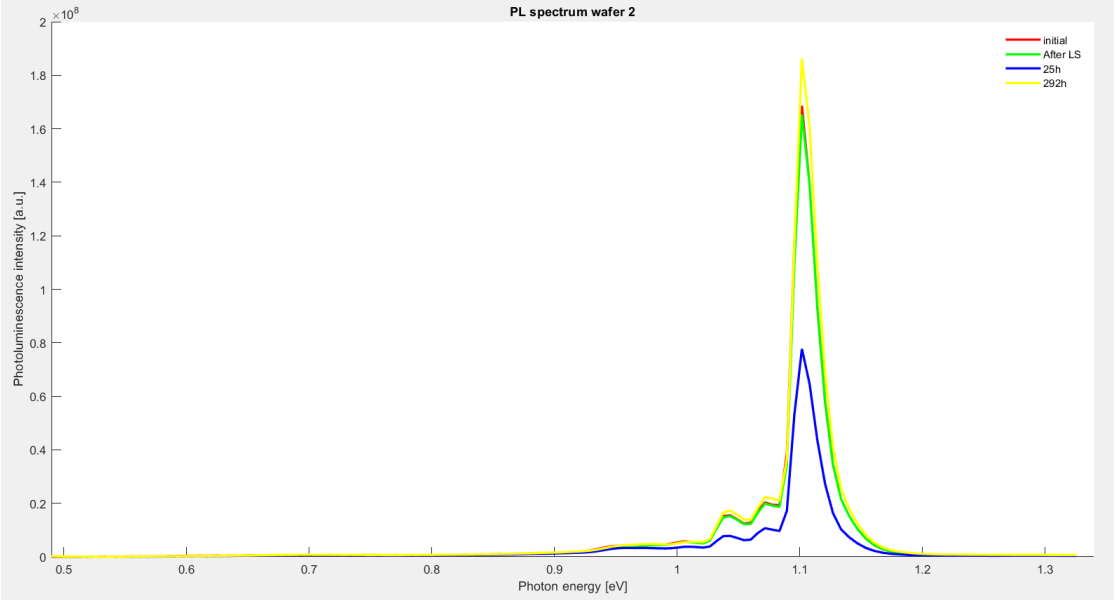

Figure 4.6: Photoluminescence spectrum of sample nr. 2. The red line is the initial spectrum, the green line is the spectrum after light soaking, the blue line is the spectrum when the sample is fully degraded and the yellow line is the spectrum after the sample has regenerated.

Figure 4.6 shows the spectrums of sample 2. The figure shows a small, if any, degradation of the BB-signal from the initial image to the image taken after light soaking. From the image after light soaking to the image taken after full degradation the signal is reduced to about 45 % of the initial signal. And after regeneration the BB-signal is approximately 10 % stonger than the initial BB-signal. Figure 4.6 shows the same degradation and regeneration as figur 4.4, for the D3 and D4 signal.

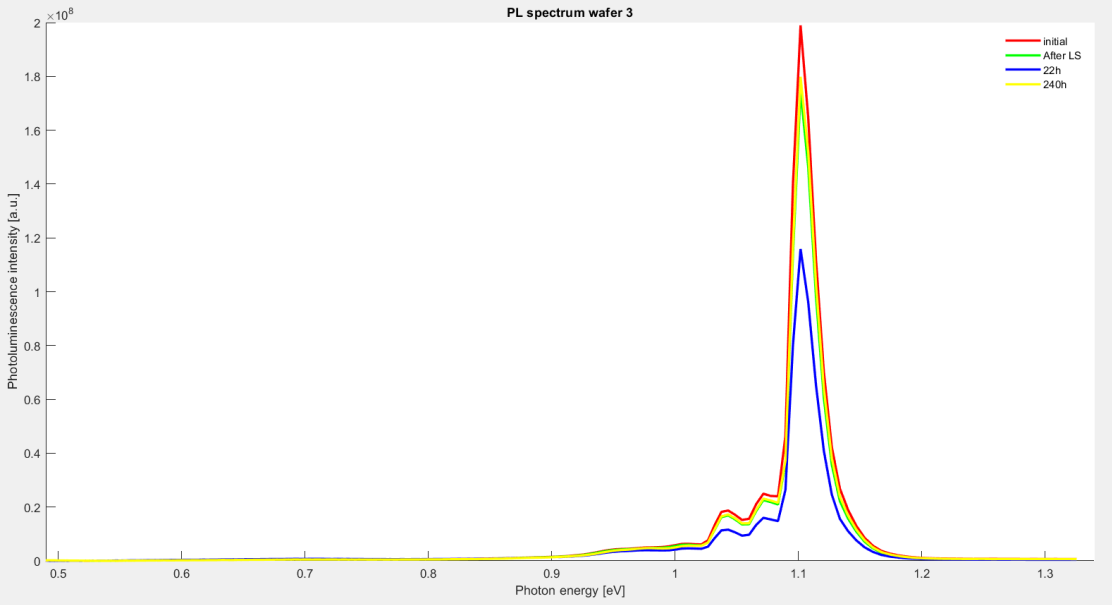

Figure 4.7: Photoluminescence spectrum of sample nr. 3. The red line is the initial spectrum, the green line is the spectrum after light soaking, the blue line is the spectrum when the sample is fully degraded and the yellow line is the spectrum after the sample has regenerated.

The spectrums of sample 3 can be seen in figure 4.7. The figure shows a degradation of the BB-signal of approximately 10 % from the initial image to the light soaked image. Further the fully degraded image shows a BB-signal that are a little bit under 60 % of initial BB-signal. After this the BB-signal regenerates to approximately the same level as after light soaking, after 240 hours of processing. This sample shows degradation of the D3 and D4 signal and some regeneration.

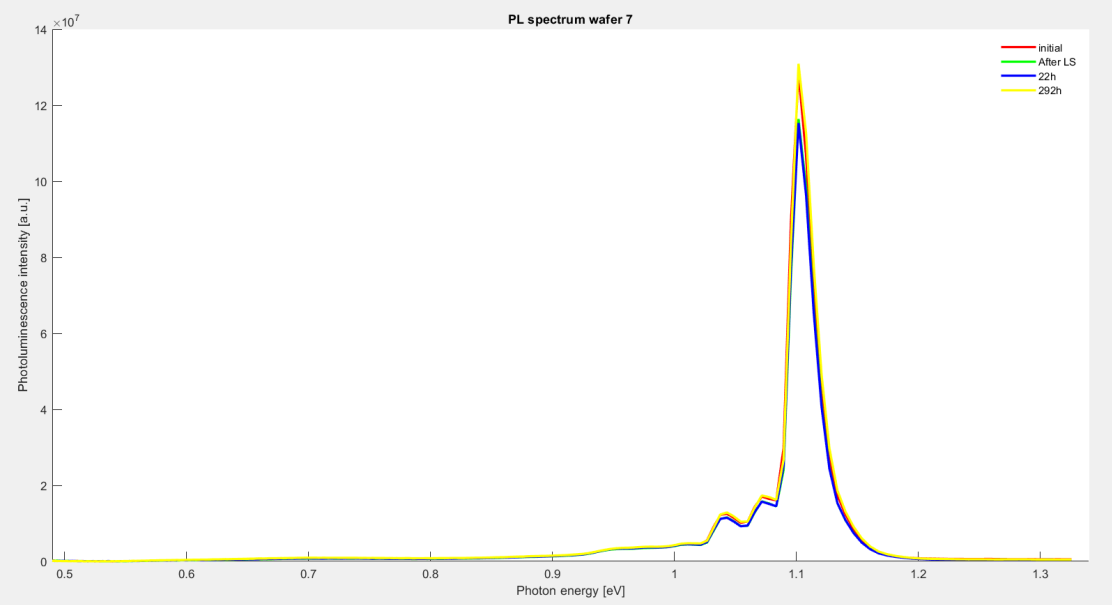

Figure 4.8: Photoluminescence spectrum of sample nr. 7. The red line is the initial spectrum, the green line is the spectrum after light soaking, the blue line is the spectrum when the sample is fully degraded and the yellow line is the spectrum after the sample has regenerated.

In figure 4.8 the spectrums of sample 7 are displayed. The BB-signal are reduced by approximately 10 % after light soaking and it is just slightly lower when fully degraded. After 292 hours the BB-signal has regenerated to 102 % of the original signal. This figure also shows a D3 and D4 signal, but no degradation and regeneration. In fact for sample 7 the D3 and D4 signal is at its lowest after light soaking and strongest after full regeneration.

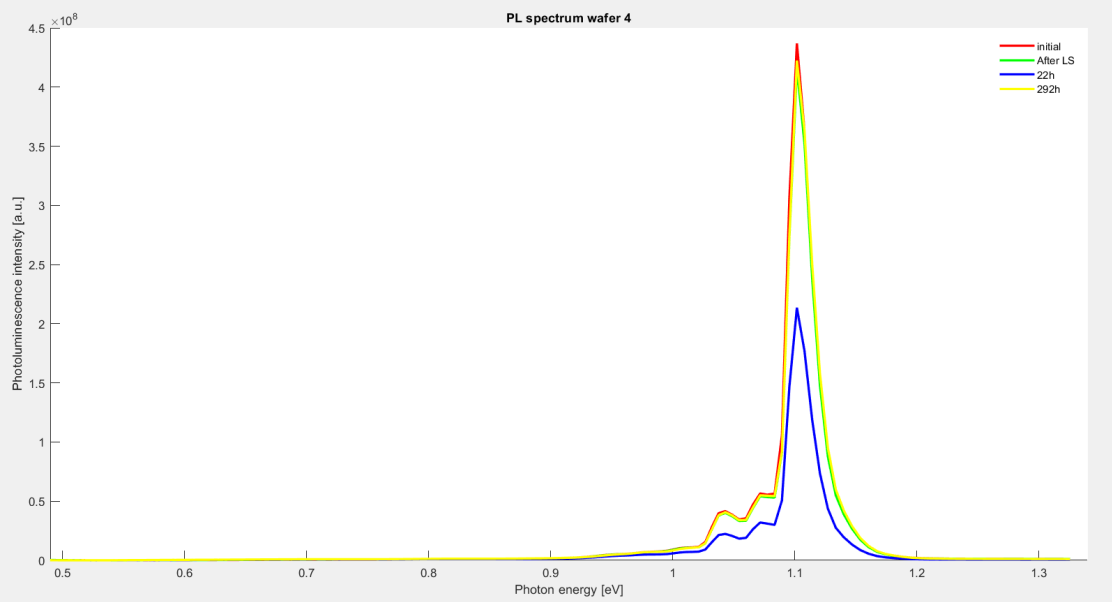

Figure 4.9: Photoluminescence spectrum of sample nr. 4. The red line is the initial spectrum, the green line is the spectrum after light soaking, the blue line is the spectrum when the sample is fully degraded and the yellow line is the spectrum after the sample has regenerated.

Figure 4.9 shows the spectrums of sample 4. The BB-signal of this sample is reduced to approximately 95 % of the initial signal after light soaking and are reduced further to about 50 % when fully degraded after 22 hours of elevated temperature treatment. After 292 hours of elevated temperature treatment the BB-signal is regenerated to almost 97 % of the initial signal. This sample shows less D3 and D4 signal compared to the BB-signal than the earlier samples shown, and in general the signals below 1 eV are weak compared to the BB-signal in this figure. The spectrums of the downside of sample 4 can be seen in figure A.1 in appendix A.

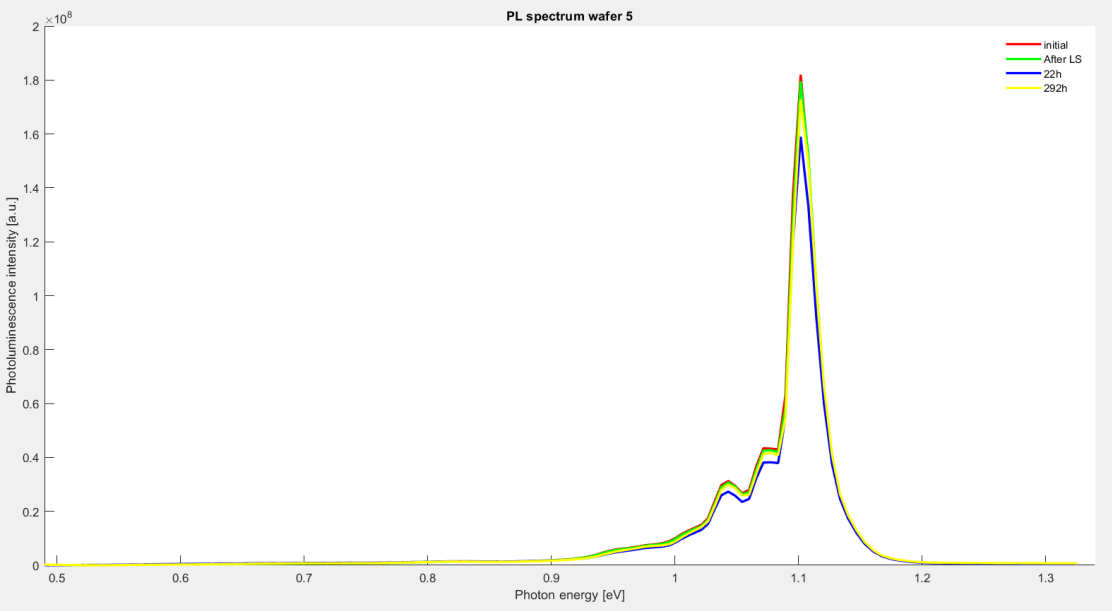

Figure 4.10: Photoluminescence spectrum of sample nr. 5. The red line is the initial spectrum, the green line is the spectrum after light soaking, the blue line is the spectrum when the sample is fully degraded and the yellow line is the spectrum after the sample has regenerated.

The spectrums of sample 5 are displayed in figure 4.10. The BB-signal of sample 5 are reduced by under 2 % by the light soaking. When fully degraded the BB-signal is reduced to approximately 87 % of the initial BB-signal. After being treated with light and elevated temperature for 292 hours the BB-signal regenerates to approximately 95 % of what it is initially. This sample shows more DRL relative to the BB-signal compared to the samples shown earlier. The spectrums of the downside of sample 5 can be seen in figure A.2 in appendix A.

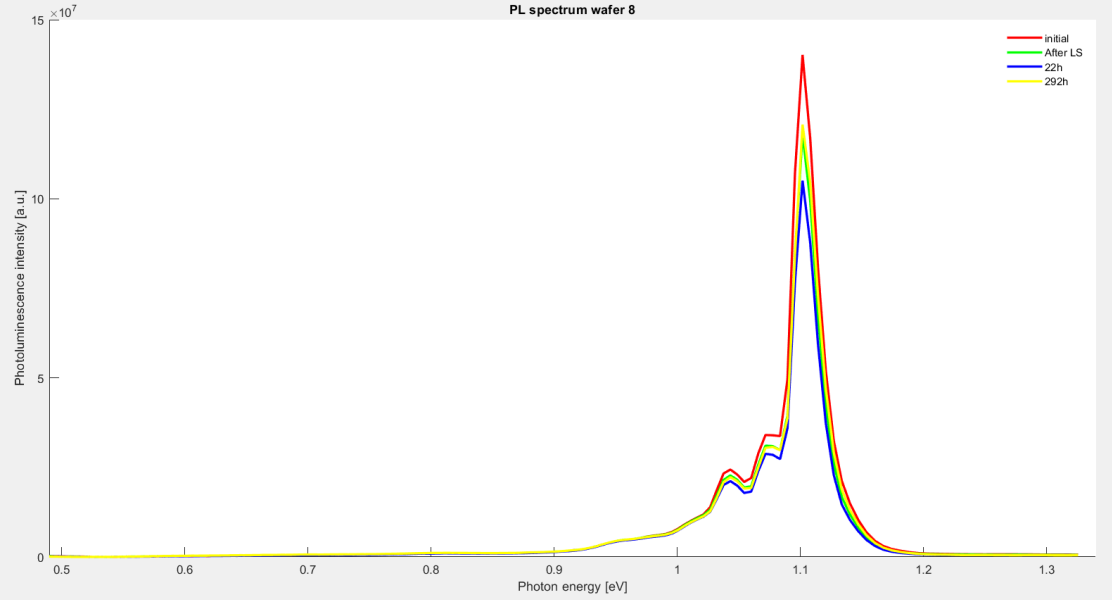

Figure 4.11: Photoluminescence spectrum of sample nr. 8. The red line is the initial spectrum, the green line is the spectrum after light soaking, the blue line is the spectrum when the sample is fully degraded and the yellow line is the spectrum after the sample has regenerated.

Figure 4.11 displays the spectrums for sample 8. The figure shows a drop in the BB-signal of around 15 % after light soaking, followed by another drop of around 10 %. After 292 hours of light and elevated temperature treatment the BB-signal regenerated to approximately 87 % of the initial signal. The spectrums shows some degradation and regeneration in the D3/D4 signal. Similar to sample 5, sample 8 shows a stronger signal below 1 eV relative to the BB-signal compared to the rest of the samples. The spectrums of the downside of sample 8 can be seen in figure A.3 in appendix A.

4.3 A deeper look on the dislocation clusters

As the PL-signal variates througout the samples, it is interesting to look at areas of the samples with a PL-signal that stands out. This section will look deeper into the PL-signal of different dislocation clusters. Since a dislocation cluster has more impurities than the rest of a sample, the PL-signal of a dislocation cluster is expected to have more DRL-signal and less BB-signal compared to the rest

of the sample. For each dislocation cluster it will first be shown a D3 image of the sample where the location of the dislocation cluster is outlined. Then the dislocation clusters spectrums of the four timesteps, initial, after light soaking, fully degraded and fully regenerated, will be displayed. The results of the hydrogenated samples will be displayed first followed by the results of the samples that are not hydrogenated.

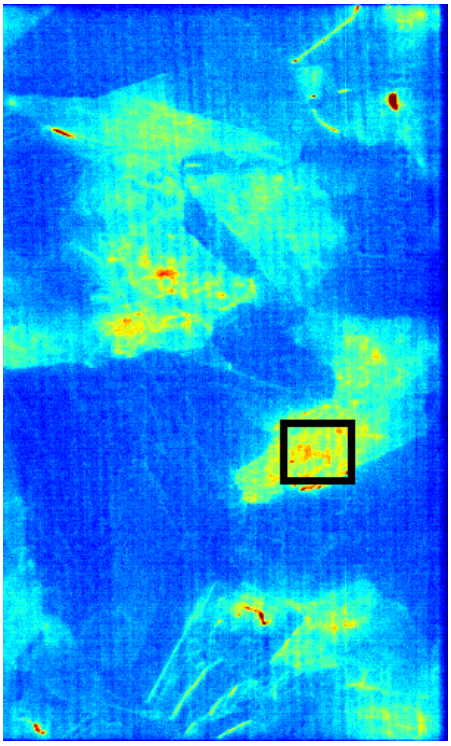

Figure 4.12: The image displays where the dislocation cluster investigated on sample 2 is situated. The image also shows the spatial distribution of the D3-signal of sample 2.

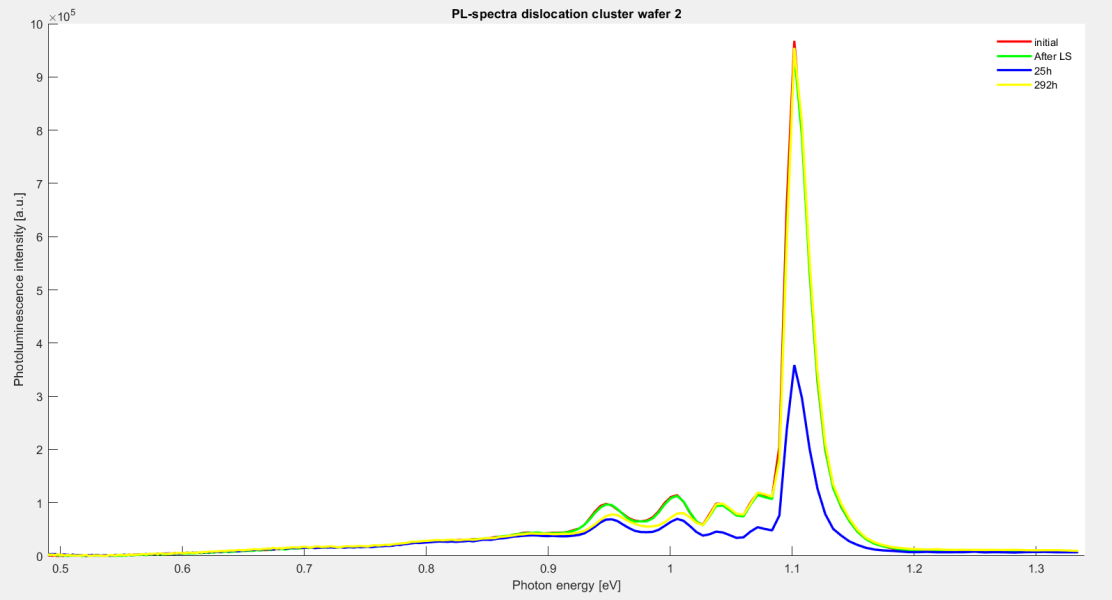

Figure 4.13: The figure shows the photoluminescence spectrum of the dislocation cluster of sample 2.

Figure 4.12 is an image of the D3 signal of sample 2 and it shows where the further investigated dislocation cluster of sample 2 is situated. In figure 4.13 the spectrums of the dislocationa cluster are presented. This figure shows a lot more DRL-signal relative to the BB-signal compared to the figures that showed the spectrums for the entire samples. The figure shows a drop in BB-signal of less than 3 % from initial to light soaked. From light soaked to fully degraded the BB-signal is reduced to less than 40 % of the initial signal. After regeneration the BB-signal has increased to almost the same level as the initial signal. The figure shows a D3 signal around 0.95 eV and a D4 signal around 1 eV, these are clear and differentiated with a little stronger D4 signal than D3 signal. For both signals the initial signal and the signal after light soaking is approximately the same. The D3 signal degrades by approximately 30 % when fully degraded and the D4 signal degrades by almost 40 %, at this point the two signals are approximately equally strong. The D3 signal then regenerates to almost 80 % of the initial signal and the D4 signal regenerates to a little over 70 % of the initial signal. Also after regeneration the signals are approximately equally strong. Both the D1 signal at approximately 0.81 eV and D2 signal at approximately 0.88 eV shows a slight degradation when fully degraded.

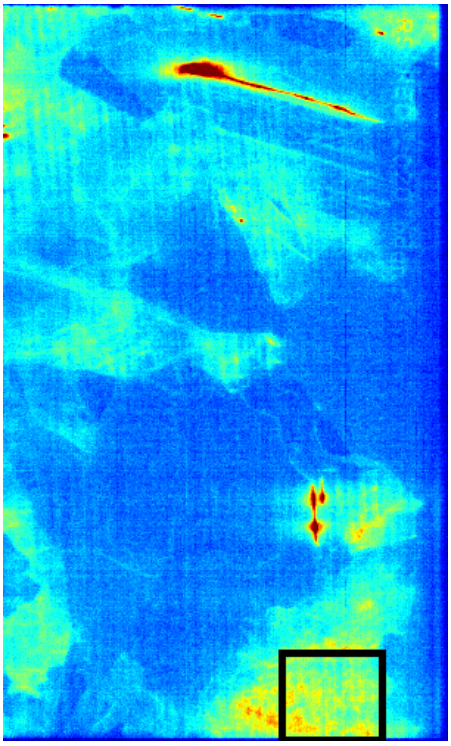

Figure 4.14: The image displays where the dislocation cluster investigated on sample 3 is situated. The image also shows the spatial distribution of the D3-signal of sample 3.

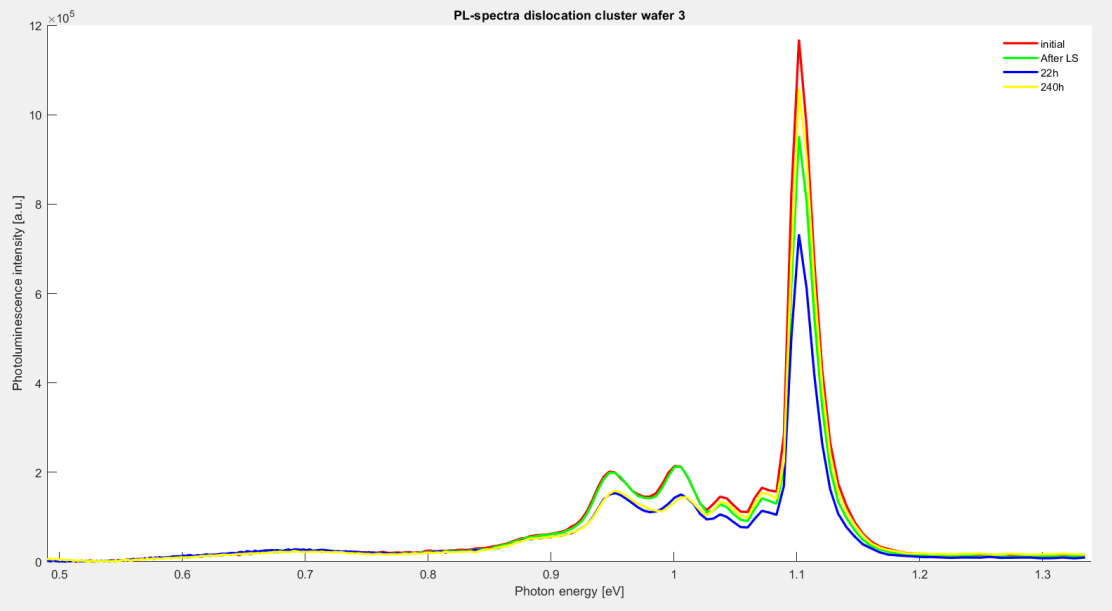

Figure 4.15: The figure shows the photoluminescence spectrum of the dislocation cluster of sample 3.

The dislocation cluster of sample 3 is outlined in the D3 signal of the sample in figure 4.14. The spectrums of this dislocation cluster is displayed in figure 4.15. The figure shows a reduction of the BB-signal between initial and after light soaking by about 20 % and further reduction by almost 20 % more. This degradation is then followed by a regeneration to approximately 90 % of the initial BB-signal. The D3 and D4 signal follows a similar pattern to the pattern seen in figure 4.13, but for this dislocation cluster none of the signals regenerates noticeably and the D4 signal actually declines slightly from when the samples BB-signal is fully degraded to fully regenerated. It can also be noticed from the figure that the D07 signal is slightly increased when the sample is fully degraded.

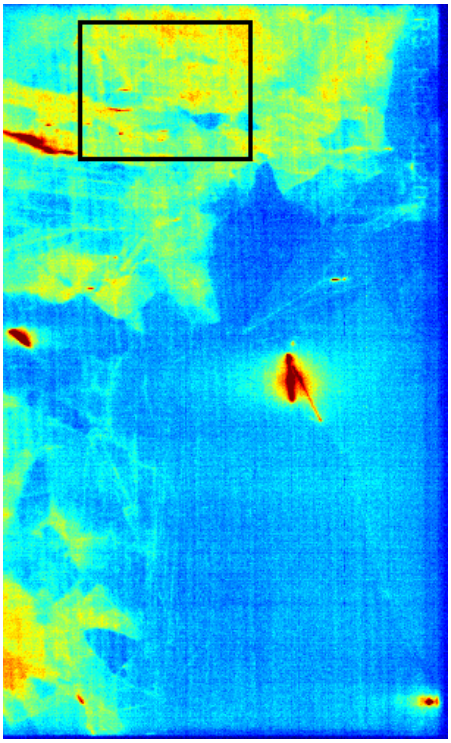

Figure 4.16: The image displays where the dislocation cluster investigated on sample 4 is situated. The image also shows the spatial distribution of the D3-signal of sample 4.

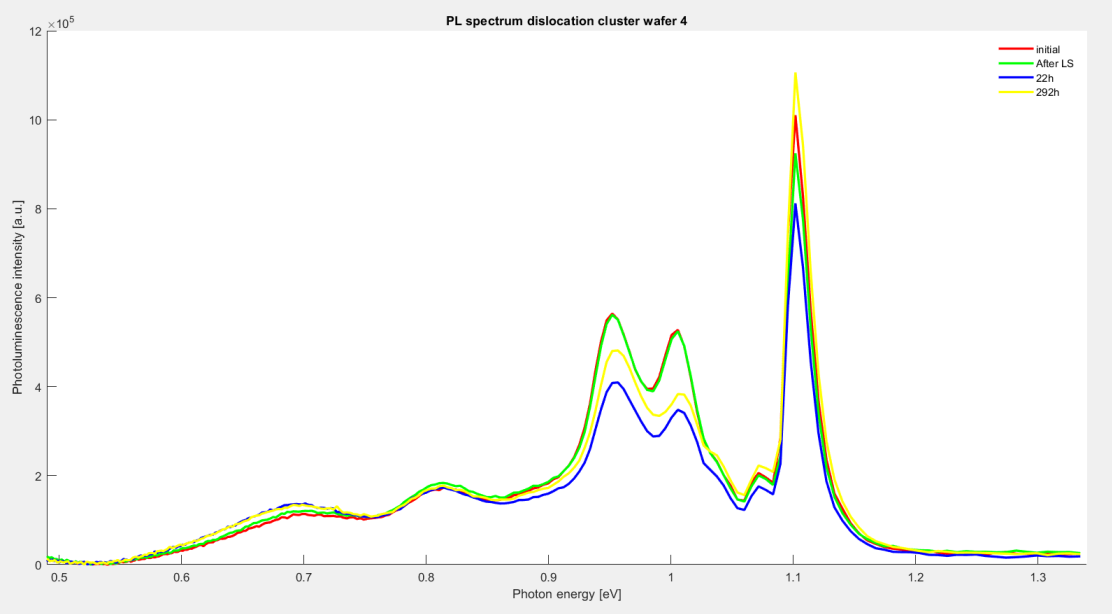

Figure 4.17: The figure shows the photoluminescence spectrum of the dislocation cluster on the upside of sample 4.

The dislocation cluster investigated from sample 4 is marked in figure 4.16. It can be seen from figure 4.17 that the BB-signal of this dislocation cluster shows a degradation to about 90 % of the initial signal after light soaking, and it then decreases further to about 80 % when fully degraded. After the degradation the BB-signal increases to a level approximately 10 % higher than the initial signal. Also the dislocation cluster of sample 4 shows a degradation of the D3 and D4 signal after treatment with illumination and elevated temperature. It can be noticed that this dislocation cluster also shows a distinct D1 signal, but this signal does not show any clear development. In figure 4.18 the spatial development of the BB, D3 and D4 signal of the dislocation cluster is shown. It shows a clear degradation of the D3 and D4 signal when the temperature is elevated, while the BB-signal shows no particular degradation. It can also be seen that the spatial distribution of the D4 signal covers the same areas as both the BB and D3 signal.

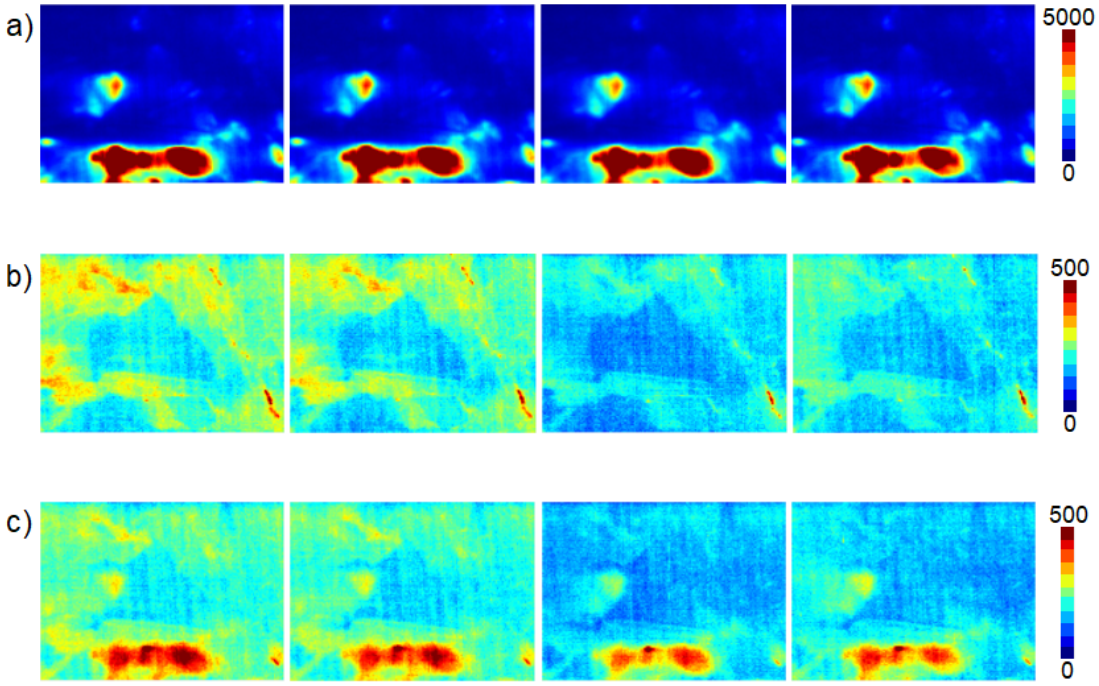

Figure 4.18: The figure shows the spatial development of a) the BB-signal, b) the D3 signal and c) the D4 signal of the dislocation cluster on the upside of sample 4. The colour of the pixels indicates the strength of the signal.

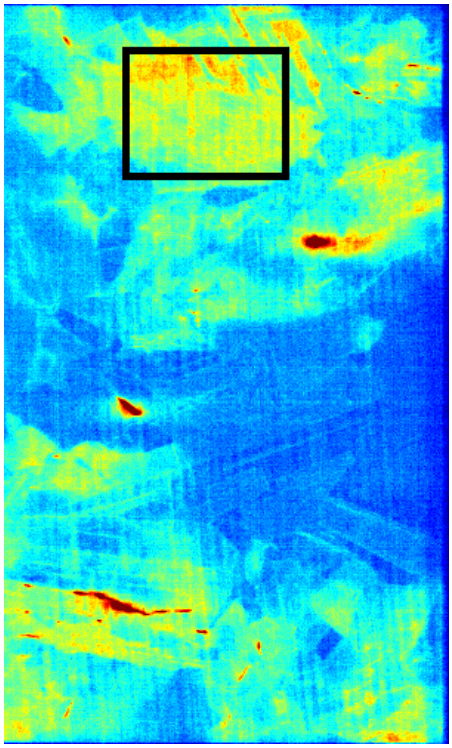

Figure 4.19: The image displays where the dislocation cluster investigated on the downside of sample 4 is situated. The image also shows the spatial distribution of D3-signal on the downside of sample 4.

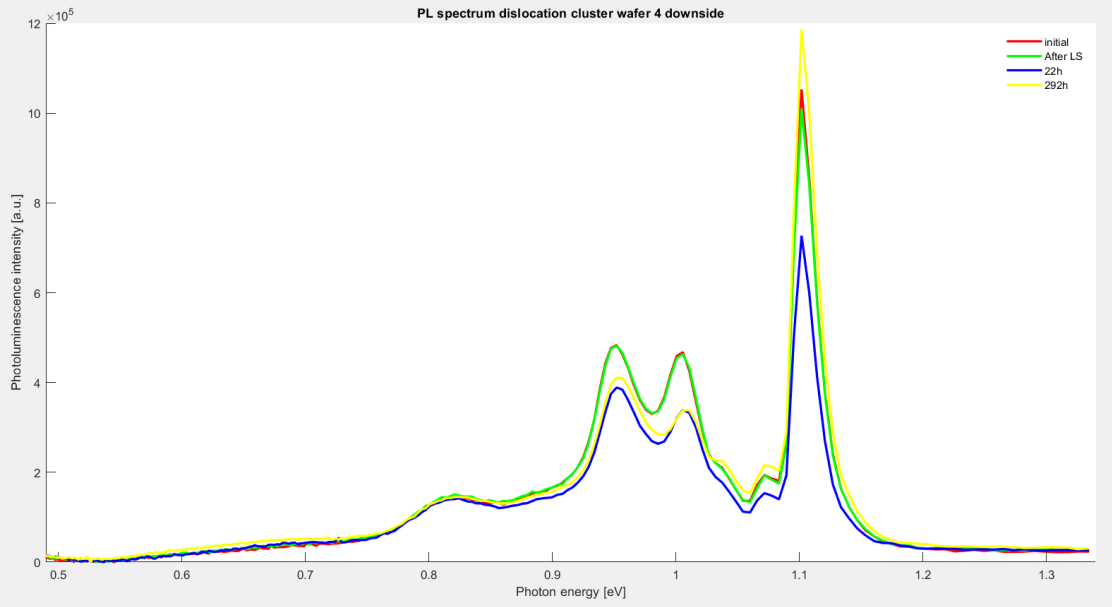

Figure 4.20: The figure shows the photoluminescence spectrum of the dislocation cluster on the downside of sample 4.

As the downside sample of sample D4 had a big dislocation cluster this was chosen to look further into, the part of the dislocation cluster looked further into is marked in figure 4.19. The spectrum development of this dislocation cluster, which is displayed in figure 4.20, shows much similarity to the spectrum development of the dislocation cluster of sample 4. It does though show a larger degradation of the BB-signal after exposure to illumination and elevated temperature.

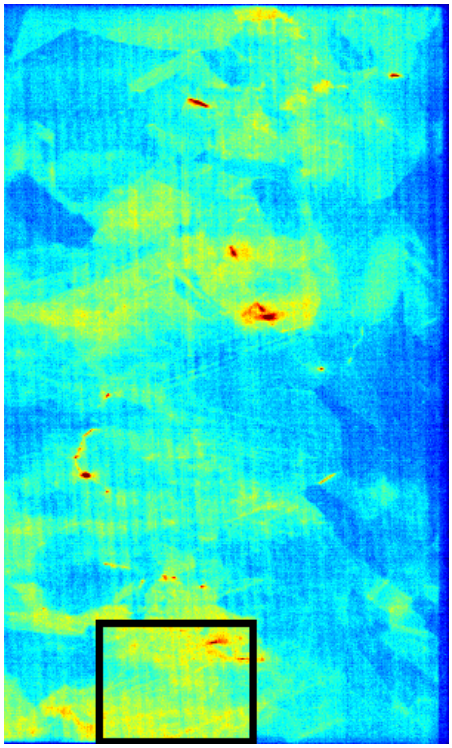

Figure 4.21: The image displays where the dislocation cluster investigated on the downside of sample 5 is situated. The image also shows the spatial distribution of the D3-signal on the downside of sample 5.

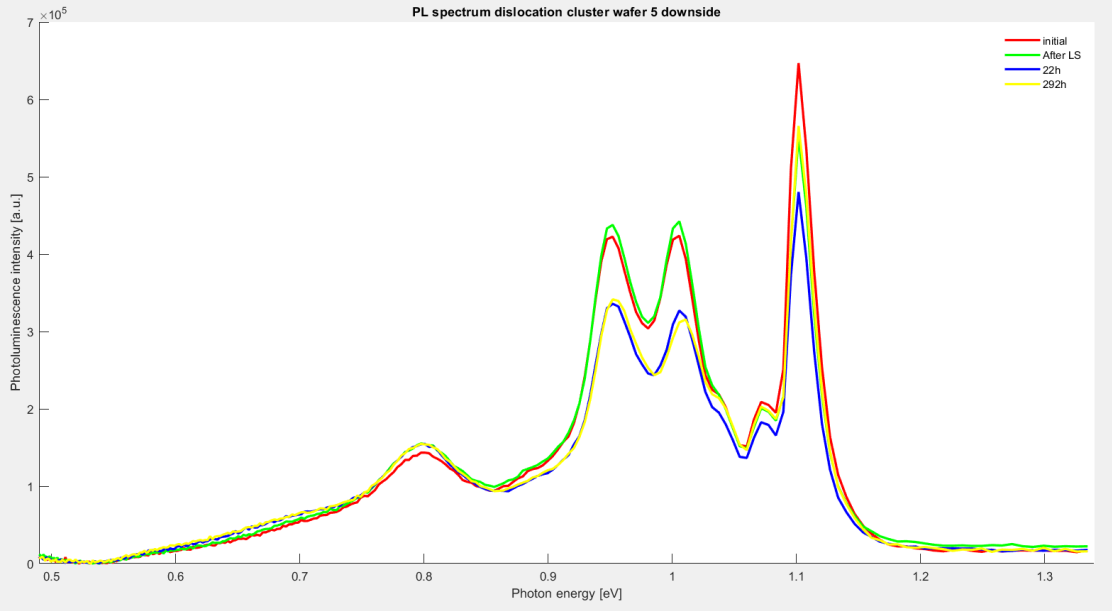

Figure 4.22: The figure shows the photoluminescence spectrum of the dislocation cluster on the downside of sample 5.

The dislocation cluster of sample 5D can be seen marked in figure 4.21. The spectrum development of this dislocation cluster can be seen in figure 4.22. It shows a BB-signal degradation of about 15 % after light soaking and further degradation of about 10 %. After 292 hours the BB-signal regenerated to around the same level as after light soaking. Also this figure shows the same pattern with regard to the D3 and D4 signal as the dislocation clusters investigated earlier. It is worth noticing that the D1 signal in this figure increases slightly after light soaking and stays stabile after that.

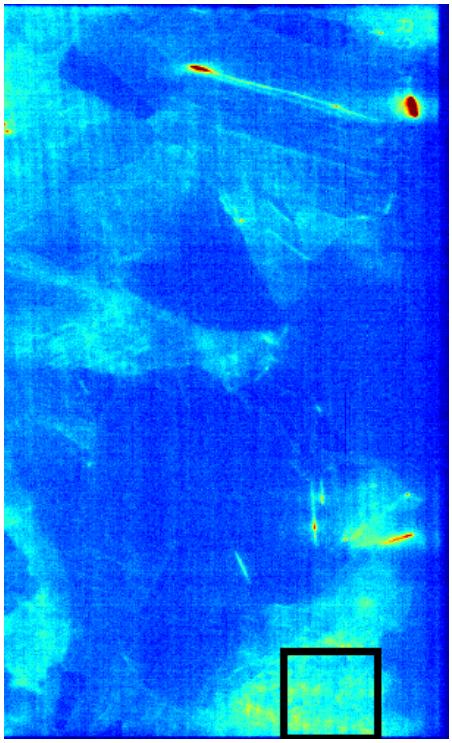

Figure 4.23: The image displays where the dislocation cluster investigated on sample 7 is situated. The image also shows the spatial distribution of the D3-signal of sample 7.

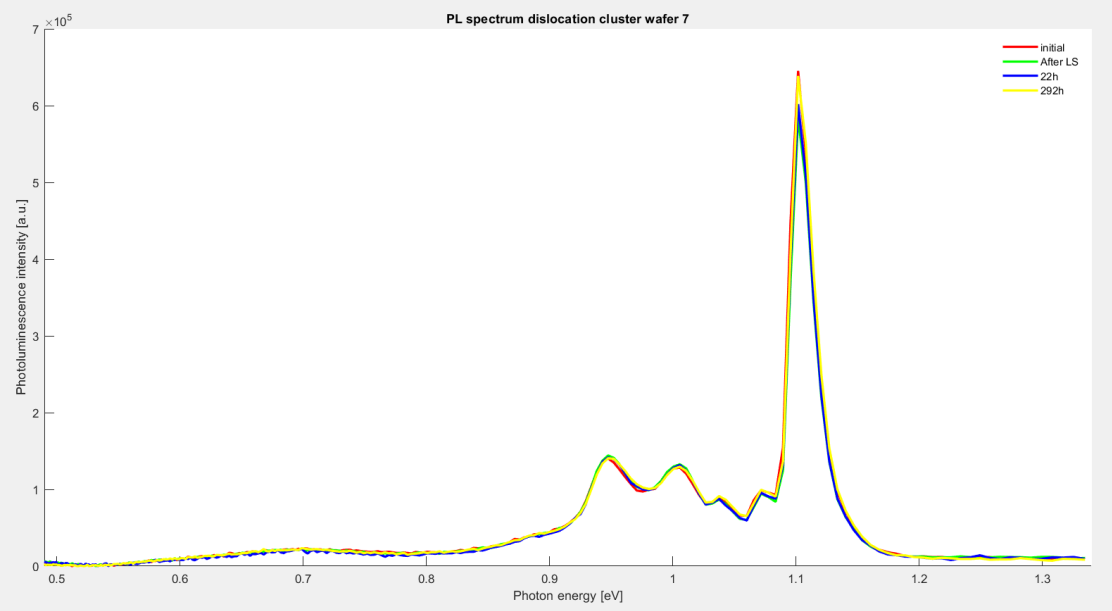

Figure 4.24: The figure shows the photoluminescence spectrum of the dislocation cluster of sample 7.

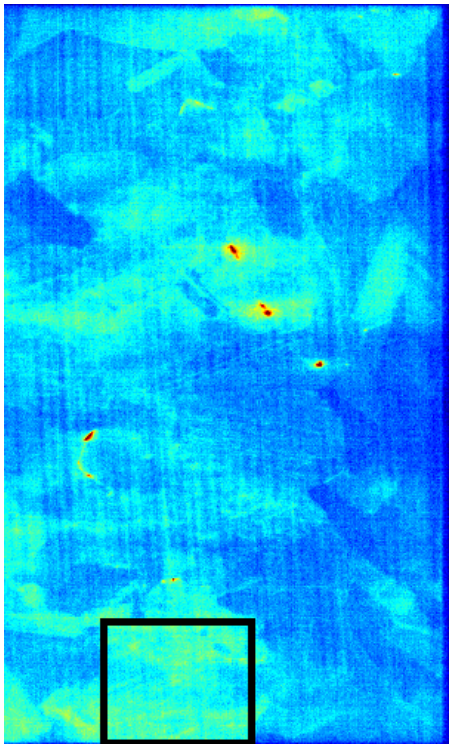

Figure 4.25: The image displays where the dislocation cluster investigated on the downside of sample 8 is situated. The image also shows the spatial distribution of the D3-signal on the downside of sample 8.

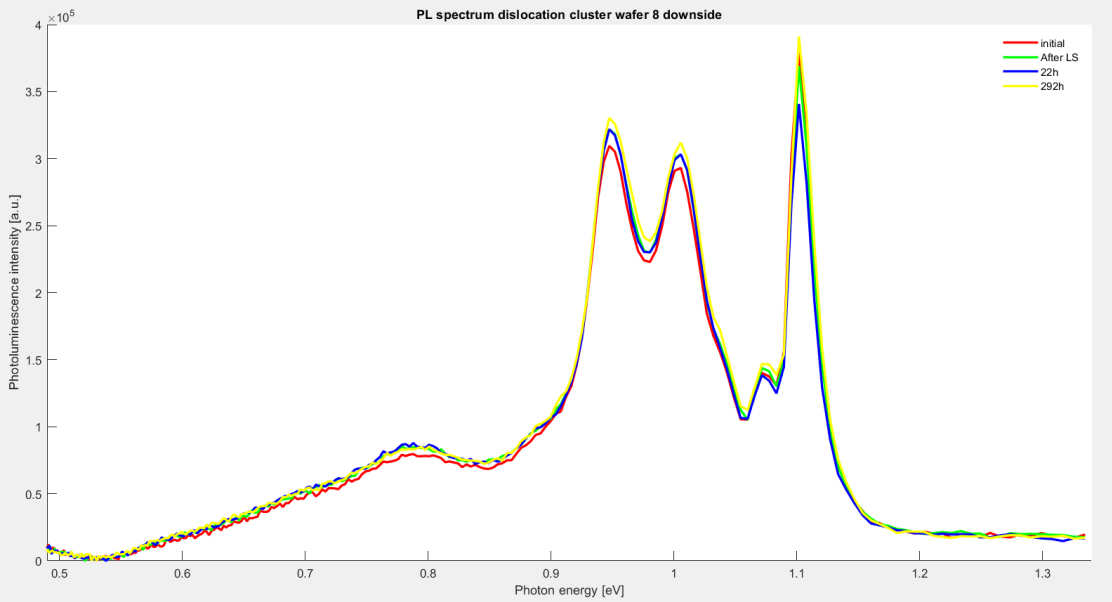

Figure 4.26: The figure shows the photoluminescence spectrum of the dislocation cluster on the downside of sample 8.

Figure 4.23 shows where the dislocation cluster of sample 7 is located and figure 4.25 shows where the dislocation cluster further investigated of sample 8D is located. Their spectrum development is shown in figure 4.24 for sample 7 and 4.26 for sample 8D, respectively. None of these dislocation clusters shows any large degradation of the BB-signal. The dislocation cluster of sample 7 is degraded by not more than 10 % when fully degraded and the BB-signal is approximately equal to the initial signal when fully regenerated. The BB-signal of the dislocation cluster of sample 8D degrades by approximately 12 % when fully degraded and when fully regenerated the signal is barely stronger than it was initially. None of these dislocation clusters shows any reduction of the D3 and D4 signal, in fact, the dislocation cluster of sample 8D shows an increase in these signals when treated with illumination and elevated temperature. It can also be noted that figure 4.26 shows and increase in D1 signal when illuminated in similar fashion as figure 4.22.

4.4 A closer look on the DRL development

When showing the spectrum development, the BB-signal is so strong that it camouflages the other signals. As it is important to show the strength of the BB-signal compared to the other signals and because of the general importance of the BB-signal it was decided to rather use an own section on the other signals. In the last section were the spectrum development of the dislocation clusters were shown, it could be seen a difference in the D3 and D4 signal for hydrogenated and not hydrogenated samples. This difference will be looked further into spatially for the entire samples in this section. This section will also show relative spectrum development for some samples, were the spectrum for each timestep is divided by the initial spectrum. This is done to get a view of the spectrum development that is not entirely dominated by the BB-signal.

As could be seen in the last section the D3 signal and D4 signal developed differently when exposed to illumination and elevated temperature. In figure 4.27 this is shown spatially for sample 3, 7, 5D and 8D. In figure 4.27a) the development of sample 3 is shown. In this figure it can be seen that the D3 signal is pretty stable from initial to after light soaking, but it decreases when exposed to illumination and higher temperature. After several hours of exposure the D3 signal increases slightly, but not to the same level as before the elevated temperature. In figure 4.27b) the D3 signal development of sample 7 can be seen. Sample 7 is from almost the same height of it's ingot as sample 3, but it is not hydrogenated. This sample show no particular development of the D3 signal. In figure 4.27c) and d) the same pattern can be seen for sample 5D and 8D respectively. Where sample 5D that is hydrogenated shows degradation of the D3 signal and 8D that is not hydrogenated does not show much development of the D3 signal. This difference between the D3 signal development of the hydrogenated and non-hydrogenated sample can be seen throughout the samples, with an exception of sample 1 and sample 6. This can be seen in figure A.4 in appendix A.

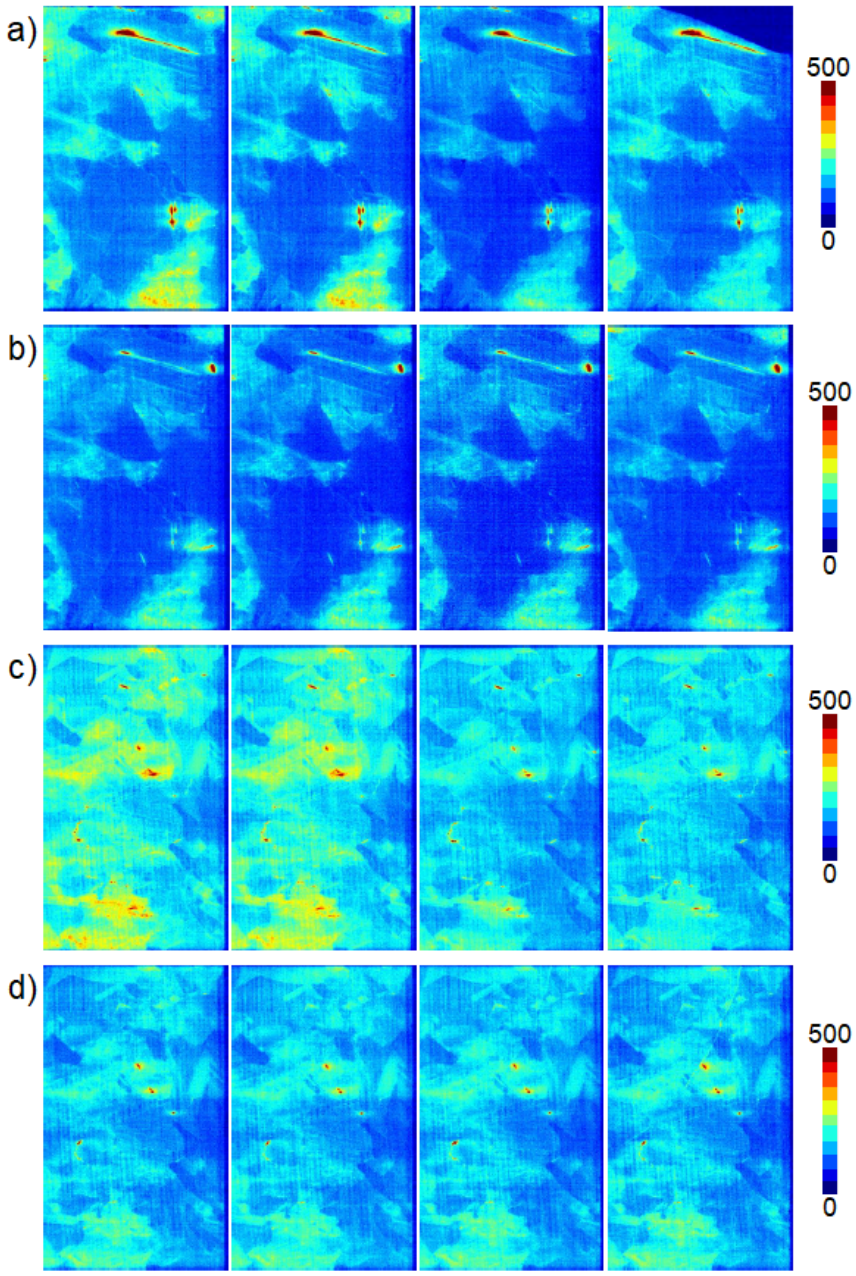

Figure 4.27: Spatial development of the D3-signal over time for: a) sample 3, b) sample 7, c) sample 5D and d) sample 8D. The images are from left the initial image, image after light soaking, fully degraded and fully regenerated. The colour of the pixel indicates the strength of the signal.

The next figures will compare the relative signal development of the different treatments, with and without hydrogenation. Figure 4.28 compares the development of a) sample 1 and b) sample 6. Figure 4.29 compares the development of a) sample 3 and b) sample 7. Figure 4.30 compares the development of a) sample 5 and b) sample 8.

a)

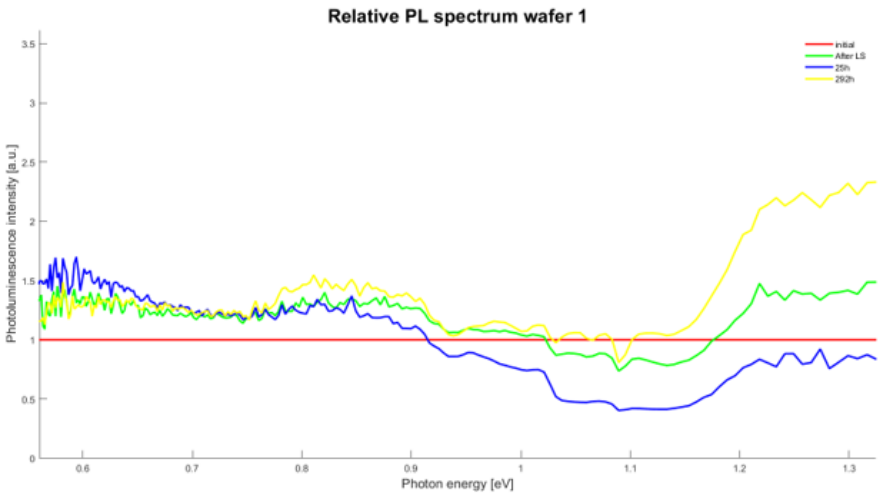

b)

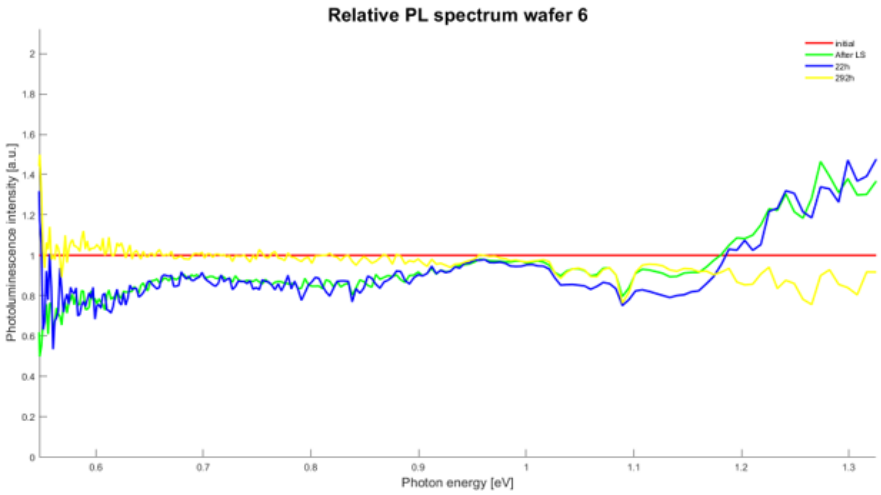

Figure 4.28: The figure compares the relative changes in the PL-signal of: a) sample 1 and b) sample 6. The PL spectrums are divided by their respective initial PL spectrum, to show how the signals develop through prossesing.

a)

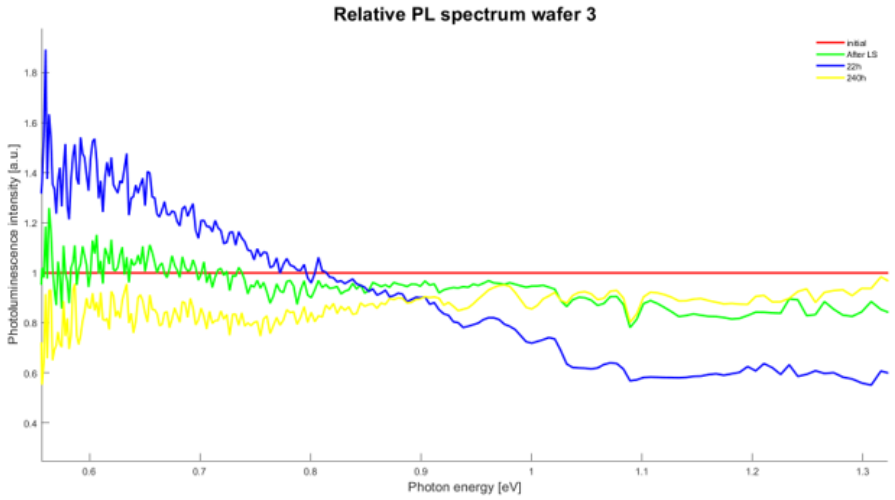

b)

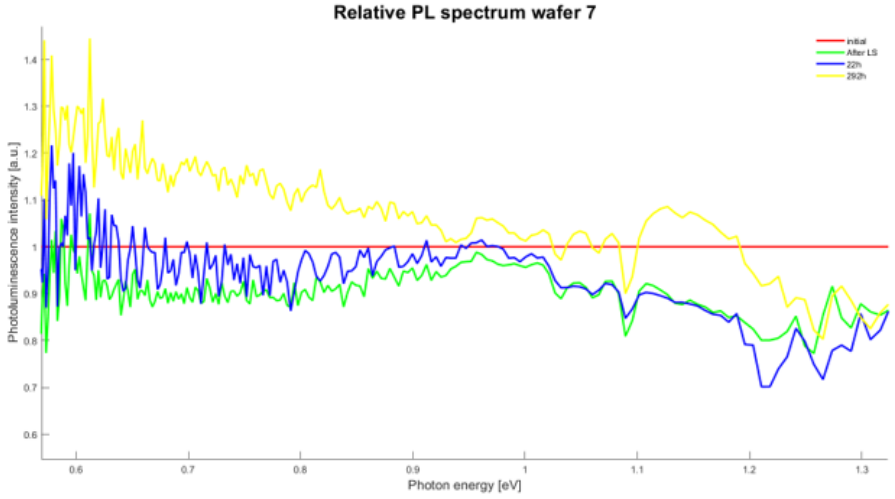

Figure 4.29: The figure compares the relative changes in the PL-signal of: a) sample 3 and b) sample 7. The PL spectrums are divided by their respective initial PL spectrum, to show how the signals develop through prossesing.

a)

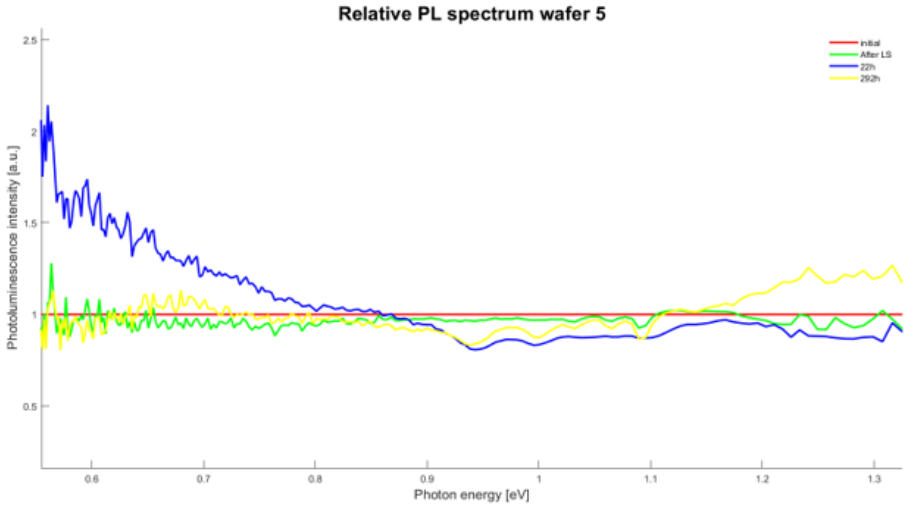

b)

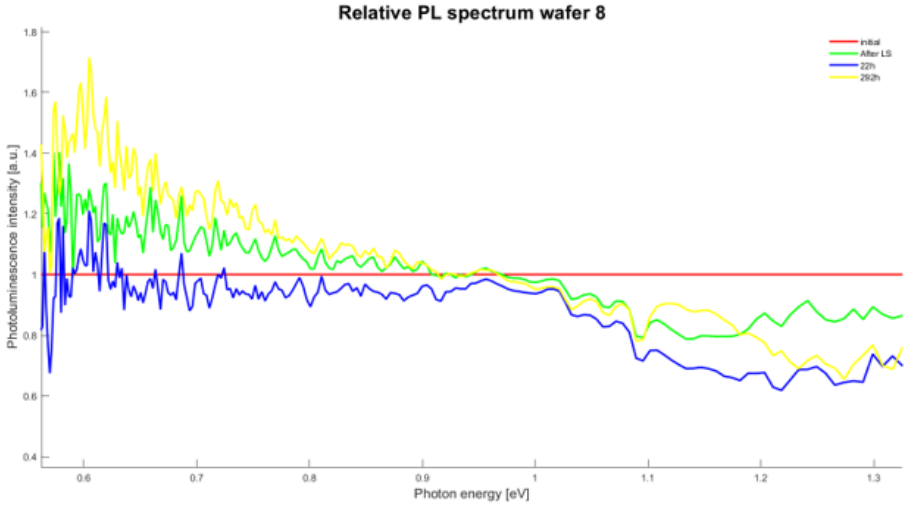

Figure 4.30: The figure compares the relative changes in the PL-signal of: a) sample 5 and b) sample 8. The PL spectrums are divided by their respective initial PL spectrum, to show how the signals develop through prossesing.

It can be seen from figure 4.28, 4.29 and 4.30 that the spectrum after light soaking and the spectrum after full degradation follows each other much closer for the samples that are non-hydrogenated than for those who are hydrogenated. In figure

4.28b) they are almost identical, the only places they really differs are the BB-signal and the BB-signal replicas. In figure 4.30b) they differ much more, but also for sample 8 their shape is similar. The difference for sample 8 is the spectrum at full degradation in general being weaker than the spectrum after light soaking.

It seems like the samples that are hydrogenated has an increase in signal from 0.8 eV and below. This increase can not be seen for the non-hydrogenated samples. Sample 2 does not show the same increase in signal below 0.8 eV as the rest of the hydrogenated samples, it actually shows a decrease. As there were no non-hydrogenated samples from the same height in the ingot as sample 2, no comparison to a similar non-hydrogenated sample can be made. The relative spectral development of sample 2 can be seen in figure A.5 in appendix A.

Chapter 5

Discussion

5.1 Discussion of methodology: Weaknesses and considerations

Only the last of the four images taken for every sample was used for tracking the time development of the BB-signal. The development can be seen in figure 3.5 and 3.6. A consequense of this is less certain approximations of the times for full degradation and full regeneration. The investigation looked for the differences between the samples initial, light soaked, fully degraded and fully regenerated images, and therefore finding the exact times for these points was not that important. The reason for this is that the images close in time will be similar. Taking the median of the three last images would make the approximations of these points more exact, but would be a challenge both for the memory and the RAM of the computer. It was thus decided against it. The tracking of the BB-signal was only done for the upside samples and not for the downside samples because it was not seen as important to track the degradation of both sides. The reason for this is LeTID's supposedly homogeneous development within the samples, stated in the theory chapter.

The lack of a reference wafer is a weakness for this thesis' methodology. Imaging without a reference wafer makes the comparison between each image less certain as the impact of external uncertainties becomes larger. A reference wafer was not used, because a reference wafer with a suiting lifetime could not be obtained. The minority carrier lifetime of the reference wafer has to be comparable to the minority carrier lifetime of the samples. Reference wafers with stabile lifetime had

been collected preceding the imaging, but these had much higher lifetime than the samples. Using these wafers would lead to saturation of their signals, as a result they could not be used. As it was hard to obtain any suitable reference sample it was decided to start the imaging without one. The number of samples used in the study, together with the number of datapoints and the immense data of each hyperspectral image compensate for the lack of a reference sample to some degree.

The choice of bottoms for the non-hydrogenated samples could be criticized, as they are not the true bottoms of their BB-signals shown in figure 3.5. Especially sample 6 and 8 seem to have a bottom point around 157 hours, but these measurements seems to be outliers. The reason for this is that they are precursed by a rapid decline, especially for sample 8 which is called data6 in the figure, followed by a rapid incline. The uncertainty regarding these bottoms could have been avoided if a reference sample had been used. The bottoms were chosen at the same time as the hydrogenated samples to make the comparison between them more correct with regards to time.

The reason why there was taken four images when only three were used to make the median image, was that the samples did not reach the bottom temperature before the second image was taken. Instead of timing the starting point of the imaging after the samples was put on, it was easier to start the imaging and use the three last images. This made less room for human errors, caused by incorrect timing.

5.2 Hydrogens role in LeTID

It seems evident from the results of this study that hydrogen plays a major part in LeTID. None of the non-hydrogenated samples showed degradation of the BB-signal above 15 % after 22 hours of light and elevated temperature treatment, compared to the light soaked image. On the contrary, all the hydrogenated samples, except sample 5, showed a degraded BB-signal of at least 30 % between light soaked and fully degraded. All of the hydrogenated samples showed more degradation between the light soaked and the fully degraded image, than between the initial and light soaked image. This could not be seen for any of the non-hydrogenated samples. The litterature supports hydrogen being an important root cause to LeTID. Luka et al. suspected that at least one fast diffuser was involved in the degradation, amongst those were hydrogen [24]. Although it is not agreed upon one theory, there seem to be a broad agreement that hydrogen is involved. It is a major part of both Chen et al.'s theory [12] and Bredemeier et al.'s theory [28].

5.3 Variation due to the samples' height in the ingot

LeTID seems to vary with the samples' height in the ingot. All the hydrogenated samples shows clear degradation and regeneration, except for sample 5 which is the sample taken from highest in the ingot. Thus, it looks like the wafers from highest in the ingot is not affected by LeTID. This is also partly supported by Petter et al. who observed that the wafers highest in the ingot was less affected by LeTID. As sample 5 has a stronger BB-signal than sample 1, it is clear that the lack of LeTID in sample 5 is not due to a low initial efficiency.

The LeTID effect being weaker in the top of the ingot does not fit well with the theory of Bredemeier et al. [28], who proposed that cobalt or nickel is causing the degradation. Both cobalt and nickel are accumulating towards the top of the ingot and if these impurities caused LeTID, one should suppose that the effect was stronger higher in the ingot. The same is the case for copper which was mentioned by Luka et al. [24]as a possible factor behind LeTID. Therefore it seems probable that amongst the fast diffusers mentioned by Luka et al. [24], hydrogen is the one causing LeTID. The level of hydrogen should be the same for all the hydrogenated samples as they were pre-processed the same way. Oxygen is the most known impurity that disappears towards the top of the ingot. Despite this it seems unlikely that oxygen is a major factor in the LeTID effect. This because there cannot be seen any clear trend of more LeTID towards the bottom, which would correspond to the higher oxygen concentration towards the bottom of the ingot.

The concentration of the dopant atoms are increasing towards the top of the ingot, and they could be a factor behind the LeTID as proposed by Chen et al. [12]. If hydrogen is somehow passivating the dopant atoms, a higher concentration of dopant atoms should make a sample more resiliant against LeTID as a lower percentage of dopant atoms are passivated. LeTID caused by migrating hydrogen that interacts with the dopant atoms, could explain a decrease of LeTID towards the top.

5.4 Discussion of the results for the dislocation clusters

At least one defect is passivated in the dislocation clusters of all the hydrogenated samples when the temperature is increased. This can be seen from the D3 and D4 signal decreasing in all of these dislocation clusters spectrums after treatment with illumination and elevated temperature. Non of the non-hydrogenated samples shows this phenomenon. This indicates that hydrogen is passivating the defect. Hydrogen is also in general known for passivating defects.

The dislocation cluster on the upside of sample 4 shows less LeTID than the rest of the sample. Under the assumption that the cause of LeTID is hydrogen passivating a portion of the dopant atoms, it could be possible that this dislocation cluster showed less LeTID, due to the passivated defect having a higher chance to interact with the hydrogen atoms than the dopant atoms. One could believe that the concentration of dopant atoms in sample 4 is too low for the sample to be resiliant to LeTID, but if the defect that is passivated is attracting the hydrogen atom at the expense of the dopant atoms, fewer dopant atoms would be passivated. This could cause the dislocation cluster to be resiliant. This seems possible as the dislocation clusters in samples from further down in the ingot shows clear LeTID. The dislocation cluster of the downside of sample 4 is not showing the same degree of resiliance towards LeTID as the dislocation cluster on the upside. However, this dislocation cluster shows less DRL compared to the BB-signal which could indicate fewer defects to passivate, which implies more passivated dopant atoms.

The analysis of the dislocation clusters strengthens Chen et al.'s theory [12], which proposes that LeTID is caused by migrating hydrogen interacting with the dopant atoms, in two ways. Firstly, the passivation of one or more defects after elevation of the temperature indicates that hydrogen becomes active in the silicon when the temperature is elevated. Secondly, this theory can explain the decreased LeTID in the dislocation cluster on the upside of sample 4.

Another interesting finding is that the D3 and D4 signal in the dislocation clusters of sample 2 and 4 regenerates from the image taken when fully degraded to the fully regenerated image. This could be caused by a general increase of the minority carrier lifetime in the samples. None of the dislocation clusters of sample 5 shows an increase in D3 and D4 signal, which indicates that this increase is due to the increased lifetime. Sample 5 does not show a high increase in the BB-signal either, and this dislocation cluster actually shows a further decrease of the D4 signal. A contradiction to this is the spectral development of sample 3's dislocation

cluster, which does not show any increase in the D3 and D4 signal. Although, this sample shows an increase in BB-signal, which indicates an increased minority carrier lifetime.

In the end it should be pointed out that the development of the D3 and D4 signals is slightly different. The D3 signal in the dislocation clusters of the hydrogenated samples consistently degrades less than the D4 signal when the temperature is elevated. This could mean that there are differences in the origin of the D3 and D4 signals. The difference could also be due to the VID3 signal, but the D3 signal in these regions is not very intense nor concentrated in specific areas. As seen in figure 4.18 the D4 signal can be disturbed by phonon replicas of the BB-signal, which could be a third potential reason for the different developments of the D3 and D4 signal. Because of this disturbance, it is hard to tell if there actually is a difference in the origin of the D3 and D4 signals.

5.5 Further discussion of the signal development

From the development of the DRL signals it seems evident that the hydrogenated samples shows a higher difference between the spectrum after light soaking and the spectrum after full degradation, compared the non-hydrogenated samples. It is still hard to see an increase in any particular signal that could cause LeTID. Nevertheless, the hydrogenated samples have an increase in the signal up to around 0.7-0.8 eV, compared to the non-hydrogenated samples. On the other hand it is hard to say that this has anything to do with LeTID, as sample 5 shows the same development of this signal. Further, as can be seen in appendix A, sample 2 shows a decrease in this signal, which makes it even harder to tie this to LeTID. From the results of this thesis it seems most likely that LeTID is caused by a non-radiative defect. This follows from the lack of any DRL signal that consistantly increases significantly in the samples when they degrade.

Chapter 6

Conclusion and further work

6.1 Conclusion

The development of LeTID in multicrystalline p-type PERC wafers, when exposed to illumination and elevated temperature, has been investigated in this thesis by hyperspectral imaging. Eight samples each from different wafers has been investigated. Among these, five were cut from wafers pre-processed with PDGH treatment and three were cut from wafers pre-processed with PDG treatment. The wafers within the groups of different pre-processings were cut from different heights in the same ingot.

Studying these samples of different pre-processings and heights in the ingot with hyperspectral imaging, led to some key observations. Firstly, the hydrogenated samples showed LeTID, while the non-hydrogenated samples did not show LeTID. Secondly, the hydrogenated sample cut from the wafer highest in the ingot did not show LeTID. Thirdly, at least one defect is passivated in the dislocation clusters of the hydrogenated samples, while this passivation cannot be seen in the dislocation clusters of the non-hydrogenated samples. Further, one dislocation cluster in the hydrogenated sample cut from the wafer second highest in the ingot shows a resiliance towards LeTID, while the rest of that sample does not show resiliance towards LeTID. Finally, it cannot be seen an increase in any DRL signal that can explain the LeTID. These obeservations leads to the conclusions of the thesis.

The first conclusion is that the hydrogen plays a part in the LeTID and that hydrogen is activated in the wafer when the temperature is increased. The second

conclusion is that LeTID decreases towards the top of the ingot, and the third conclusion is that LeTID is mainly caused by non-radiative recombination. The results of this thesis strongly indicates that neither cobalt nor nickel is playing a part in the LeTID, which contradicts the proposition by Bredemeier et al. [28]. On the other hand, the results of the thesis supports the theory of LeTID being caused by migrating hydrogen that interacts with the dopant atoms, proposed by Chen et al. [12].

The main goal of this thesis was to contribute to the research on LeTID utilizing hyperspectral imaging. This has been acheived by completing three of the thesis' four sub goals. The thesis has contributed to a deeper understanding of the role of hydrogen in the LeTID, as it has verified the participation of hydrogen. In addition, the results indicates that hydrogen is simultaneuously causing LeTID and passivating defects. The results of the study shows that LeTID is disappearing towards the top of the ingot, which completes sub goal two. The most plausible reason for this seems to be the increased level of dopant atoms towards the top. Sub goal number four was also completed. The results of the study is indicating that Chen et al.'s theory [12] is plausible, while they contradict the theory of Bredemeier et al. [28]. The third sub goal, finding a DRL signal that could be tied to the LeTID, was not completed. The inability to find a signal that could be tied to LeTID led to the third conclusion of LeTID mainly being caused by non-radiative recombination.

6.2 Further work

The main uncertainty tied to the results of this thesis is the lack of a reference wafer during the hyperspectral imaging. To diminsh this uncertainty, the experiment of the thesis could be repeated with a reference wafer and the set of the reserve samples from the thesis. Repeating the experiment with a reference wafer could verify the results of this thesis.

As the involvement of hydrogen in LeTID seems to be indisputable, further work should focus on hydrogenated samples. A further study of non-hydrogenated samples seems superfluous. Since the concentration of numerous elements varies with regard to height in a silicon ingot, it is hard to draw a clear conclusion for the involvement of the dopant atoms in LeTID when studying wafers of different heights. A further reasearch on the involvement of dopant atoms in LeTID could thus be recommendable. This could be done by comparing wafers cut from the same height of ingots with different initial concentrations of dopant atoms, and

with the methodology performed in this thesis.

Bibliography

[1] IEA, *Data and statistics*, Available at https://www.iea.org/reports/world-energy-outlook-2019#shale-and-solar-revolutions (2020/05/24).

[2] IPCC, *Climate change 2014 synthesis report summary for policymakers*, Available at https://www.ipcc.ch/site/assets/uploads/2018/02/AR5_SYR_FINAL_SPM.pdf (2020/05/25).

[3] O. Edenhofer, R. Pichs-Madruga, Y. Sokona, J. C. Minx, E. Farahani *et al.*, *Climate change 2014 mitigation of climate change working group iii contribution to the fifth assessment report of the intergovernmental panel on climate change*, Available at https://www.ipcc.ch/site/assets/uploads/2018/02/ipcc_wg3_ar5_full.pdf (2020/05/25).

[4] A. Detollenaere, J. Wetter, G. Masson, I. Kaizuka, A. Jäger-Waldau and J. Donoso, 'Snapshot of global pv markets 2020 pvps task 1 strategic pv analysis and outreach', IAE-PVPS, Tech. Rep., Apr. 2020. DOI: 10.13140/RG.2.2.24096.74248.

[5] IEA, *World energy outlook 2019*, Available at https://www.iea.org/reports/world-energy-outlook-2019#shale-and-solar-revolutions (2020/05/24), 2019.

[6] ITRPV, 'International technology roadmap for photovoltaic (itrpv) - 2019 results', Tech. Rep., 2020. [Online]. Available: https://itrpv.vdma.org/documents/27094228/29066965/ITRPV02020.pdf/ba3da187-3186-83de-784e-6e3b10d96f3f.

[7] K. Ramspeck, S. Zimmermann, H. Nagel, A. Metz, Y. Gassenbauer, B. Birkmann and A. Seidl, 'Light induced degradation of rear passivated mc-si solar cells', *Proc. 27th Eur. Photovoltaic Solar Energy Conf.*, pp. 861–865, Jan. 2012. DOI: 10.4229/27thEUPVSEC2012-2DO.3.4.

[8] F. Kersten, P. Engelhart, H.-C. Ploigt, A. Stekolnikov, T. Lindner, F. Stenzel, M. Bartzsch, A. Szpeth, K. Petter, J. Heitmann and J. W. Müller, 'Degradation of multicrystalline silicon solar cells and modules after illumination at elevated temperature', *Solar Energy Materials and Solar Cells*, vol. 142, pp. 83 –86, 2015, Proceedings of the 5th International Conference on Crystalline Silicon Photovoltaics (SiliconPV 2015), ISSN: 0927-0248. DOI: https://doi.org/10.1016/j.solmat.2015.06.015. [Online]. Available: http://www.sciencedirect.com/science/article/pii/S0927024815002846.

[9] D. L. I. B. E. O. Torbjørn Mehl Tabea Luka, 'Study of changes in pl spectrum from defects in perc solar cells with respect to letid', *SiliconPV 2019*, 2019.

[10] R. Eberle, W. Kwapil, F. Schindler, M. C. Schubert and S. W. Glunz, 'Impact of the firing temperature profile on light induced degradation of multicrystalline silicon', *physica status solidi (RRL) – Rapid Research Letters*, vol. 10, no. 12, pp. 861–865, 2016. DOI: 10.1002/pssr.201600272. eprint: https://onlinelibrary.wiley.com/doi/pdf/10.1002/pssr.201600272. [Online]. Available: https://onlinelibrary.wiley.com/doi/abs/10.1002/pssr.201600272.

[11] C. Chan, T. H. Fung, M. Abbott, D. Payne, A. Wenham, B. Hallam, R. Chen and S. Wenham, 'Modulation of carrier-induced defect kinetics in multi-crystalline silicon perc cells through dark annealing', *Solar RRL*, vol. 1, no. 2, p. 1 600 028, 2017. DOI: 10.1002/solr.201600028. eprint: https://onlinelibrary.wiley.com/doi/pdf/10.1002/solr.201600028. [Online]. Available: https://onlinelibrary.wiley.com/doi/abs/10.1002/solr.201600028.

[12] D. Chen, P. Hamer, M. Kim, C. Chan, A. C. nee Wenham], F. Rougieux, Y. Zhang, M. Abbott and B. Hallam, 'Hydrogen-induced degradation: Explaining the mechanism behind light- and elevated temperature-induced degradation in n- and p-type silicon', *Solar Energy Materials and Solar Cells*, vol. 207, p. 110 353, 2020, ISSN: 0927-0248. DOI: https://doi.org/10.1016/j.solmat.2019.110353. [Online]. Available: http://www.sciencedirect.com/science/article/pii/S0927024819306798.

[13] R. Søndenå, H. Haug, C. C. You, J. Zhu and M. S. Wiig, 'Evolution of defect densities with height in a hpmc-si ingot', *AIP Conference Proceedings*, vol. 2147, no. 1, p. 140 010, 2019. DOI: 10.1063/1.5123897. eprint: https://aip.scitation.org/doi/pdf/10.1063/1.5123897. [Online]. Available: https://aip.scitation.org/doi/abs/10.1063/1.5123897.

[14] K. Petter, K. Hübener, F. Kersten, M. Bartzsch, F. Fertig and J. Müller, *Dependence of letid on brick height for different wafer suppliers with several resistivities and dopants*, Available at https://tu-freiberg.de/sites/

default/files/media/institut-fuer-angewandte-physik-7681/paper/petter2016.pdf (2020/05/26), 2016.

[15] O. I. R. v. S. M. Z. Arno Smets Klaus Jäger, *Solar Energy, The Physics and Engineering of Photovoltaic conversion, technologies and systems*. UiT Cambridge Ltd, 2016.

[16] L. N. Robert L. Boylestad, *Electronic Devices and Circuit Theory*, eleventh. Pearson Education Limited, 2014.

[17] A. Hangleiter, 'Experimental proof of impurity auger recombination in silicon', *Phys. Rev. Lett.*, vol. 55, pp. 2976–2978, 27 1985. DOI: 10.1103/PhysRevLett.55.2976. [Online]. Available: https://link.aps.org/doi/10.1103/PhysRevLett.55.2976.

[18] T. Mehl, 'Hyperspectral photoluminescence of silicon wafers and solar cells', PhD thesis, Norwegian University of Life Sciences, 2018.

[19] N. Drozdov, A. Patryn and V. Tkachev, 'Recombination radiation on dislocations in silicon', *Soviet Journal of Experimental and Theoretical Physics Letters*, vol. 23, Jun. 1976.

[20] S. Pizzini, M. Acciarri, E. Leoni and A. Le Donne, 'About the d1 and d2 dislocation luminescence and its correlation with oxygen segregation', *physica status solidi (b)*, vol. 222, no. 1, pp. 141–150, 2000. DOI: 10.1002/1521-3951(200011)222:1⟨141::AID-PSSB141⟩3.0.CO;2-H. eprint: https://onlinelibrary.wiley.com/doi/pdf/10.1002/1521-3951%28200011%29222%3A1%3C141%3A%3AAID-PSSB141%3E3.0.CO%3B2-H. [Online]. Available: https://onlinelibrary.wiley.com/doi/abs/10.1002/1521-3951%28200011%29222%3A1%3C141%3A%3AAID-PSSB141%3E3.0.CO%3B2-H.

[21] A. Flø, I. Burud, K. Kvaal, R. Søndenå and E. Olsen, 'Distribution of radiative crystal imperfections through a silicon ingot', *AIP Advances*, vol. 3, no. 11, p. 112 120, 2013. DOI: 10.1063/1.4834155. eprint: https://doi.org/10.1063/1.4834155. [Online]. Available: https://doi.org/10.1063/1.4834155.

[22] A. Flø, 'Hyperspectral imaging as a tool for characterization of multicrystalline silicon wafers', PhD thesis, Norwegian University of Life Sciences, 2014.

[23] M. A. Green and U. of New South Wales., *Solar cells : operating principles, technology and system applications / Martin A. Green*, English. University of New South Wales Kensington, N.S.W, 1992, xiv, 274 pages : ISBN: 0858235803.

[24] S. G. C. H. Tabea Luka Marko Turek, 'Light induced degradation - defect gettering at grain boundaries', *EU PVSEC 2017*, 2017.

[25] C. Vargas, Y. Zhu, G. Coletti, C. Chan, D. Payne, M. Jensen and Z. Hameiri, 'Recombination parameters of lifetime-limiting carrier-induced defects in multicrystalline silicon for solar cells', *Applied Physics Letters*, vol. 110, no. 9, p. 092 106, 2017. DOI: 10.1063/1.4977906. eprint: https://doi.org/10.1063/1.4977906. [Online]. Available: https://doi.org/10.1063/1.4977906.

[26] R. Søndenå and M. S. Wiig, 'Evolution of the light sensitive defects in high performance multicrystalline silicon wafers', *Journal of Applied Physics*, vol. 125, no. 8, p. 085 701, 2019. DOI: 10.1063/1.5079496. eprint: https://doi.org/10.1063/1.5079496. [Online]. Available: https://doi.org/10.1063/1.5079496.

[27] A. Herguth, G. Schubert, M. Kaes and G. Hahn, 'Investigations on the long time behavior of the metastable boron–oxygen complex in crystalline silicon', *Progress in Photovoltaics: Research and Applications*, vol. 16, no. 2, pp. 135–140, 2008. DOI: 10.1002/pip.779. eprint: https://onlinelibrary.wiley.com/doi/pdf/10.1002/pip.779. [Online]. Available: https://onlinelibrary.wiley.com/doi/abs/10.1002/pip.779.

[28] D. Bredemeier, D. C. Walter and J. Schmidt, 'Possible candidates for impurities in mc-si wafers responsible for light-induced lifetime degradation and regeneration', *Solar RRL*, vol. 2, no. 1, p. 1 700 159, 2018. DOI: 10.1002/solr.201700159. eprint: https://onlinelibrary.wiley.com/doi/pdf/10.1002/solr.201700159. [Online]. Available: https://onlinelibrary.wiley.com/doi/abs/10.1002/solr.201700159.

[29] J. M. Amigo, 'Chapter 1.1 - hyperspectral and multispectral imaging: Setting the scene', in *Hyperspectral Imaging*, ser. Data Handling in Science and Technology, J. M. Amigo, Ed., vol. 32, Elsevier, 2020, pp. 3 –16. DOI: https://doi.org/10.1016/B978-0-444-63977-6.00001-8. [Online]. Available: http://www.sciencedirect.com/science/article/pii/B9780444639776000018.

[30] A. I. L. Maldonado, H. R. Fuentes and J. A. V. Contreras, *Hyperspectral imaging in Agriculture, Food and Evironment*. IntechOpen, 2018. [Online]. Available: https://www.intechopen.com/books/hyperspectral-imaging-in-agriculture-food-and-environment.

[31] Y. Yoshida and G. Langouche, *Defects and Impurities in Silicon Materials: An Introduction to Atomic-Level Silicon Engineering*, ser. Lecture Notes in Physics. Springer Japan, 2016, ISBN: 9784431558002. [Online]. Available: https://books.google.no/books?id=YF3eCwAAQBAJ.

[32] K. Nakajima, 'Chapter 1 - basic growth and crystallographic quality of si crystals for solar cells', in *Crystal Growth of Si Ingots for Solar Cells Using Cast Furnaces*, K. Nakajima, Ed., Elsevier, 2020, pp. 1 –61, ISBN: 978-0-12-819748-6. DOI: https://doi.org/10.1016/B978-0-12-819748-6.00001-3. [Online]. Available: http://www.sciencedirect.com/science/article/pii/B9780128197486000013.

[33] R. Søndenå, H. Haug, A. Song, C.-C. Hsueh and J. O. Odden, 'Resistivity profiles in multicrystalline silicon ingots featuring gallium co-doping', *AIP Conference Proceedings*, vol. 1999, no. 1, p. 130 016, 2018. DOI: 10.1063/1.5049335. eprint: https://aip.scitation.org/doi/pdf/10.1063/1.5049335. [Online]. Available: https://aip.scitation.org/doi/abs/10.1063/1.5049335.

[34] D. Oriwol, M. Trempa, L. Sylla and H. S. Leipner, 'Investigation of dislocation cluster evolution during directional solidification of multicrystalline silicon', *Journal of Crystal Growth*, vol. 463, pp. 1 –9, 2017, ISSN: 0022-0248. DOI: https://doi.org/10.1016/j.jcrysgro.2017.01.027. [Online]. Available: http://www.sciencedirect.com/science/article/pii/S0022024817300337.

[35] M. Kivambe, G. Stokkan, T. Ervik, S. Castellanos, J. Hofstetter and T. Buonassisi, 'The impact of dislocation structure on impurity decoration of dislocation clusters in multicrystalline silicon', *Solid State Phenomena*, vol. 205-206, pp. 71–76, Oct. 2013. DOI: 10.4028/www.scientific.net/SSP.205-206.71.

[36] Sumino, K., 'Interaction between dislocations and impurities in silicon', *J. Phys. Colloques*, vol. 44, pp. C4–195–C4–205, 1983. DOI: 10.1051/jphyscol:1983424. [Online]. Available: https://doi.org/10.1051/jphyscol:1983424.

[37] B. Ryningen, G. Stokkan, M. Kivambe, T. Ervik and O. Lohne, 'Growth of dislocation clusters during directional solidification of multicrystalline silicon ingots', *Acta Materialia - ACTA MATER*, vol. 59, pp. 7703–7710, Dec. 2011. DOI: 10.1016/j.actamat.2011.09.002.

[38] B. J. Hallam, P. G. Hamer, A. M. Ciesla née Wenham, C. E. Chan, B. Vicari Stefani and S. Wenham, 'Development of advanced hydrogenation processes for silicon solar cells via an improved understanding of the behaviour of hydrogen in silicon', *Progress in Photovoltaics: Research and Applications*, vol. n/a, no. n/a, DOI: 10.1002/pip.3240. eprint: https://onlinelibrary.wiley.com/doi/pdf/10.1002/pip.3240. [Online]. Available: https://onlinelibrary.wiley.com/doi/abs/10.1002/pip.3240.

[39] K. Adamczyk, 'Recombination strength of dislocations in high-performance multicrystalline/quasi-mono hybrid wafers during solar cell processing', *Physica Status Solidi*, 2017.

[40] S. G. C. H. Tabea Luka Marko Turek, 'Microstructure and recombination activity of grain boundaries from front and rear side during a lid-cycle of mc-perc solar cells', *IEEE PVSC 2017*, 2017.

Appendix A

Extra figures

A.1 Extra spectrum development figures

This section displays the figures of the spectral development for sample 4D, sample 5D and 8D, refered to in the main text.

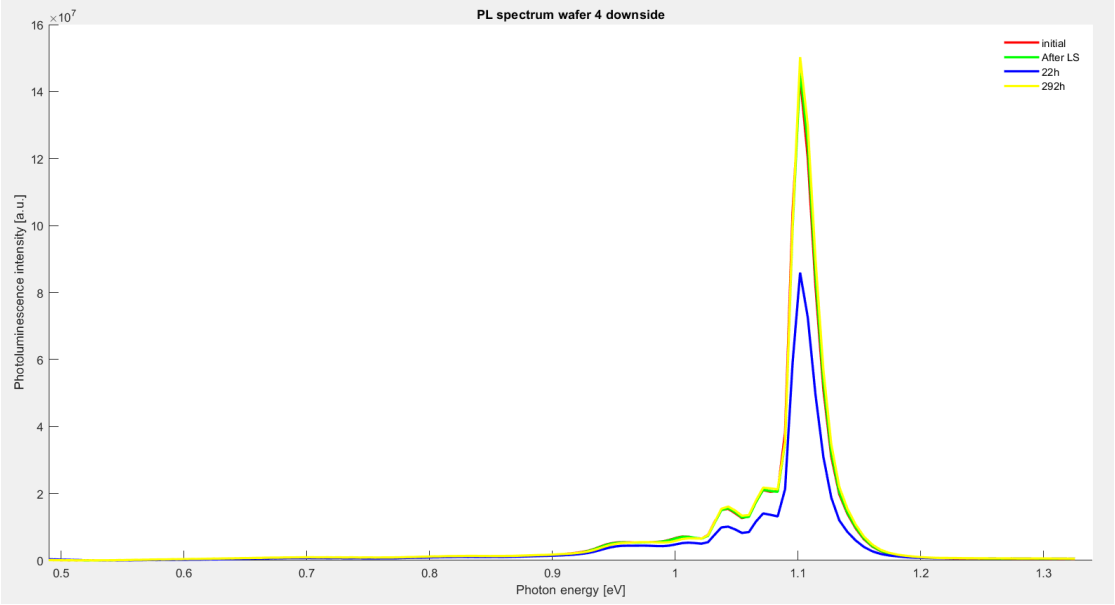

Figure A.1: Photoluminescence spectrum of the downside of sample nr. 4. The red line is the initial spectrum, the green line is the spectrum after light soaking, the blue line is the spectrum when the sample is fully degraded and the yellow line is the spectrum after the sample has regenerated.

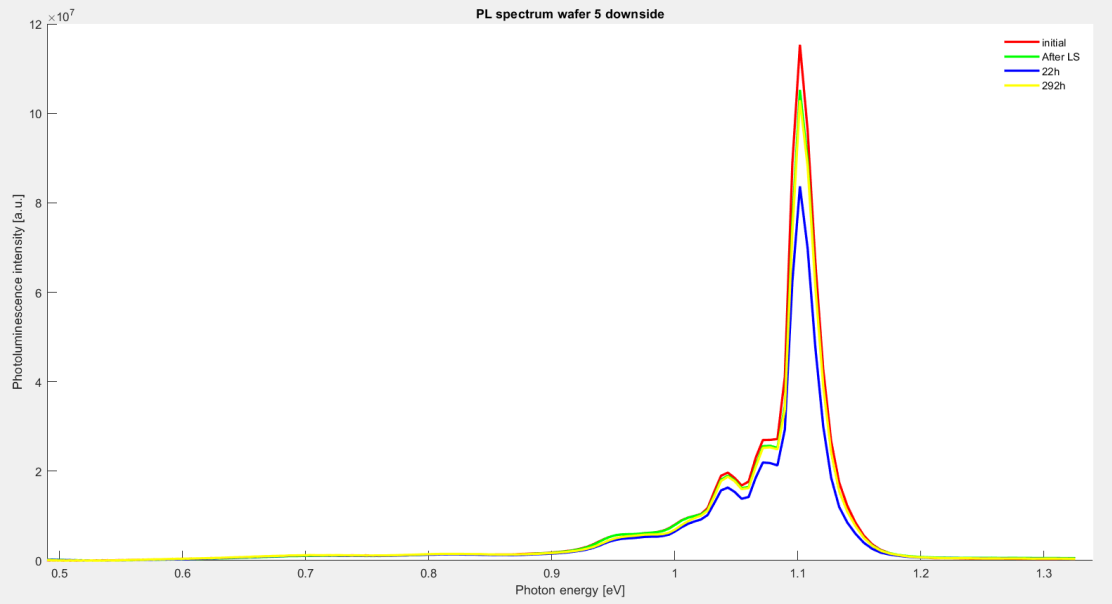

Figure A.2: Photoluminescence spectrum of the downside of sample nr. 5. The red line is the initial spectrum, the green line is the spectrum after light soaking, the blue line is the spectrum when the sample is fully degraded and the yellow line is the spectrum after the sample has regenerated.

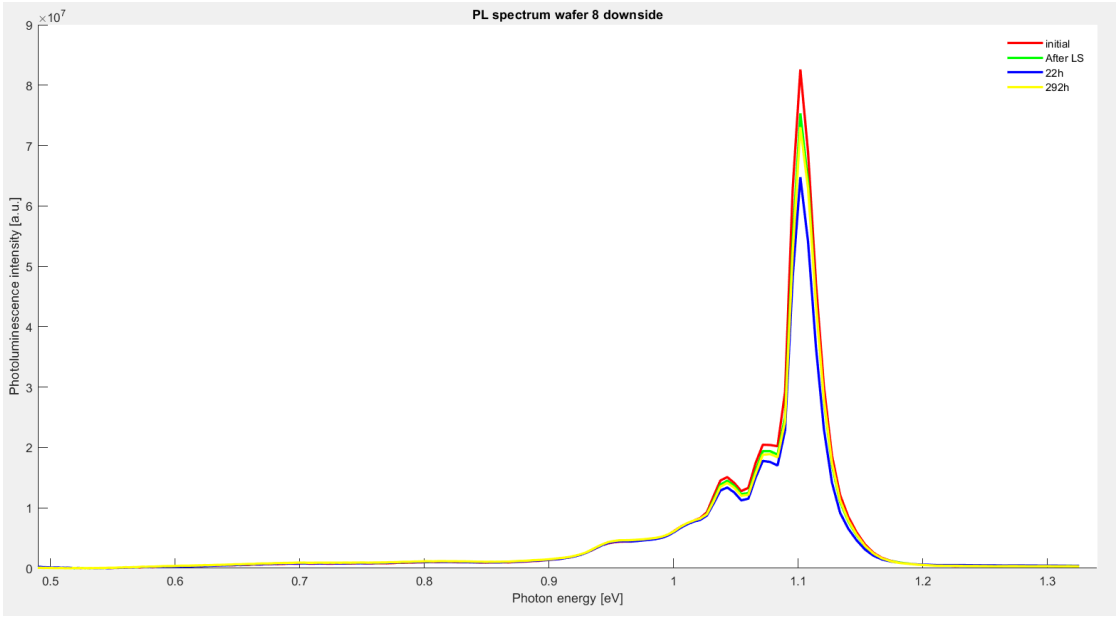

Figure A.3: Photoluminescence spectrum of the downside of sample nr. 8. The red line is the initial spectrum, the green line is the spectrum after light soaking, the blue line is the spectrum when the sample is fully degraded and the yellow line is the spectrum after the sample has regenerated.

A.2 Extra figures relative DRL development

This section shows the extra figure of the spatial development of the D3-signal for sample 1 and 6. It also shows the figure of the relative photoluminescence specturm development for sample 2 and 4. Both of which are refered to in the main text.

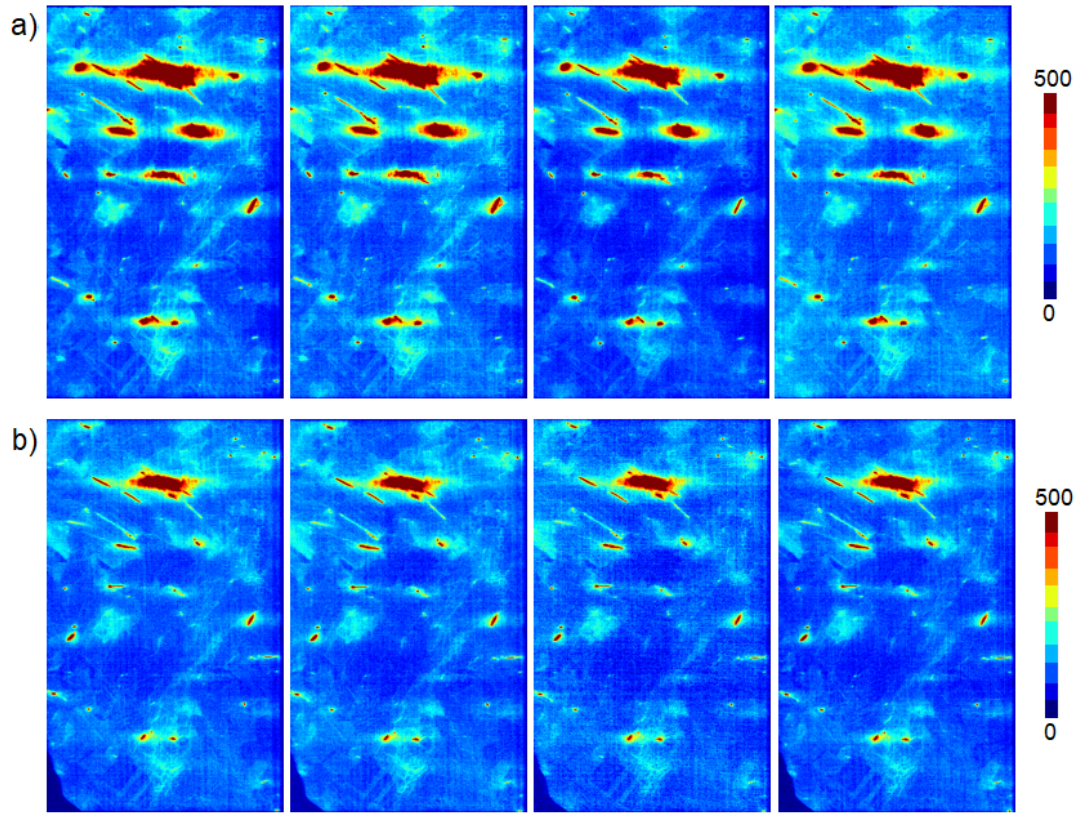

Figure A.4: Spatial development of the D3-signal over time for: a) sample 1 and b) sample 6. The images are from left the initial image, image after light soaking, fully degraded and fully regenerated. The colour of the pixel indicates the strength of the signal.

a)

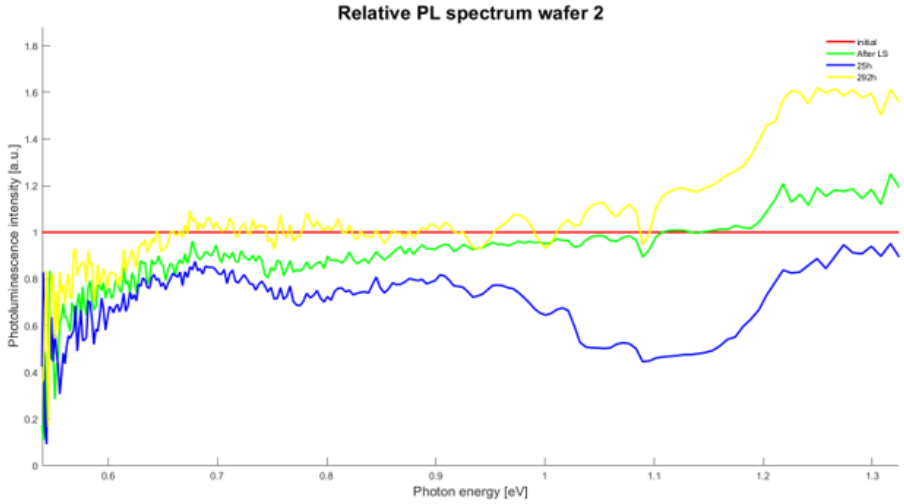

b)

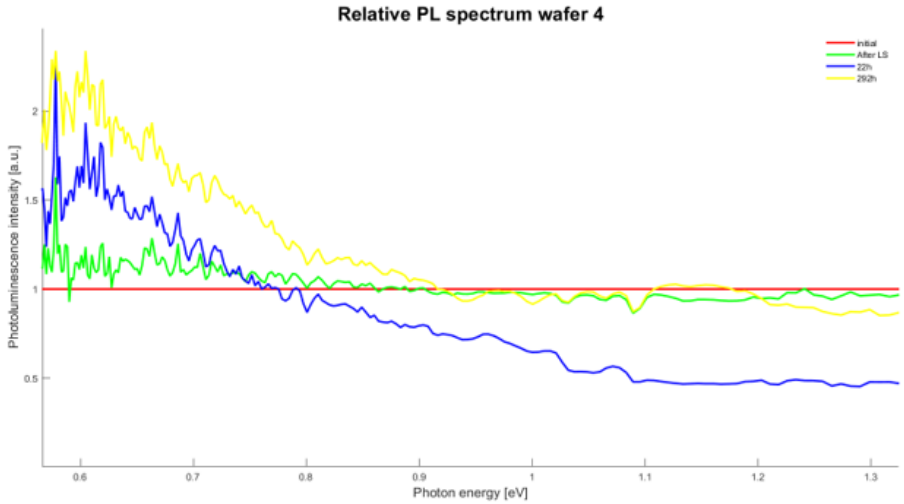

Figure A.5: The figure compares the relative changes in the PL-signal of: a) sample 2 and b) sample 4. The PL spectrums are divided by their respective initial PL spectrum, to show how the signals develop through prossesing.

Appendix B

Example Matlab Codes

This appendix shows examples of the scripts used in this thesis for the data analysis. The appendix contains the script used to create the medaian of 3 images. The script used to display the spatial development of the different PL-signals is also contained in this appendix. Thirdly, the script used to generate the spectrum of the different images and plot them together can be seen. The last script displayed in this appendix is the script used initially to track the development of the samples' BB-signal during the imaging. All of the scripts is heavily based on scripts written by Torbjørn Mehl and they all makes use of functions written by Torbjørn Mehl.

The Matlab-script used to create the median of 3 images

```
1  %MakeMedianOfThree_example.m
2
3  addpath ('C:\Users\Rasmus Svebestad\Documents\Skole\Masteroppgave\
       Matlab\0Kode');
4
5  addpath ('C:\Users\Rasmus Svebestad\Documents\Skole\Masteroppgave\
       Matlab\0Kode\LoadImage');
6
7  addpath ('C:\Users\Rasmus Svebestad\OneDrive - Norwegian University
       of Life Sciences\Data Master');
8
9  %load('Energi_specimOct2014.mat')
10
11 BB=(30:34); D4=(48:52); D3=(59:64); D2=(77:82); D1=(93:99); D07
       =(116:143);
12
```

```
13 SUB=(67:124); TD=(110:149); ALT=(25:250);
14
15
16 %%
17
18 % load images and view them
19
20 fn1 = 'REC_pdgh_init_34D-2';
21
22 fn2 = 'REC_pdgh_init_34D-3';
23
24 fn3 = 'REC_pdgh_init_34D-4';
25
26 img1 = load_subtract_correct_v20200101(fn1);
27
28 img2 = load_subtract_correct_v20200101(fn2);
29
30 img3 = load_subtract_correct_v20200101(fn3);
31
32
33 PL = BB;
34
35
36 imtool(sum(img1(:,:,PL),3),[],'Colormap',jet)
37
38 imtool(sum(img2(:,:,PL),3),[],'Colormap',jet)
39
40 imtool(sum(img3(:,:,PL),3),[],'Colormap',jet)
41
42
43 %%
44
45 % crop images
46
47 % x : horizontal   y : vertical
48
49 PL = ALT;
50
51 Magn = 400;
52
53
54 %Q4_143um90K_REF_75C_0_2sun_048h 0 -1 0
55
56 %x1 = 4;       y1 = 7;
57
58 %x2 = x1+298; y2 = y1+599;
59
60
61 %Q4_143um90K_REF_75C_0_2sun_050h 0 0 1
```

```
% 0 0 1 er justering - er opp og + er ned
% dx dy dz


x1 = 1;        y1 = 539;

x2 = x1+300;   y2 = y1+500;


dy1 = 0;    % align up/down (try to not use, only use dy2 and dy3)

dx1 = 0;    % align sidewise(try to not use, only use dx2 and dx3)

imtool(sum(img1((y1+dy1):(y2+dy1), (x1+dx1):(x2+dx1),PL),3),[],'
    Colormap',jet,'InitialMagnification',Magn)


dy2 = 0;  % align up/down

dx2 = 0;  % align sidewise

imtool(sum(img2((y1+dy2):(y2+dy2), (x1+dx2):(x2+dx2),PL),3),[],'
    Colormap',jet,'InitialMagnification',Magn)


dy3 = 0;  % align up/down

dx3 = 0;  % align sidewise

imtool(sum(img3((y1+dy3):(y2+dy3), (x1+dx3):(x2+dx3),PL),3),[],'
    Colormap',jet,'InitialMagnification',Magn)


%%

% make median of 3 images and save to file

REC_pdgh_init_4D = MakeMedianImg(img1((y1+dy1):(y2+dy1), (x1+dx1):(
    x2+dx1),:),img2((y1+dy2):(y2+dy2), (x1+dx2):(x2+dx2),:), img3((
    y1+dy3):(y2+dy3), (x1+dx3):(x2+dx3),:));


save('REC_pdgh_init_4D.mat','REC_pdgh_init_4D','-v7.3');


imtool(sum(REC_pdgh_init_4D(:,:,PL),3),[],'Colormap',jet)
```

The Matlab-script used to display the spatial development of the different PL-signals

```
% Setup

clc, clear

load('Energi_specimOct2014.mat')

BB=(30:34); D4=(48:52); D3=(59:64); D2=(77:82); D1=(93:99); D07
    =(116:143);

%%
% Loading the saved images

% Loading the initial image
load('REC_pdgh_init_4D.mat')

% Loading the image after lightsoaking
load('REC_pdgh_LS66h_4D.mat')

% Loading the bottom image
load('REC_pdgh_022h_4D.mat')

% Loading the top image
load('REC_pdgh_292h_4D.mat')

%%
% Loading extra image
load('REC_pdgh_292h_3.mat')

%%
% Displaying the images of the samples with PL-signal PL

PL = D4;

Magn = 100;

range = [0 500];


imtool(sum(REC_pdgh_init_3(:, :, PL),3),range,'Colormap',jet,'
    InitialMagnification',Magn)

imtool(sum(REC_pdgh_LS66h_4(:, :, PL),3),range,'Colormap',jet,'
    InitialMagnification',Magn)

```

```
imtool(sum(REC_pdgh_022h_3(:, :, PL),3),range,'Colormap',jet,'
    InitialMagnification',Magn)

imtool(sum(REC_pdgh_240h_3(:, :, PL),3),range,'Colormap',jet,'
    InitialMagnification',Magn)

%%
% Display extra image

imtool(sum(REC_pdgh_292h_3(:, :, PL),3),range,'Colormap',jet,'
    InitialMagnification',Magn)
```

The Matlab-script used to generate spectrums and plot them together

```
% To generate spectras with the imgSpectrum function

spec11 = imgSpectrum(REC_pdgh_init_3(440-1:500-1, 189-2:257-2, :));
spec12 = imgSpectrum(REC_pdgh_LS66h_4(440-1:500-1, 189-3:257-3, :));
spec13 = imgSpectrum(REC_pdgh_022h_3(440:500, 189-4:257-4, :));
spec14 = imgSpectrum(REC_pdgh_240h_3(440-1:500-1, 189:257, :));

%%
spec11 = imgSpectrum(REC_pdgh_init_4D(418:498, 64:168, :));
spec12 = imgSpectrum(REC_pdgh_LS66h_4D(418:498, 64+1:168+1, :));
spec13 = imgSpectrum(REC_pdgh_022h_4D(418+2:498+2, 64:168, :));
spec14 = imgSpectrum(REC_pdgh_292h_4D(418:498, 64+3:168+3, :));

%%
% To compare spectras of different samples new variables are made

spec21 = imgSpectrum(REC_pdgh_init_4D(:, :, :));
spec22 = imgSpectrum(REC_pdgh_LS66h_4D(:, :, :));
spec23 = imgSpectrum(REC_pdgh_022h_4D(:, :, :));
spec24 = imgSpectrum(REC_pdgh_292h_4D(:, :, :));
%%
% Generating curves to compare time development
PL = D07;

spectra1 = [sum(spec11(PL)), sum(spec12(PL)), sum(spec13(PL)), sum(
    spec14(PL))] / sum(spec12(PL));
spectra2 = [sum(spec21(PL)), sum(spec22(PL)), sum(spec23(PL)), sum(
    spec24(PL))] / sum(spec22(PL));
time = [0, 66, 88, 358];

%%
```

```
30 % Plotting the time development of PL-signals of the two different
       spectras
31
32 figure;
33 hold on;
34
35 xlabel('Time [h]');
36 ylabel('Photoluminescence intensity [a.u.]');
37
38 title('D07-signal')
39
40 plot(time,spectra1,'r','LineWidth',2)
41 plot(time,spectra2,'b','LineWidth',2)
42
43 legend('Dislocation cluster', 'BB-region');
44
45 hold off;
46
47 %%
48 % Plotting the 4 spectrums initial, LS, degraded and regenerated
49
50 figure;
51 hold on;
52
53 xlim([0.49 1.34]);
54 xlabel('Photon energy [eV]', 'FontSize', 14);
55 ylabel('Photoluminescence intensity [a.u.]', 'FontSize', 14);
56
57 title('Relative PL spectrum wafer 5 downside', 'FontSize', 20)
58
59 plot(Ev,spec21,'r','LineWidth',2)
60
61 plot(Ev,spec22,'g','LineWidth',2)
62
63 plot(Ev,spec23,'b','LineWidth',2)
64
65 plot(Ev,spec24,'y','LineWidth',2)
66
67 legend('initial', 'After LS', '22h', '292h');
68
69 hold off;
70
71 %%
72 % Plotting the 4 spectrums initial, LS, degraded and regenerated of
       two
73 % different samples
74
75 figure;
76 hold on;
```

```
77
78  xlim([0.49 1.34])
79  xlabel('Photon energy [eV]')
80  ylabel('Photoluminescence intensity [a.u.]')
81  legend("initial", "After LS", "22h", "240h");
82
83  title('Comparing 4 and 6')
84
85  plot(Ev,spec11,'r','LineWidth',2)
86
87  plot(Ev,spec12,'g','LineWidth',2)
88
89  plot(Ev,spec13,'b','LineWidth',2)
90
91  plot(Ev,spec14,'y','LineWidth',2)
92
93  plot(Ev,spec21,'-.r','LineWidth',2)
94
95  plot(Ev,spec22,'-.g','LineWidth',2)
96
97  plot(Ev,spec23,'-.b','LineWidth',2)
98
99  plot(Ev,spec24,'-.y','LineWidth',2)
```

The Matlab-script used to track the development of the samples' BB-signal during the imaging process

```
1  addpath ('C:\Users\Rasmus Svebestad\Documents\Skole\Masteroppgave\
       Matlab\0Kode');
2
3  addpath ('C:\Users\Rasmus Svebestad\Documents\Skole\Masteroppgave\
       Matlab\0Kode\LoadImage');
4
5  load('Energi_specimOct2014.mat')
6
7  BB=(30:34);D4=(48:52);D3=(59:64);D2=(77:82);D1=(93:99);D07=(116:143)
       ;NEW=(95:105);NEW2=(120:190);
8
9
10 %%
11
12 fn1 = 'REC_pdgh_init_78D-4';
13 meanspec1 = mean_spectra(fn1);
14
15 fn2 = 'REC_pdgh_LS66h_78D-4';
16 meanspec2 = mean_spectra(fn2);
```

```
17
18 fn3 = 'REC_pdgh_010h_78D-4';
19 meanspec3 = mean_spectra(fn3);
20
21 fn4 = 'REC_pdgh_022h_78D-4';
22 meanspec4 = mean_spectra(fn4);
23
24 fn5 = 'REC_pdgh_025h_78D-4';
25 meanspec5 = mean_spectra(fn5);
26
27 fn6 = 'REC_pdgh_044h_78D-4';
28 meanspec6 = mean_spectra(fn6);
29
30 fn7 = 'REC_pdgh_066h_78D-4';
31 meanspec7 = mean_spectra(fn7);
32
33 fn8 = 'REC_pdgh_075h_78D-4';
34 meanspec8 = mean_spectra(fn8);
35
36 fn9 = 'REC_pdgh_087h_78D-4';
37 meanspec9 = mean_spectra(fn9);
38
39 fn10 = 'REC_pdgh_108h_78D-4';
40 meanspec10 = mean_spectra(fn10);
41
42 fn11 = 'REC_pdgh_127h_78D-4';
43 meanspec11 = mean_spectra(fn11);
44
45 fn12 = 'REC_pdgh_157h_78D-4';
46 meanspec12 = mean_spectra(fn12);
47
48 fn13 = 'REC_pdgh_177h_78D-4';
49 meanspec13 = mean_spectra(fn13);
50
51 fn14 = 'REC_pdgh_214h_78D-4';
52 meanspec14 = mean_spectra(fn14);
53
54 fn15 = 'REC_pdgh_240h_78D-4';
55 meanspec15 = mean_spectra(fn15);
56
57 fn16 = 'REC_pdgh_273h_78D-4';
58 meanspec16 = mean_spectra(fn16);
59
60 fn17 = 'REC_pdgh_292h_78D-4';
61 meanspec17 = mean_spectra(fn17);
62
63 fn18 = 'REC_pdgh_314h_78D-4';
64 meanspec18 = mean_spectra(fn18);
65
```

```
fn19 = 'REC_pdgh_356h_78D-4';
meanspec19 = mean_spectra(fn19);

fn20 = 'REC_pdgh_381h_78D-4';
meanspec20 = mean_spectra(fn20);



%%


fn1 = 'REC_pdgh_init_12-4';
spec1 = load_spectra(fn1, 25, 525);
spec1 = spec1./meanspec1;

fn2 = 'REC_pdgh_LS66h_12D-4';
spec2 = load_spectra(fn2, 25, 525);
spec2 = spec2./meanspec2;

fn3 = 'REC_pdgh_010h_12D-4';
spec3 = load_spectra(fn3, 25, 525);
spec3 = spec3./meanspec3;

fn4 = 'REC_pdgh_022h_12D-4';
spec4 = load_spectra(fn4, 25, 525);
spec4 = spec4./meanspec4;

fn5 = 'REC_pdgh_025h_12D-4';
spec5 = load_spectra(fn5, 25, 525);
spec5 = spec5./meanspec5;

fn6 = 'REC_pdgh_044h_12D-4';
spec6 = load_spectra(fn6, 25, 525);
spec6 = spec6./meanspec6;

fn7 = 'REC_pdgh_066h_12D-4';
spec7 = load_spectra(fn7, 25, 525);
spec7 = spec7./meanspec7;

fn8 = 'REC_pdgh_075h_12D-4';
spec8 = load_spectra(fn8, 25, 525);
spec8 = spec8./meanspec8;

fn9 = 'REC_pdgh_087h_12D-4';
spec9 = load_spectra(fn9, 25, 525);
spec9 = spec9./meanspec9;

fn10 = 'REC_pdgh_108h_12D-4';
spec10 = load_spectra(fn10, 25, 525);
```

```
115 spec10 = spec10./meanspec10;
116
117 fn11 = 'REC_pdgh_127h_12D-4';
118 spec11 = load_spectra(fn11, 25, 525);
119 spec11 = spec11./meanspec11;
120
121 fn12 = 'REC_pdgh_157h_12D-4';
122 spec12 = load_spectra(fn12, 25, 525);
123 spec12 = spec12./meanspec12;
124
125 fn13 = 'REC_pdgh_177h_12D-4';
126 spec13 = load_spectra(fn13, 25, 525);
127 spec13 = spec13./meanspec13;
128
129 fn14 = 'REC_pdgh_214h_12D-4';
130 spec14 = load_spectra(fn14, 25, 525);
131 spec14 = spec14./meanspec14;
132
133 fn15 = 'REC_pdgh_240h_12D-4';
134 spec15 = load_spectra(fn15, 25, 525);
135 spec15 = spec15./meanspec15;
136
137 fn16 = 'REC_pdgh_273h_12D-4';
138 spec16 = load_spectra(fn16, 25, 525);
139 spec16 = spec16./meanspec16;
140
141 fn17 = 'REC_pdgh_292h_12D-4';
142 spec17 = load_spectra(fn17, 25, 525);
143 spec17 = spec17./meanspec17;
144
145 fn18 = 'REC_pdgh_314h_12D-4';
146 spec18 = load_spectra(fn18, 25, 525);
147 spec18 = spec18./meanspec18;
148
149 fn19 = 'REC_pdgh_356h_12D-4';
150 spec19 = load_spectra(fn19, 25, 525);
151 spec19 = spec19./meanspec19;
152
153 fn20 = 'REC_pdgh_381h_12D-4';
154 spec20 = load_spectra(fn20, 25, 525);
155 spec20 = spec20./meanspec20;
156
157 curve1 = [sum(spec1(BB)), sum(spec2(BB)), sum(spec3(BB)), sum(spec4(
        BB)), sum(spec5(BB)), sum(spec6(BB)), sum(spec7(BB)), sum(spec8(
        BB)), sum(spec9(BB)), sum(spec10(BB)), sum(spec11(BB)), sum(
        spec12(BB)), sum(spec13(BB)), sum(spec14(BB)), sum(spec15(BB)),
        sum(spec16(BB)), sum(spec17(BB)), sum(spec18(BB)), sum(spec19(BB
        )), sum(spec20(BB))]./sum(spec2(BB));
158
```

```
159
160 fn1 = 'REC_pdgh_init_12D-4';
161 spec1 = load_spectra(fn1, 530, 1100);
162 spec1 = spec1./meanspec1;
163
164 fn2 = 'REC_pdgh_LS66h_12D-4';
165 spec2 = load_spectra(fn2, 530, 1100);
166 spec2 = spec2./meanspec2;
167
168 fn3 = 'REC_pdgh_010h_12D-4';
169 spec3 = load_spectra(fn3, 530, 1100);
170 spec3 = spec3./meanspec3;
171
172 fn4 = 'REC_pdgh_022h_12-4';
173 spec4 = load_spectra(fn4, 530, 1100);
174 spec4 = spec4./meanspec4;
175
176 fn5 = 'REC_pdgh_025h_12D-4';
177 spec5 = load_spectra(fn5, 530, 1100);
178 spec5 = spec5./meanspec5;
179
180 fn6 = 'REC_pdgh_044h_12D-4';
181 spec6 = load_spectra(fn6, 530, 1100);
182 spec6 = spec6./meanspec6;
183
184 fn7 = 'REC_pdgh_066h_12D-4';
185 spec7 = load_spectra(fn7, 530, 1100);
186 spec7 = spec7./meanspec7;
187
188 fn8 = 'REC_pdgh_075h_12D-4';
189 spec8 = load_spectra(fn8, 530, 1100);
190 spec8 = spec8./meanspec8;
191
192 fn9 = 'REC_pdgh_087h_12D-4';
193 spec9 = load_spectra(fn9, 530, 1100);
194 spec9 = spec9./meanspec9;
195
196 fn10 = 'REC_pdgh_108h_12D-4';
197 spec10 = load_spectra(fn10, 530, 1100);
198 spec10 = spec10./meanspec10;
199
200 fn11 = 'REC_pdgh_127h_12D-4';
201 spec11 = load_spectra(fn11, 530, 1100);
202 spec11 = spec11./meanspec11;
203
204 fn12 = 'REC_pdgh_157h_12D-4';
205 spec12 = load_spectra(fn12, 530, 1100);
206 spec12 = spec12./meanspec12;
207
```

```
208 fn13 = 'REC_pdgh_177h_12D-4';
209 spec13 = load_spectra(fn13, 530, 1100);
210 spec13 = spec13./meanspec13;
211
212 fn14 = 'REC_pdgh_214h_12D-4';
213 spec14 = load_spectra(fn14, 530, 1100);
214 spec14 = spec14./meanspec14;
215
216 fn15 = 'REC_pdgh_240h_12D-4';
217 spec15 = load_spectra(fn15, 530, 1100);
218 spec15 = spec15./meanspec15;
219
220 fn16 = 'REC_pdgh_273h_12D-4';
221 spec16 = load_spectra(fn16, 530, 1100);
222 spec16 = spec16./meanspec16;
223
224 fn17 = 'REC_pdgh_292h_12D-4';
225 spec17 = load_spectra(fn17, 530, 1100);
226 spec17 = spec17./meanspec17;
227
228 fn18 = 'REC_pdgh_314h_12D-4';
229 spec18 = load_spectra(fn18, 530, 1100);
230 spec18 = spec18./meanspec18;
231
232 fn19 = 'REC_pdgh_356h_12D-4';
233 spec19 = load_spectra(fn19, 530, 1100);
234 spec19 = spec19./meanspec19;
235
236 fn20 = 'REC_pdgh_381h_12D-4';
237 spec20 = load_spectra(fn20, 530, 1100);
238 spec20 = spec20./meanspec20;
239
240 curve2 = [sum(spec1(BB)), sum(spec2(BB)), sum(spec3(BB)), sum(spec4(
        BB)), sum(spec5(BB)), sum(spec6(BB)), sum(spec7(BB)), sum(spec8(
        BB)), sum(spec9(BB)), sum(spec10(BB)), sum(spec11(BB)), sum(
        spec12(BB)), sum(spec13(BB)), sum(spec14(BB)), sum(spec15(BB)),
        sum(spec16(BB)), sum(spec17(BB)), sum(spec18(BB)), sum(spec19(BB
        )), sum(spec20(BB))]./sum(spec2(BB));
241
242 fn1 = 'REC_pdgh_init_34D-4';
243 spec1 = load_spectra(fn1, 125, 525);
244 spec1 = spec1./meanspec1;
245
246 fn2 = 'REC_pdgh_LS66h_34D-4';
247 spec2 = load_spectra(fn2, 125, 525);
248 spec2 = spec2./meanspec2;
249
250 fn3 = 'REC_pdgh_010h_34D-4';
251 spec3 = load_spectra(fn3, 125, 525);
```

```
spec3 = spec3./meanspec3;

fn4 = 'REC_pdgh_022h_34D-4';
spec4 = load_spectra(fn4, 125, 525);
spec4 = spec4./meanspec4;

fn5 = 'REC_pdgh_025h_34D-4';
spec5 = load_spectra(fn5, 125, 525);
spec5 = spec5./meanspec5;

fn6 = 'REC_pdgh_044h_34D-4';
spec6 = load_spectra(fn6, 125, 525);
spec6 = spec6./meanspec6;

fn7 = 'REC_pdgh_066h_34D-4';
spec7 = load_spectra(fn7, 125, 525);
spec7 = spec7./meanspec7;

fn8 = 'REC_pdgh_075h_34D-4';
spec8 = load_spectra(fn8, 125, 525);
spec8 = spec8./meanspec8;

fn9 = 'REC_pdgh_087h_34D-4';
spec9 = load_spectra(fn9, 125, 525);
spec9 = spec9./meanspec9;

fn10 = 'REC_pdgh_108h_34D-4';
spec10 = load_spectra(fn10, 125, 525);
spec10 = spec10./meanspec10;

fn11 = 'REC_pdgh_127h_34D-4';
spec11 = load_spectra(fn11, 125, 525);
spec11 = spec11./meanspec11;

fn12 = 'REC_pdgh_157h_34D-4';
spec12 = load_spectra(fn12, 125, 525);
spec12 = spec12./meanspec12;

fn13 = 'REC_pdgh_177h_34D-4';
spec13 = load_spectra(fn13, 125, 525);
spec13 = spec13./meanspec13;

fn14 = 'REC_pdgh_214h_34D-4';
spec14 = load_spectra(fn14, 125, 525);
spec14 = spec14./meanspec14;

fn15 = 'REC_pdgh_240h_34D-4';
spec15 = load_spectra(fn15, 125, 525);
spec15 = spec15./meanspec15;
```

```
301
302 fn16 = 'REC_pdgh_273h_34D-4';
303 spec16 = load_spectra(fn16, 125, 525);
304 spec16 = spec16./meanspec16;
305
306 fn17 = 'REC_pdgh_292h_34D-4';
307 spec17 = load_spectra(fn17, 125, 525);
308 spec17 = spec17./meanspec17;
309
310 fn18 = 'REC_pdgh_314h_34D-4';
311 spec18 = load_spectra(fn18, 125, 525);
312 spec18 = spec18./meanspec18;
313
314 fn19 = 'REC_pdgh_356h_34D-4';
315 spec19 = load_spectra(fn19, 125, 525);
316 spec19 = spec19./meanspec19;
317
318 fn20 = 'REC_pdgh_381h_34D-4';
319 spec20 = load_spectra(fn20, 125, 525);
320 spec20 = spec20./meanspec20;
321
322 curve3 = [sum(spec1(BB)), sum(spec2(BB)), sum(spec3(BB)), sum(spec4(
       BB)), sum(spec5(BB)), sum(spec6(BB)), sum(spec7(BB)), sum(spec8(
       BB)), sum(spec9(BB)), sum(spec10(BB)), sum(spec11(BB)), sum(
       spec12(BB)), sum(spec13(BB)), sum(spec14(BB)), sum(spec15(BB)),
       sum(spec16(BB)), sum(spec17(BB)), sum(spec18(BB)), sum(spec19(BB
       )), sum(spec20(BB))]./sum(spec2(BB));
323
324
325 fn1 = 'REC_pdgh_init_34D-4';
326 spec1 = load_spectra(fn1, 530, 1100);
327 spec1 = spec1./meanspec1;
328
329 fn2 = 'REC_pdgh_LS66h_34D-4';
330 spec2 = load_spectra(fn2, 530, 1100);
331 spec2 = spec2./meanspec2;
332
333 fn3 = 'REC_pdgh_010h_34D-4';
334 spec3 = load_spectra(fn3, 530, 1100);
335 spec3 = spec3./meanspec3;
336
337 fn4 = 'REC_pdgh_022h_34D-4';
338 spec4 = load_spectra(fn4, 530, 1100);
339 spec4 = spec4./meanspec4;
340
341 fn5 = 'REC_pdgh_025h_34D-4';
342 spec5 = load_spectra(fn5, 530, 1100);
343 spec5 = spec5./meanspec5;
344
```

```
fn6 = 'REC_pdgh_044h_34D-4';
spec6 = load_spectra(fn6, 530, 1100);
spec6 = spec6./meanspec6;

fn7 = 'REC_pdgh_066h_34D-4';
spec7 = load_spectra(fn7, 530, 1100);
spec7 = spec7./meanspec7;

fn8 = 'REC_pdgh_075h_34D-4';
spec8 = load_spectra(fn8, 530, 1100);
spec8 = spec8./meanspec8;

fn9 = 'REC_pdgh_087h_34D-4';
spec9 = load_spectra(fn9, 530, 1100);
spec9 = spec9./meanspec9;

fn10 = 'REC_pdgh_108h_34D-4';
spec10 = load_spectra(fn10, 530, 1100);
spec10 = spec10./meanspec10;

fn11 = 'REC_pdgh_127h_34D-4';
spec11 = load_spectra(fn11, 530, 1100);
spec11 = spec11./meanspec11;

fn12 = 'REC_pdgh_157h_34D-4';
spec12 = load_spectra(fn12, 530, 1100);
spec12 = spec12./meanspec12;

fn13 = 'REC_pdgh_177h_34D-4';
spec13 = load_spectra(fn13, 530, 1100);
spec13 = spec13./meanspec13;

fn14 = 'REC_pdgh_214h_34D-4';
spec14 = load_spectra(fn14, 530, 1100);
spec14 = spec14./meanspec14;

fn15 = 'REC_pdgh_240h_34D-4';
spec15 = load_spectra(fn15, 530, 1100);
spec15 = spec15./meanspec15;

fn16 = 'REC_pdgh_273h_34D-4';
spec16 = load_spectra(fn16, 530, 1100);
spec16 = spec16./meanspec16;

fn17 = 'REC_pdgh_292h_34D-4';
spec17 = load_spectra(fn17, 530, 1100);
spec17 = spec17./meanspec17;

fn18 = 'REC_pdgh_314h_34D-4';
```

```
394 spec18 = load_spectra(fn18, 530, 1100);
395 spec18 = spec18./meanspec18;
396
397 fn19 = 'REC_pdgh_356h_34D-4';
398 spec19 = load_spectra(fn19, 530, 1100);
399 spec19 = spec19./meanspec19;
400
401 fn20 = 'REC_pdgh_381h_34D-4';
402 spec20 = load_spectra(fn20, 530, 1100);
403 spec20 = spec20./meanspec20;
404
405 curve4 = [sum(spec1(BB)), sum(spec2(BB)), sum(spec3(BB)), sum(spec4(
    BB)), sum(spec5(BB)), sum(spec6(BB)), sum(spec7(BB)), sum(spec8(
    BB)), sum(spec9(BB)), sum(spec10(BB)), sum(spec11(BB)), sum(
    spec12(BB)), sum(spec13(BB)), sum(spec14(BB)), sum(spec15(BB)),
    sum(spec16(BB)), sum(spec17(BB)), sum(spec18(BB)), sum(spec19(BB
    )), sum(spec20(BB))]./sum(spec2(BB));
406
407
408 fn1 = 'REC_pdgh_init_56D-4';
409 spec1 = load_spectra(fn1, 25, 525);
410 spec1 = spec1./meanspec1;
411
412 fn2 = 'REC_pdgh_LS66h_56D-4';
413 spec2 = load_spectra(fn2, 25, 525);
414 spec2 = spec2./meanspec2;
415
416 fn3 = 'REC_pdgh_010h_56D-4';
417 spec3 = load_spectra(fn3, 25, 525);
418 spec3 = spec3./meanspec3;
419
420 fn4 = 'REC_pdgh_022h_56D-4';
421 spec4 = load_spectra(fn4, 25, 525);
422 spec4 = spec4./meanspec4;
423
424 fn5 = 'REC_pdgh_025h_56D-4';
425 spec5 = load_spectra(fn5, 25, 525);
426 spec5 = spec5./meanspec5;
427
428 fn6 = 'REC_pdgh_044h_56D-4';
429 spec6 = load_spectra(fn6, 25, 525);
430 spec6 = spec6./meanspec6;
431
432 fn7 = 'REC_pdgh_066h_56D-4';
433 spec7 = load_spectra(fn7, 25, 525);
434 spec7 = spec7./meanspec7;
435
436 fn8 = 'REC_pdgh_075h_56D-4';
437 spec8 = load_spectra(fn8, 25, 525);
```

```
spec8 = spec8./meanspec8;

fn9 = 'REC_pdgh_087h_56D-4';
spec9 = load_spectra(fn9, 25, 525);
spec9 = spec9./meanspec9;

fn10 = 'REC_pdgh_108h_56D-4';
spec10 = load_spectra(fn10, 25, 525);
spec10 = spec10./meanspec10;

fn11 = 'REC_pdgh_127h_56D-4';
spec11 = load_spectra(fn11, 25, 525);
spec11 = spec11./meanspec11;

fn12 = 'REC_pdgh_157h_56-4';
spec12 = load_spectra(fn12, 25, 525);
spec12 = spec12./meanspec12;

fn13 = 'REC_pdgh_177h_56D-4';
spec13 = load_spectra(fn13, 25, 525);
spec13 = spec13./meanspec13;

fn14 = 'REC_pdgh_214h_56D-4';
spec14 = load_spectra(fn14, 25, 525);
spec14 = spec14./meanspec14;

fn15 = 'REC_pdgh_240h_56D-4';
spec15 = load_spectra(fn15, 25, 525);
spec15 = spec15./meanspec15;

fn16 = 'REC_pdgh_273h_56D-4';
spec16 = load_spectra(fn16, 25, 525);
spec16 = spec16./meanspec16;

fn17 = 'REC_pdgh_292h_56D-4';
spec17 = load_spectra(fn17, 25, 525);
spec17 = spec17./meanspec17;

fn18 = 'REC_pdgh_314h_56D-4';
spec18 = load_spectra(fn18, 25, 525);
spec18 = spec18./meanspec18;

fn19 = 'REC_pdgh_356h_56D-4';
spec19 = load_spectra(fn19, 25, 525);
spec19 = spec19./meanspec19;

fn20 = 'REC_pdgh_381h_56D-4';
spec20 = load_spectra(fn20, 25, 525);
spec20 = spec20./meanspec20;
```

```
487
488 curve5 = [sum(spec1(BB)), sum(spec2(BB)), sum(spec3(BB)), sum(spec4(
        BB)), sum(spec5(BB)), sum(spec6(BB)), sum(spec7(BB)), sum(spec8(
        BB)), sum(spec9(BB)), sum(spec10(BB)), sum(spec11(BB)), sum(
        spec12(BB)), sum(spec13(BB)), sum(spec14(BB)), sum(spec15(BB)),
        sum(spec16(BB)), sum(spec17(BB)), sum(spec18(BB)), sum(spec19(BB
        )), sum(spec20(BB))]./sum(spec2(BB));
489
490
491 fn1 = 'REC_pdgh_init_56D-4';
492 spec1 = load_spectra(fn1, 530, 1100);
493 spec1 = spec1./meanspec1;
494
495 fn2 = 'REC_pdgh_LS66h_56D-4';
496 spec2 = load_spectra(fn2, 530, 1100);
497 spec2 = spec2./meanspec2;
498
499 fn3 = 'REC_pdgh_010h_56D-4';
500 spec3 = load_spectra(fn3, 530, 1100);
501 spec3 = spec3./meanspec3;
502
503 fn4 = 'REC_pdgh_022h_56D-4';
504 spec4 = load_spectra(fn4, 530, 1100);
505 spec4 = spec4./meanspec4;
506
507 fn5 = 'REC_pdgh_025h_56D-4';
508 spec5 = load_spectra(fn5, 530, 1100);
509 spec5 = spec5./meanspec5;
510
511 fn6 = 'REC_pdgh_044h_56D-4';
512 spec6 = load_spectra(fn6, 530, 1100);
513 spec6 = spec6./meanspec6;
514
515 fn7 = 'REC_pdgh_066h_56D-4';
516 spec7 = load_spectra(fn7, 530, 1100);
517 spec7 = spec7./meanspec7;
518
519 fn8 = 'REC_pdgh_075h_56D-4';
520 spec8 = load_spectra(fn8, 530, 1100);
521 spec8 = spec8./meanspec8;
522
523 fn9 = 'REC_pdgh_087h_56D-4';
524 spec9 = load_spectra(fn9, 530, 1100);
525 spec9 = spec9./meanspec9;
526
527 fn10 = 'REC_pdgh_108h_56D-4';
528 spec10 = load_spectra(fn10, 530, 1100);
529 spec10 = spec10./meanspec10;
530
```

```
fn11 = 'REC_pdgh_127h_56D-4';
spec11 = load_spectra(fn11, 530, 1100);
spec11 = spec11./meanspec11;

fn12 = 'REC_pdgh_157h_56D-4';
spec12 = load_spectra(fn12, 530, 1100);
spec12 = spec12./meanspec12;

fn13 = 'REC_pdgh_177h_56D-4';
spec13 = load_spectra(fn13, 530, 1100);
spec13 = spec13./meanspec13;

fn14 = 'REC_pdgh_214h_56D-4';
spec14 = load_spectra(fn14, 530, 1100);
spec14 = spec14./meanspec14;

fn15 = 'REC_pdgh_240h_56D-4';
spec15 = load_spectra(fn15, 530, 1100);
spec15 = spec15./meanspec15;

fn16 = 'REC_pdgh_273h_56D-4';
spec16 = load_spectra(fn16, 530, 1100);
spec16 = spec16./meanspec16;

fn17 = 'REC_pdgh_292h_56D-4';
spec17 = load_spectra(fn17, 530, 1100);
spec17 = spec17./meanspec17;

fn18 = 'REC_pdgh_314h_56D-4';
spec18 = load_spectra(fn18, 530, 1100);
spec18 = spec18./meanspec18;

fn19 = 'REC_pdgh_356h_56D-4';
spec19 = load_spectra(fn19, 530, 1100);
spec19 = spec19./meanspec19;

fn20 = 'REC_pdgh_381h_56D-4';
spec20 = load_spectra(fn20, 530, 1100);
spec20 = spec20./meanspec20;

curve6 = [sum(spec1(BB)), sum(spec2(BB)), sum(spec3(BB)), sum(spec4(
    BB)), sum(spec5(BB)), sum(spec6(BB)), sum(spec7(BB)), sum(spec8(
    BB)), sum(spec9(BB)), sum(spec10(BB)), sum(spec11(BB)), sum(
    spec12(BB)), sum(spec13(BB)), sum(spec14(BB)), sum(spec15(BB)),
    sum(spec16(BB)), sum(spec17(BB)), sum(spec18(BB)), sum(spec19(BB
    )), sum(spec20(BB))]./sum(spec2(BB));


fn1 = 'REC_pdgh_init_78D-4';
```

```
575 spec1 = load_spectra(fn1, 25, 525);
576 spec1 = spec1./meanspec1;
577
578 fn2 = 'REC_pdgh_LS66h_78D-4';
579 spec2 = load_spectra(fn2, 25, 525);
580 spec2 = spec2./meanspec2;
581
582 fn3 = 'REC_pdgh_010h_78D-4';
583 spec3 = load_spectra(fn3, 25, 525);
584 spec3 = spec3./meanspec3;
585
586 fn4 = 'REC_pdgh_022h_78D-4';
587 spec4 = load_spectra(fn4, 25, 525);
588 spec4 = spec4./meanspec4;
589
590 fn5 = 'REC_pdgh_025h_78D-4';
591 spec5 = load_spectra(fn5, 25, 525);
592 spec5 = spec5./meanspec5;
593
594 fn6 = 'REC_pdgh_044h_78D-4';
595 spec6 = load_spectra(fn6, 25, 525);
596 spec6 = spec6./meanspec6;
597
598 fn7 = 'REC_pdgh_066h_78D-4';
599 spec7 = load_spectra(fn7, 25, 525);
600 spec7 = spec7./meanspec7;
601
602 fn8 = 'REC_pdgh_075h_78D-4';
603 spec8 = load_spectra(fn8, 25, 525);
604 spec8 = spec8./meanspec8;
605
606 fn9 = 'REC_pdgh_087h_78D-4';
607 spec9 = load_spectra(fn9, 25, 525);
608 spec9 = spec9./meanspec9;
609
610 fn10 = 'REC_pdgh_108h_78D-4';
611 spec10 = load_spectra(fn10, 25, 525);
612 spec10 = spec10./meanspec10;
613
614 fn11 = 'REC_pdgh_127h_78D-4';
615 spec11 = load_spectra(fn11, 25, 525);
616 spec11 = spec11./meanspec11;
617
618 fn12 = 'REC_pdgh_157h_78D-4';
619 spec12 = load_spectra(fn12, 25, 525);
620 spec12 = spec12./meanspec12;
621
622 fn13 = 'REC_pdgh_177h_78D-4';
623 spec13 = load_spectra(fn13, 25, 525);
```

```
624 spec13 = spec13./meanspec13;
625
626 fn14 = 'REC_pdgh_214h_78D-4';
627 spec14 = load_spectra(fn14, 25, 525);
628 spec14 = spec14./meanspec14;
629
630 fn15 = 'REC_pdgh_240h_78D-4';
631 spec15 = load_spectra(fn15, 25, 525);
632 spec15 = spec15./meanspec15;
633
634 fn16 = 'REC_pdgh_273h_78D-4';
635 spec16 = load_spectra(fn16, 25, 525);
636 spec16 = spec16./meanspec16;
637
638 fn17 = 'REC_pdgh_292h_78D-4';
639 spec17 = load_spectra(fn17, 25, 525);
640 spec17 = spec17./meanspec17;
641
642 fn18 = 'REC_pdgh_314h_78D-4';
643 spec18 = load_spectra(fn18, 25, 525);
644 spec18 = spec18./meanspec18;
645
646 fn19 = 'REC_pdgh_356h_78D-4';
647 spec19 = load_spectra(fn19, 25, 525);
648 spec19 = spec19./meanspec19;
649
650 fn20 = 'REC_pdgh_381h_78D-4';
651 spec20 = load_spectra(fn20, 25, 525);
652 spec20 = spec20./meanspec20;
653
654 curve7 = [sum(spec1(BB)), sum(spec2(BB)), sum(spec3(BB)), sum(spec4(
       BB)), sum(spec5(BB)), sum(spec6(BB)), sum(spec7(BB)), sum(spec8(
       BB)), sum(spec9(BB)), sum(spec10(BB)), sum(spec11(BB)), sum(
       spec12(BB)), sum(spec13(BB)), sum(spec14(BB)), sum(spec15(BB)),
       sum(spec16(BB)), sum(spec17(BB)), sum(spec18(BB)), sum(spec19(BB
       )), sum(spec20(BB))]./sum(spec2(BB));
655
656
657 fn1 = 'REC_pdgh_init_78D-4';
658 spec1 = load_spectra(fn1, 530, 1100);
659 spec1 = spec1./meanspec1;
660
661 fn2 = 'REC_pdgh_LS66h_78D-4';
662 spec2 = load_spectra(fn2, 530, 1100);
663 spec2 = spec2./meanspec2;
664
665 fn3 = 'REC_pdgh_010h_78D-4';
666 spec3 = load_spectra(fn3, 530, 1100);
667 spec3 = spec3./meanspec3;
```

```
668
669 fn4 = 'REC_pdgh_022h_78D-4';
670 spec4 = load_spectra(fn4, 530, 1100);
671 spec4 = spec4./meanspec4;
672
673 fn5 = 'REC_pdgh_025h_78D-4';
674 spec5 = load_spectra(fn5, 530, 1100);
675 spec5 = spec5./meanspec5;
676
677 fn6 = 'REC_pdgh_044h_78D-4';
678 spec6 = load_spectra(fn6, 530, 1100);
679 spec6 = spec6./meanspec6;
680
681 fn7 = 'REC_pdgh_066h_78D-4';
682 spec7 = load_spectra(fn7, 530, 1100);
683 spec7 = spec7./meanspec7;
684
685 fn8 = 'REC_pdgh_075h_78D-4';
686 spec8 = load_spectra(fn8, 530, 1100);
687 spec8 = spec8./meanspec8;
688
689 fn9 = 'REC_pdgh_087h_78D-4';
690 spec9 = load_spectra(fn9, 530, 1100);
691 spec9 = spec9./meanspec9;
692
693 fn10 = 'REC_pdgh_108h_78D-4';
694 spec10 = load_spectra(fn10, 530, 1100);
695 spec10 = spec10./meanspec10;
696
697 fn11 = 'REC_pdgh_127h_78D-4';
698 spec11 = load_spectra(fn11, 530, 1100);
699 spec11 = spec11./meanspec11;
700
701 fn12 = 'REC_pdgh_157h_78D-4';
702 spec12 = load_spectra(fn12, 530, 1100);
703 spec12 = spec12./meanspec12;
704
705 fn13 = 'REC_pdgh_177h_78D-4';
706 spec13 = load_spectra(fn13, 530, 1100);
707 spec13 = spec13./meanspec13;
708
709 fn14 = 'REC_pdgh_214h_78D-4';
710 spec14 = load_spectra(fn14, 530, 1100);
711 spec14 = spec14./meanspec14;
712
713 fn15 = 'REC_pdgh_240h_78D-4';
714 spec15 = load_spectra(fn15, 530, 1100);
715 spec15 = spec15./meanspec15;
716
```

```
717 fn16 = 'REC_pdgh_273h_78D-4';
718 spec16 = load_spectra(fn16, 530, 1100);
719 spec16 = spec16./meanspec16;
720
721 fn17 = 'REC_pdgh_292h_78D-4';
722 spec17 = load_spectra(fn17, 530, 1100);
723 spec17 = spec17./meanspec17;
724
725 fn18 = 'REC_pdgh_314h_78D-4';
726 spec18 = load_spectra(fn18, 530, 1100);
727 spec18 = spec18./meanspec18;
728
729 fn19 = 'REC_pdgh_356h_78D-4';
730 spec19 = load_spectra(fn19, 530, 1100);
731 spec19 = spec19./meanspec19;
732
733 fn20 = 'REC_pdgh_381h_78D-4';
734 spec20 = load_spectra(fn20, 530, 1100);
735 spec20 = spec20./meanspec20;
736
737 curve8 = [sum(spec1(BB)), sum(spec2(BB)), sum(spec3(BB)), sum(spec4(
        BB)), sum(spec5(BB)), sum(spec6(BB)), sum(spec7(BB)), sum(spec8(
        BB)), sum(spec9(BB)), sum(spec10(BB)), sum(spec11(BB)), sum(
        spec12(BB)), sum(spec13(BB)), sum(spec14(BB)), sum(spec15(BB)),
        sum(spec16(BB)), sum(spec17(BB)), sum(spec18(BB)), sum(spec19(BB
        )), sum(spec20(BB))]./sum(spec2(BB));
738
739
740
741 %%
742 time = [-66, 0, 10, 22, 25, 44, 66, 75, 87, 108, 127, 157, 177, 214,
         240, 273, 292, 314, 356, 381];
743
744 %%
745
746 figure; hold on;
747
748 xlim([-66 381])
749
750 ylim([0 1.4])
751
752 plot(time,curve1,'r','LineWidth',2)
753
754 plot(time,curve2,'g','LineWidth',2)
755
756 plot(time,curve3,'b','LineWidth',2)
757
758 plot(time,curve4,'m','LineWidth',2)
759
```

```
760 plot(time,curve5,'k','LineWidth',2)
761
762 plot(time,curve6,'c','LineWidth',2)
763
764 plot(time,curve7,'y','LineWidth',2)
765
766 plot(time,curve8,'-.b','LineWidth',2)
767
768 xlabel('Time [h]')
769
770 ylabel('Relative BB-signal')
771
772 title('BB-signal development')
773
774 legend;
775
776 hold off;
```

Thank you.

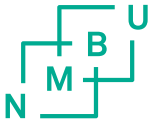

Norges miljø- og biovitenskapelige universitet
Noregs miljø- og biovitskapelege universitet
Norwegian University of Life Sciences

Postboks 5003
NO-1432 Ås
Norway